



National Aeronautics and
Space Administration

CURATORIAL BRANCH

Lyndon B. Johnson Space Center
Houston, Texas 77058

Publication 55

JSC - 17243

March 1981

GUIDEBOOK FOR
THE BOULDERS AT STATION 6,
APOLLO 17

Compiled by:

W. C. Phinney

Planetary and Earth Sciences Division
National Aeronautics and Space Administration
Lyndon B. Johnson Space Center
Houston, Texas

TABLE OF CONTENTS

	Page
ACKNOWLEDGEMENTS.....	i.
SUMMARY.....	1.
PRELIMINARY STUDIES.....	3.
INTRODUCTION.....	3.
GEOLOGIC SETTING.....	3.
BOULDER DESCRIPTIONS.....	4.
ROCK DESCRIPTIONS.....	5.
PETROGRAPHY.....	24.
SLAB DESCRIPTIONS AND ALLOCATIONS.....	25.
DETAILED STUDIES.....	54.
PETROGRAPHY.....	54.
CRYSTALLOGRAPHY.....	78.
MAJOR ELEMENT CHEMISTRY.....	80.
LITHOPHILE TRACE ELEMENTS.....	80.
METEORITIC AND VOLATILE ELEMENTS.....	87.
CARBON AND SULFUR.....	91.
NOBLE GASES.....	93.
GAMMA COUNTING.....	99.
GEOCHRONOLOGY.....	99.
URANIUM-THORIUM-LEAD.....	108.
SURFACE EXPOSURE EFFECTS.....	109.
MAGNETIZATION.....	115.
INTERESTING PROBLEMS THAT REMAIN.....	117.

(continued)

TABLE OF CONTENTS (continued)

	Page
REFERENCES.....	118.
GENERAL.....	118.
PETROLOGY.....	118.
CRYSTALLOGRAPHY.....	120.
THERMAL MODELS.....	121.
GEOCHEMISTRY.....	121.
GEOCHRONOLOGY.....	123.
SURFACE EXPOSURE EFFECTS.....	123.
MAGNETIZATION.....	125.

Acknowledgements

A consortium effort on the boulders at Station 6, Apollo 17 was initiated in the spring of 1973 and continued for a period of three years. Most of this Guide Book is a compilation of published data resulting from the consortium effort. However, much of the published data is scattered throughout several publications as a consequence of the continuing allocations of the boulder samples over a period of nearly three years. This resulted in serial publications of data sets that have never been published as a single set. In addition to the published data there is also a significant amount of unpublished information that should be presented in conjunction with what is published. **This document is an attempt to** compile all of the published and unpublished data as well as point out some of the significant conclusions which can be studied in more detail by referring to the reference list at the end of the text. Included are all of the references that resulted from allocations of the boulder samples that were made during the period of the consortium effort on the boulder. Rather than listing the many names that should be acknowledged the reader should realize that I am indebted to all of the authors of the 67 papers listed at the end of the text for the data and conclusions compiled here.

THE BOULDERS AT STATION 6, APOLLO 17

Summary

The North Massif at the Taurus-Littrow (Apollo 17) landing site is characterized by high albedo; it has been interpreted as ejecta from the Serenitatis Basin. The cluster of boulders at Station 6 may be derived from one larger boulder which rolled to its present location from an outcrop high on the North Massif about 21 m.y. ago according to cosmic ray exposure ages.

Four lithologic units within the boulder cluster have been identified, based on photography and descriptions by the crew of Apollo 17. Unit A is characterized by abundant vesicles >5 cm long, flattened along a plane parallel to the contact with the adjacent unit. Unit B is characterized by well-developed foliation or banding. Unit C is massive, with no obvious foliation and contains angular clasts up to 0.8 m long. Unit A-B is a discontinuous transition zone up to a few meters wide between units A and B.

All samples collected from the boulder are impact melts and a variety of clasts. Matrix samples were collected from all of the photogeologic units except unit A and two large clasts were sampled from unit C. The matrices contain 50-60% modal feldspar, ~45% orthopyroxene and 1-7% Fe-Ti oxide. The clasts contain 70% feldspar, 30% orthopyroxene and olivine and a trace of Fe-Ti oxide.

The impact melt comprising the matrix of the boulder was formed about 4.0 b.y. ago and was homogenized extremely well chemically by the impact process. The matrix is enriched in KREEP components and siderophile elements. The latter are considered to be a result of meteoritic enrichment and form such a tight cluster on a Au-Ir-Re plot that a meteorite group may be assigned to the projectile which produced the impact. Several anorthositic clasts which significantly predate the formation of impact melt in which they were incorporated display various degrees of brecciation and shock

metamorphism. Some of the clasts appear to be of plutonic origin. In fact one contains pyroxene with exsolution lamellae whose widths and compositions suggest formation at a depth of a few kilometers.

Chemical and petrographic data from the boulder are consistent with a thermal model for the formation of impact melts by mixing of superheated melt and relatively cool clastic debris. The model includes two stages of cooling. The initial stage results from rapid mixing and extensive dissemination of the fine grained debris to produce a thermal equilibration in tens of seconds at temperatures below the liquidus. The second stage is that of slow conductive cooling typical of sheet-like or pond-like igneous bodies. This model fits the boulder and is reflected in the finer-grained, rapidly chilled textures at the margins of the melt sheet where there is a higher content of both refractory and non-refractory clasts. Further into the sheet the grain-size increases, the content of clasts decreases, and most clasts are of very refractory minerals. Studies of the boulder combined with studies of terrestrial impact craters have led to a significant improvement in our understanding of the processes that occur during impacts.

Rock surfaces exposed to the lunar environment are pitted by micrometeorite impact craters, contain solar flare tracks, and are covered with a thin patina of brown glass. These studies suggest invariant fluxes for solar flares and interplanetary micrometeoroids over a 10^6 year period. Also the upper limit of solar wind erosion is placed at 0.03\AA per year under recent lunar conditions.

A study of the natural remanent magnetization of the boulder indicates two sources of magnetization. One results from the clast population which was not heated enough to reset its magnetization. The other results from the matrix which was largely heated to melt temperatures and reflects the field at the time of breccia formation.

Preliminary Studies

Introduction

In preparation for an integrated consortium approach to the study of large boulder samples from Station 6 at the Apollo 17 landing site a number of preliminary studies were accomplished. Lunar surface photographs allowed rather detailed mapping of the large boulders as well as the determination of locations for six of the seven samples chipped from the boulder (76315 could not be accurately located). Maps of the individual samples and the locations of chips for preliminary analysis were compiled. Other preliminary studies included petrographic descriptions, chemistry, gamma-ray counting results, rare gas contents (with estimated exposure ages), and natural remanent magnetization data. These preliminary data were compiled in Ref. 1 and are summarized in the next three sections.

Geologic Setting

The 2000 m high North Massif rises to an altitude of 6500 m. (6180 m in the vicinity of Station 6) from the Valley of Taurus-Littrow at 4530 m and is characterized by steep slopes (20° - 30°) and high albedo; it has been interpreted as ejecta from large ring basins, subsequently uplifted by the impact which formed the Serenitatis Basin (Ref. 1). Apollo 15 orbital photography of the site indicated that several large boulders at low elevations were derived from outcrops high on the slopes of the massif; the boulders left tracks as they rolled downslope. According to photogeologic interpretation (Ref. 1), the boulders at Station 6 originated from a field of boulders that extends for about one kilometer horizontally, high on the north massif. From this apparently horizontal lens of consolidated material the Station 6 boulder rolled somewhat cross-slope for 1230 m while dropping from an altitude of 5030 m to 4590 m (440 m).

Boulder Descriptions

A cluster of boulders covering an area 10 x 24 m constitutes Station 6. It appears that many (or most) of these may be derived from one larger boulder which split into several pieces when it stopped rolling or afterwards. The largest boulders in the cluster were numbered, north to south, 1 through 5 (Figure 1). They were photographed on all sides except within the narrow cracks between boulders 1 and 2 and the northwest side of boulder 1. The maps (Figures 2-6) are based on the photographs and astronaut descriptions.

All boulders at Station 6 appear to be breccias; the samples collected are from large clasts and matrices. Boulders 1, 2, and 3 readily fit together; the fit of boulders 4 and 5 is less obvious. Three basic lithologic units are here defined photogeologically; they are labeled A, B, and C for convenience and do not imply a top or base. Descriptions of these units, based mainly on boulders 1, 2, and 3, are outlined in Figure 7. In boulders 4 and 5 and parts of boulder 2, the contact between units A and B is sharp; in boulder 2 it defines a plane oriented about N20W and dipping 65°W. In other parts of boulder 2 (see Figure 1) zones A and B are not well defined and a contact zone or transitional area, several meters wide, has been defined. If this plane were originally horizontal, the boulders are now turned on their sides relative to their original position. The foliation in boulder 2 is defined by aligned, flattened vesicles, "trains" of small clasts, and differentially eroded linear depressions in the rock surface; it is parallel to the contact between units A and B.

A sharp contact cuts across boulder 5 then folds over the present top of the boulder at a steep angle (Figure 5). It is possible that this contact is equivalent to that between units A and B; this relationship places samples 76015 and 76215 in unit B. If this is the case, then boulders 4 and 5 rolled over during separation from boulder 2. Folds defined by the foliation are visible in several places on the face of boulder 4.

The stratigraphic "section" of breccia units defined in the boulders at Station 6 is given in Figure 7. It is not possible to determine which end is top or bottom. Unit A is a highly vesicular unit (est. 30-35%), with large, flattened vesicles up to 15 cm long and 5-6 cm wide in sharp contact with the foliated, less vesicular unit B. Unit C is a massive unit exhibiting low vesicularity and large (up to 0.8 m long) clasts.

An apparently close terrestrial analogue is an 8-40 m thick ash flow tuff unit in Central Oregon (see Ref. 1). From the base upward, it consists of (1) ~1-2 m thick, densely welded vitrophyre zone, (2) 1-2 m thick vesicular (or vuggy) lithophysal zone, (3) 4-5 m thick strongly foliated zone which is internally deformed in places, forming slump structures, and (4) unwelded to welded tuffs (>10 m thick) which exhibit only poor foliation. The zonation of the ash flow tuff results from different degrees of compaction and welding and from primary and secondary vapor-phase crystallization. The relation between the vesicular zone and foliation zone may be analogous to units A and B, respectively, in the boulders at Station 6. If this analogy is carried through, then unit A is below unit B in the Station 6 "section." Unit C is also compatible with this model.

At present, there is no way to establish the thickness of the depositional unit from which the Station 6 boulders are derived or the composition of the gases which formed the vesicles.

Rock Descriptions

Sample 76315 is from the south face of boulder 2. Astronaut descriptions and photographs indicate that it is from a highly vesicular zone, possibly photogeologic unit A but more probably the transition zone between photogeologic units A and B.

Samples 76215 and 76015 are from vesicular, banded areas of boulders 4 and 5. If this unit is the same as the banded unit in boulder 2, then they are characteristic of photogeologic unit B.

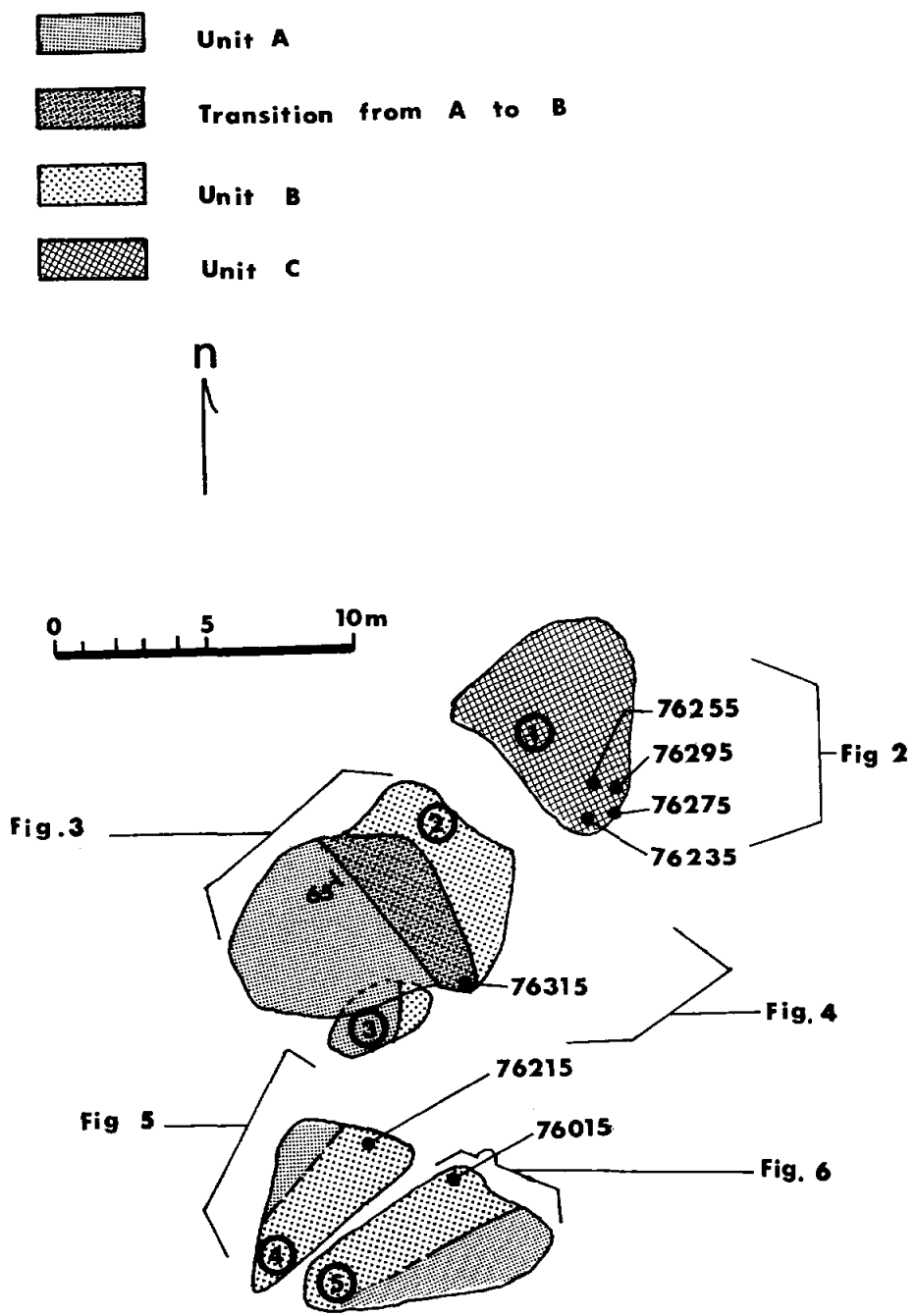


Figure 1. - Map of the boulder cluster at Station 6, showing sample locations, location of lithologic units, and index to boulder maps.

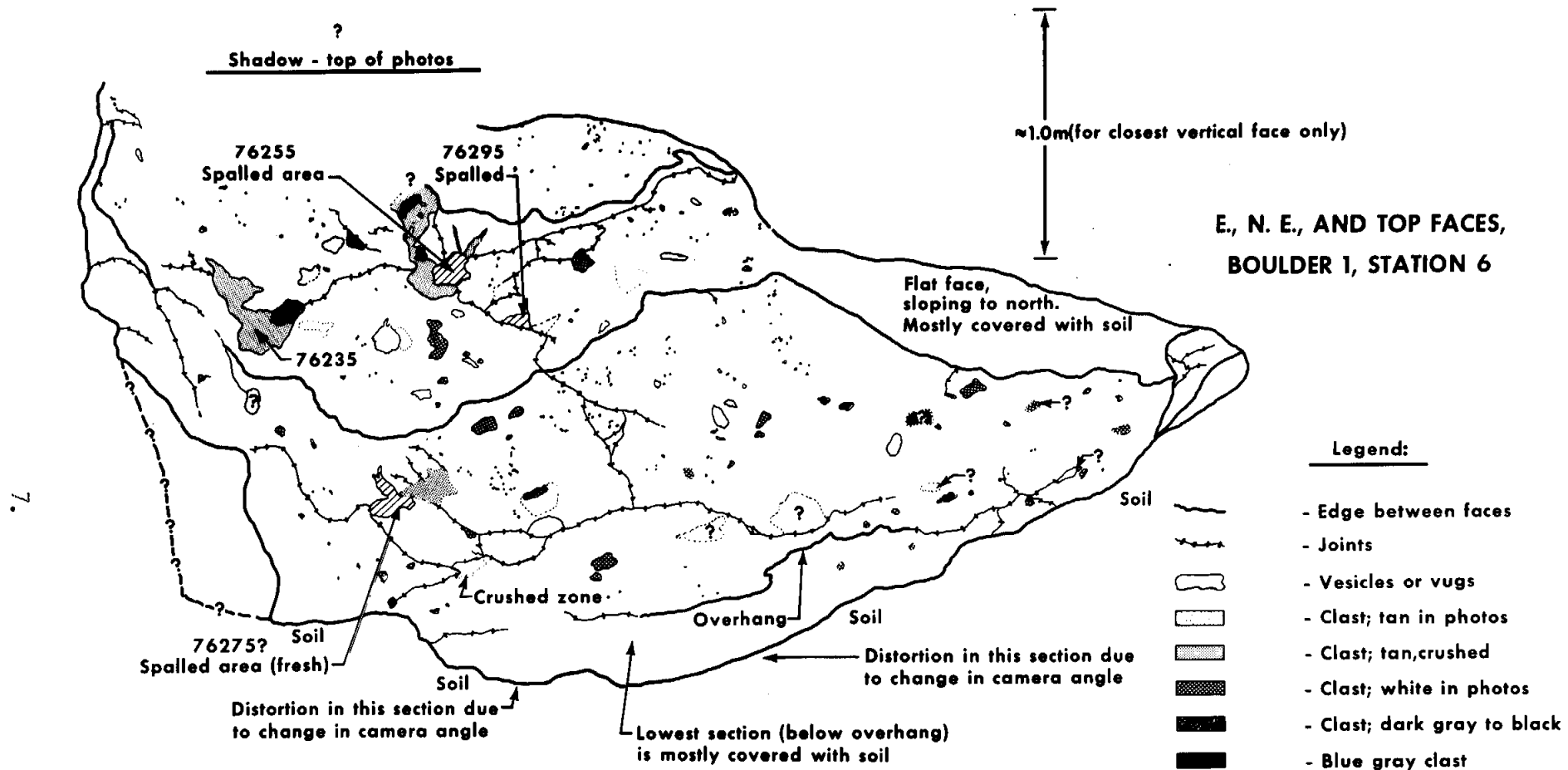


Figure 2. - Map of the East, Northeast and top faces of Boulder 1.

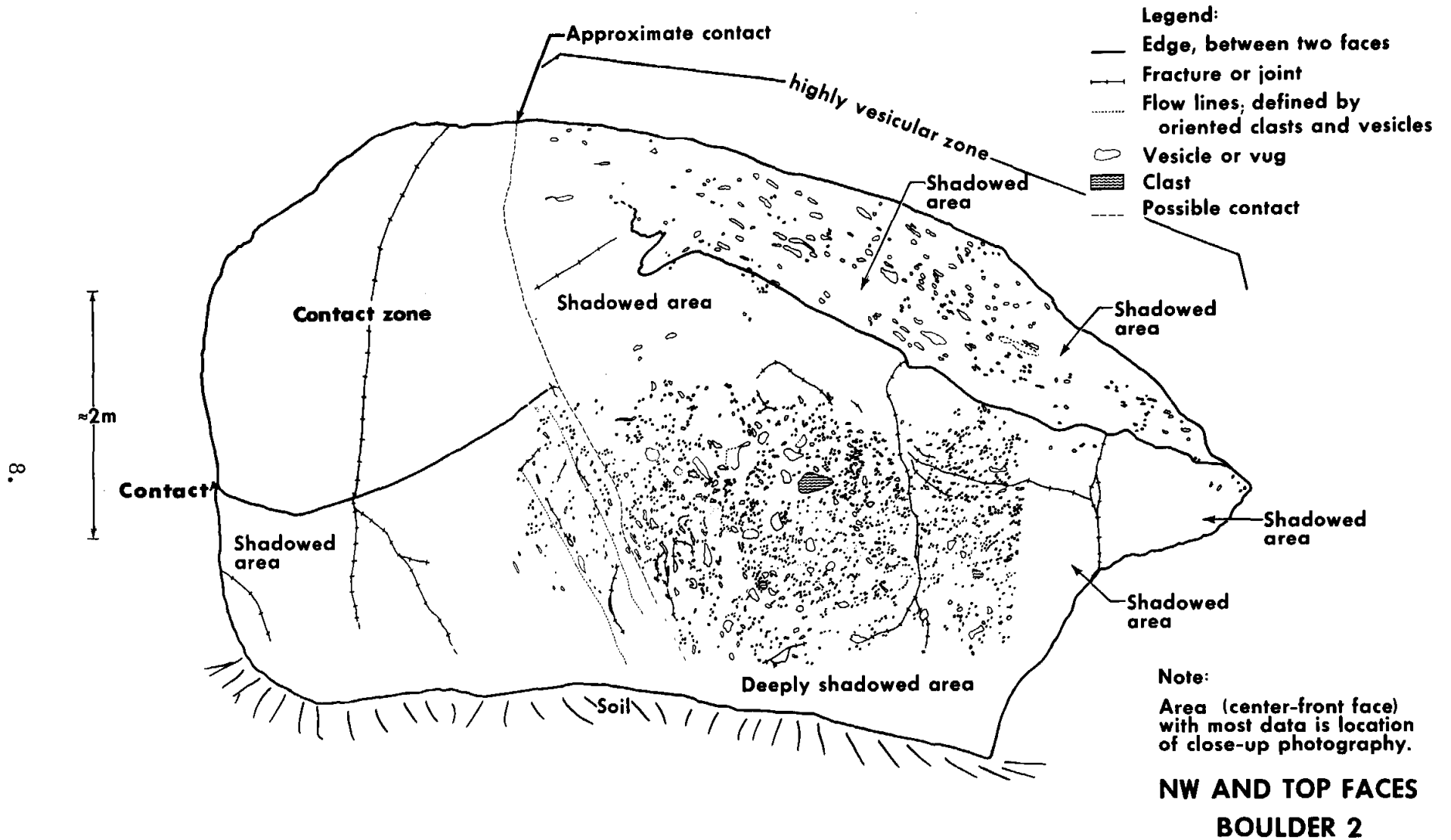


Figure 3. - Map of the Northwest and top faces of Boulder 2.

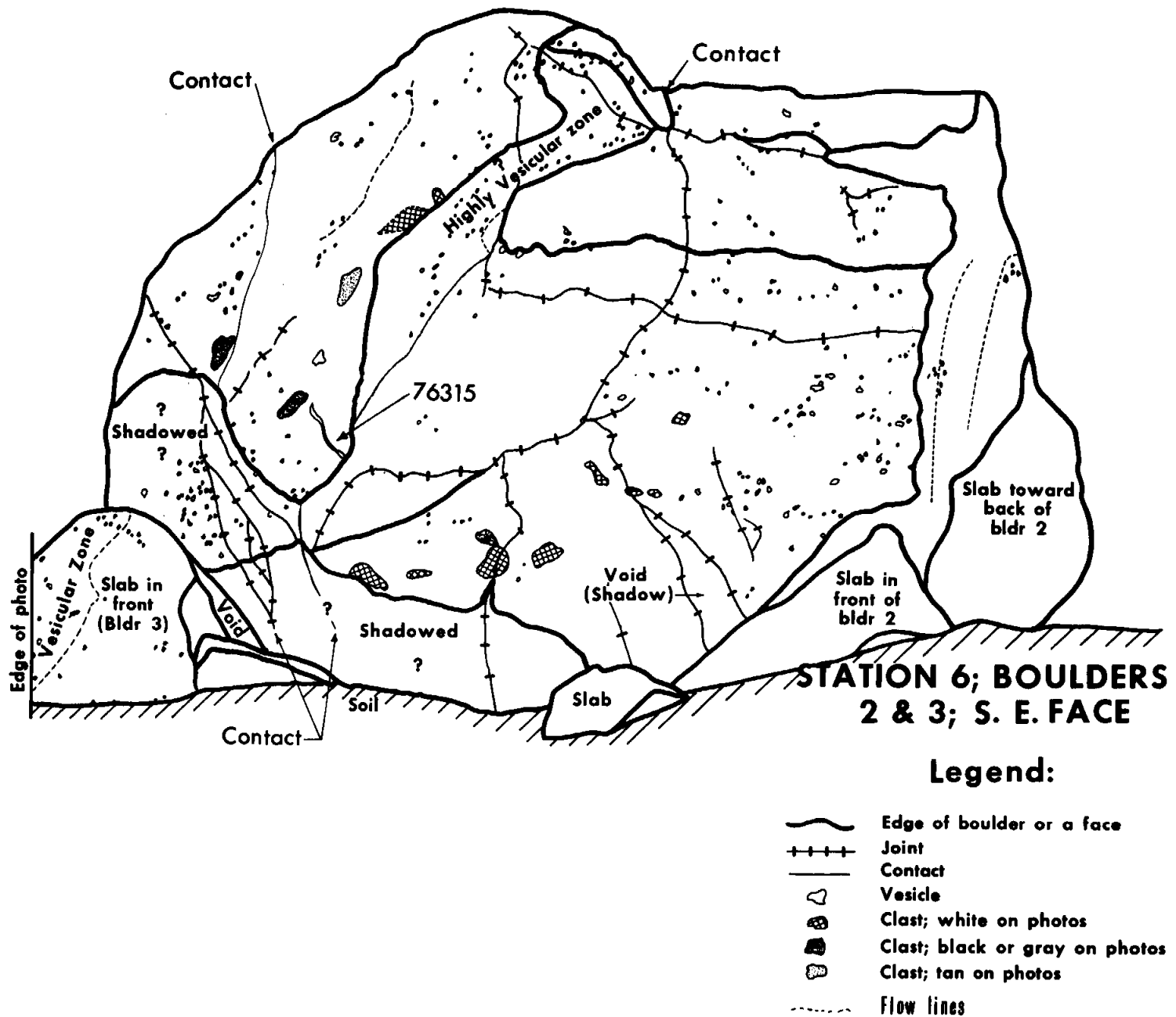
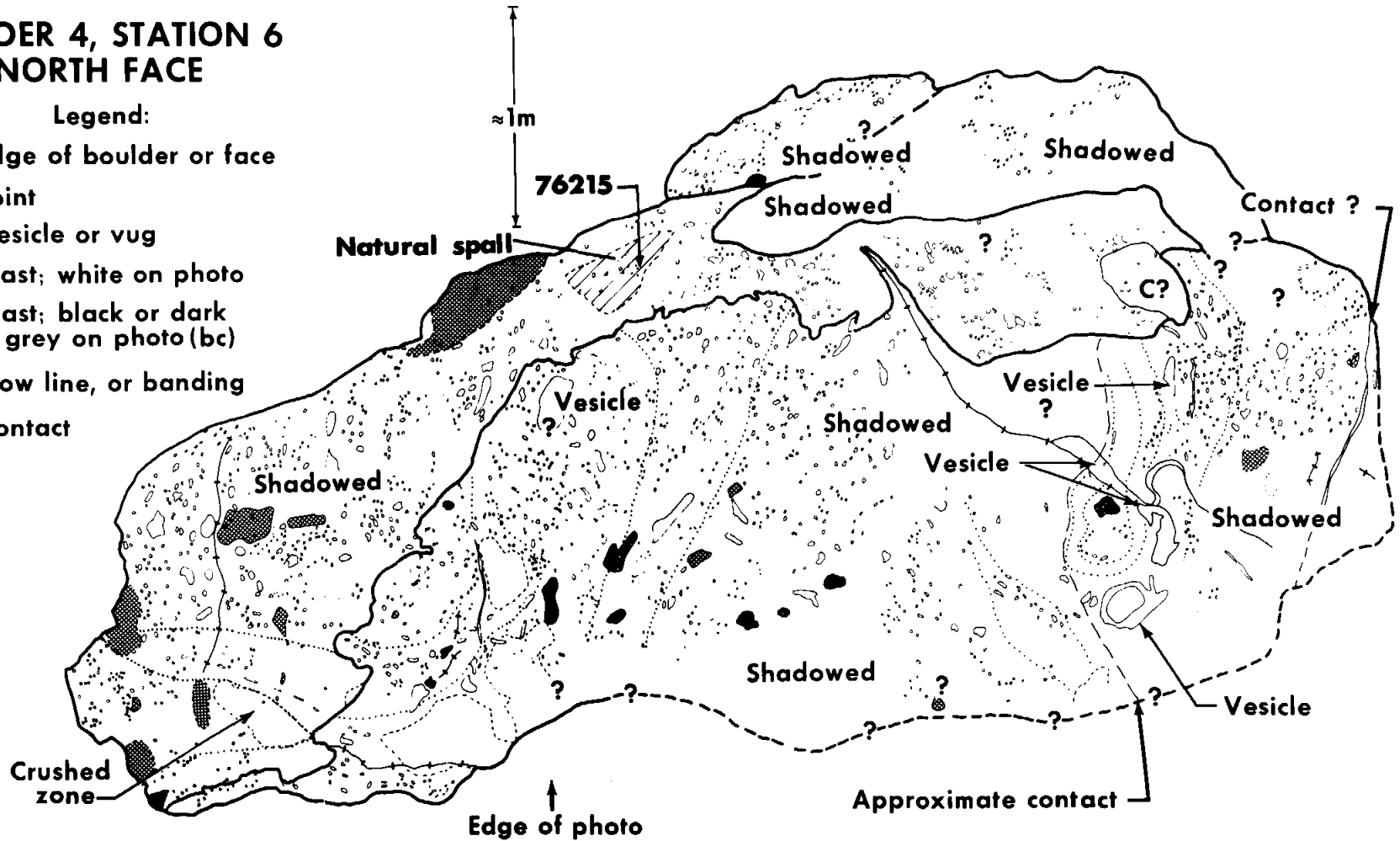


Figure 4. - Map of the Southeast face of Boulders 2 and 3.

**BOULDER 4, STATION 6
NORTH FACE**

Legend:

- Edge of boulder or face
- - - Joint
- Vesicle or vug
- ▨ Clast; white on photo
- Clast; black or dark grey on photo (bc)
- ⋯ Flow line, or banding
- - - Contact



10.

Figure 5. - Map of the North face of Boulder 4.

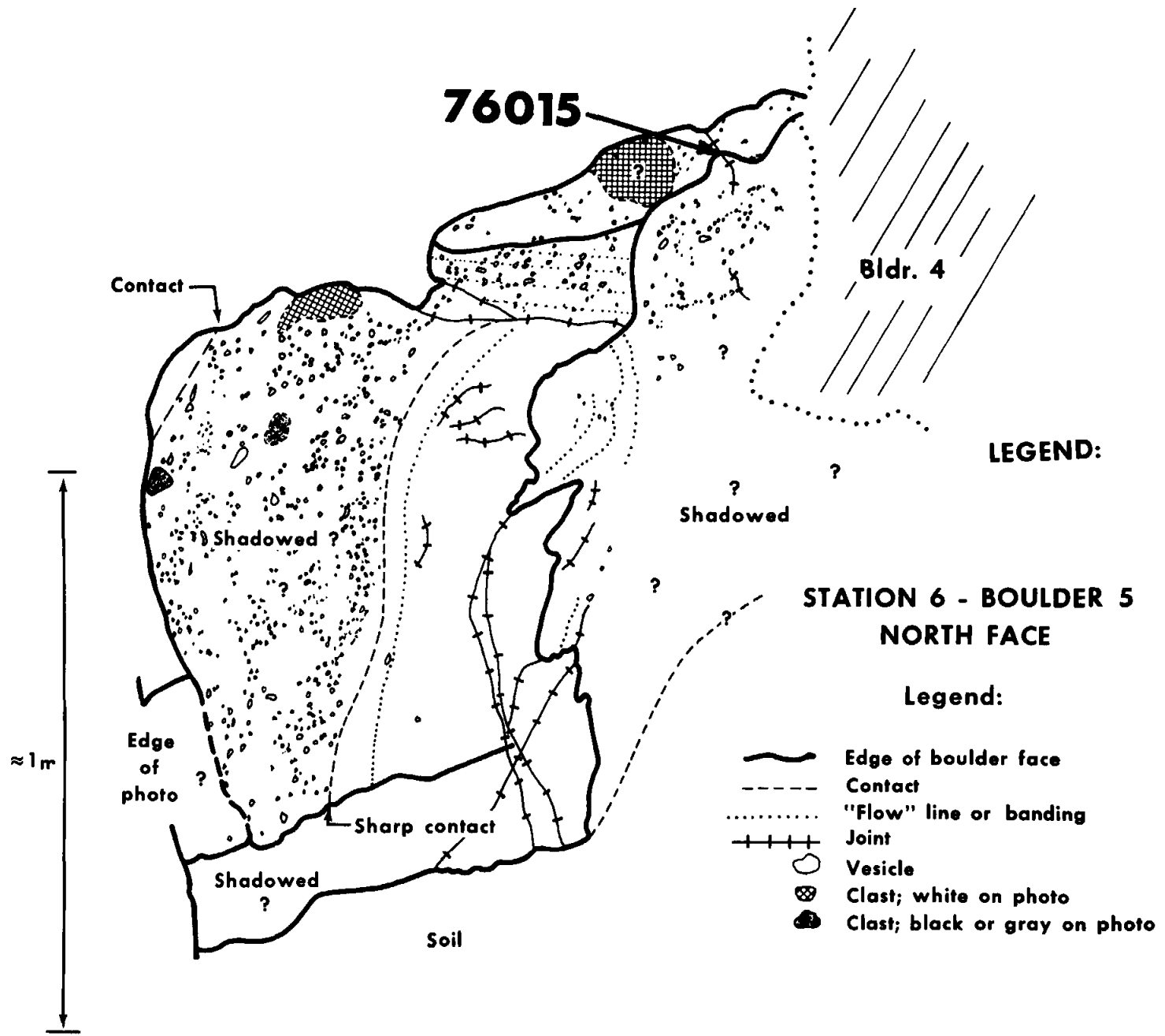


Figure 6. - Map of the North face of Boulder 5.

UNIT AND THICKNESS	A; 6m +	GRADATION FROM A TO B; 0-2.5 m	B; 2-4 m	C; 6m +
Description	Highly vesicular, with abundant large vesicles (>5 cm); many vesicles are flattened along a plane parallel to the contact with unit B. There is an increase in the number of large vesicles toward the "center" of this unit.	Irregular zone across present top side of Boulder 2 (see map)	Characterized by well-developed foliation or banding. Some of the bands are folded. Vesicular, with only a trace of vesicles >5 cm long. There are very few clasts visible in the photographs.	Contains blue-gray to white clasts, up to 0.8 m long, in a pale brown to light gray matrix. There is <u>no</u> obvious banding or foliation. Vesicular, with only a <u>trace</u> of vesicles >5 cm long.
Samples	76315	--	76215 and 76015	76295, 76275 (matrix) 76235, 76255 (clasts)
Comments	Near the ground surface on the NW side of Boulder 2, the contact between A and B is very sharp.			Contact with unit B may be gradational?

Figure 7. - Stratigraphic "Section" represented in the boulders of Station 6.

Samples 76275, 76295, 76255, and 76235 are from the east and southeast faces of boulder 1 in photogeologic unit C. Samples 76275 and 76295 are characteristic of the matrix. Sample 76255 is partially from a 0.5 m long tan clast but partially mixed with matrix. Sample 76235 is from a 0.8 m long, irregular white clast from which a total of eight fragments (76235-76239 and 76305-76307) were collected.

Sample 76315 - Blue-Gray Breccia

The lithologic character of the rock (Figure 8) is generally obscured by pitting and patination on all but the fresh B₁ surface. The dark gray, fine-grained, breccia that forms about two-thirds of the B₁ base seems to compose an even greater part of the rest of the rock since the large, irregular patches of pinkish-gray material on the B₁ face should be visible on the other surfaces if they were present. The various types of gray clasts visible on B₁, however, would be obscured on the other faces if present. The occurrence of relatively large minerals, both as individual clasts and as parts of lithic clasts, is mapped in the few cases where they occur.

Sample 76215 - Green-Gray Breccia; 643.9 gms

On a fresh face, this breccia is medium light gray (N6 to N7) - See Figure 9. The "matrix" or groundmass has a crystalline, equigranular texture and is vesicular to vuggy. It consists of about 75% 50-120 μ m long plagioclase crystals, 15-20% pale reddish-brown pyroxene and very pale green olivine crystals, and 5% 20-200 μ m long flakes of opaque minerals. There is a trace of a 100 μ m diameter pale red mineral.

Clasts consist of ~2% 0.5 to 1.0 mm long plagioclase grains, 1-2% olivine crystals (up to 2.4 mm long), and 1% gray anorthosite (5-8 mm diameter). On a fresh surface, 4-5 mm diameter white oikocrysts are visible.

LEGEND

LITHOLOGIES

-  LITHOLOGIC BOUNDARY; QUERIED WHERE OBTAINED BY PITTING OR PATINA
 -  BOUNDARY OF SURFACE FEATURE
 -  BOUNDARY BETWEEN FACES OR OUTLINE OF ROCK
 -  COINCIDENT BOUNDARY BETWEEN FACES AND SURFACE FEATURES
 -  PITTED SURFACE; MICROMETEORITE IMPACT PITS
 -  PAT PATINATED SURFACES
 -  F FRESH, UNPITTED SURFACE
 -  PO SURFACE WITH POWDER COVERING
 -  4 SAMPLING LOCATION FOR 76315,4
- 1 cm

-  MATRIX - DARK GREY (N3) WITH MEDIUM DARK GRAY (N4) VEINS. 80% VITREOUS, APHANITIC MATERIAL; 15% WHITE TO LT. GRAY PLAGIOCLASE GRAINS (UP TO 1 MM); 1% OPAQUE MINERALS; 1% MAFIC MINERAL CLASTS (PALE GREEN OLIVINE AND CINNAMON BROWN PYROXENE); 2% SMALL VUGS.
-  MM MOTTLED MATRIX, PRODUCED BY FINE-GRAINED INTERSTITIAL WHITE MATERIAL IN DARK GREY GROUND MASS.
-  VM VUGGY MATRIX, 10% VOID SPACE
-  BRECCIA, PINKISH GRAY (5YR 8/1): 20% GRAY CLASTS OF MATRIX-LIKE MATERIAL; 80% WHITE, CRUSHED FRIABLE MATERIAL (20% OLIVINE, 75% PLAGIOCLASE, 5% GRAY FRAGMENTS).
-  AC APHANITIC GRAY CLAST (N5), WITH VITREOUS LUSTER
-  LIGHT GRAY CLASTS (N6) WITH A VITREOUS LUSTER
-  PC PLAGIOCLASE CLASTS
-  TC TROCTOLITIC CLASTS; UP TO 40% OLIVINE WITH PLAGIOCLASE. MAY BE UNCRUSHED EQUIVALENTS TO WHITE BRECCIA MATRIX.
-  SPC SPINEL-PLAGIOCLASE CLAST; 3% RED SPINEL.
-  S SPINEL, RED SINGLE CRYSTALS OR AN AGGREGATE OF SPINEL
-  PX PYROXENE, YELLOWISH-BROWN

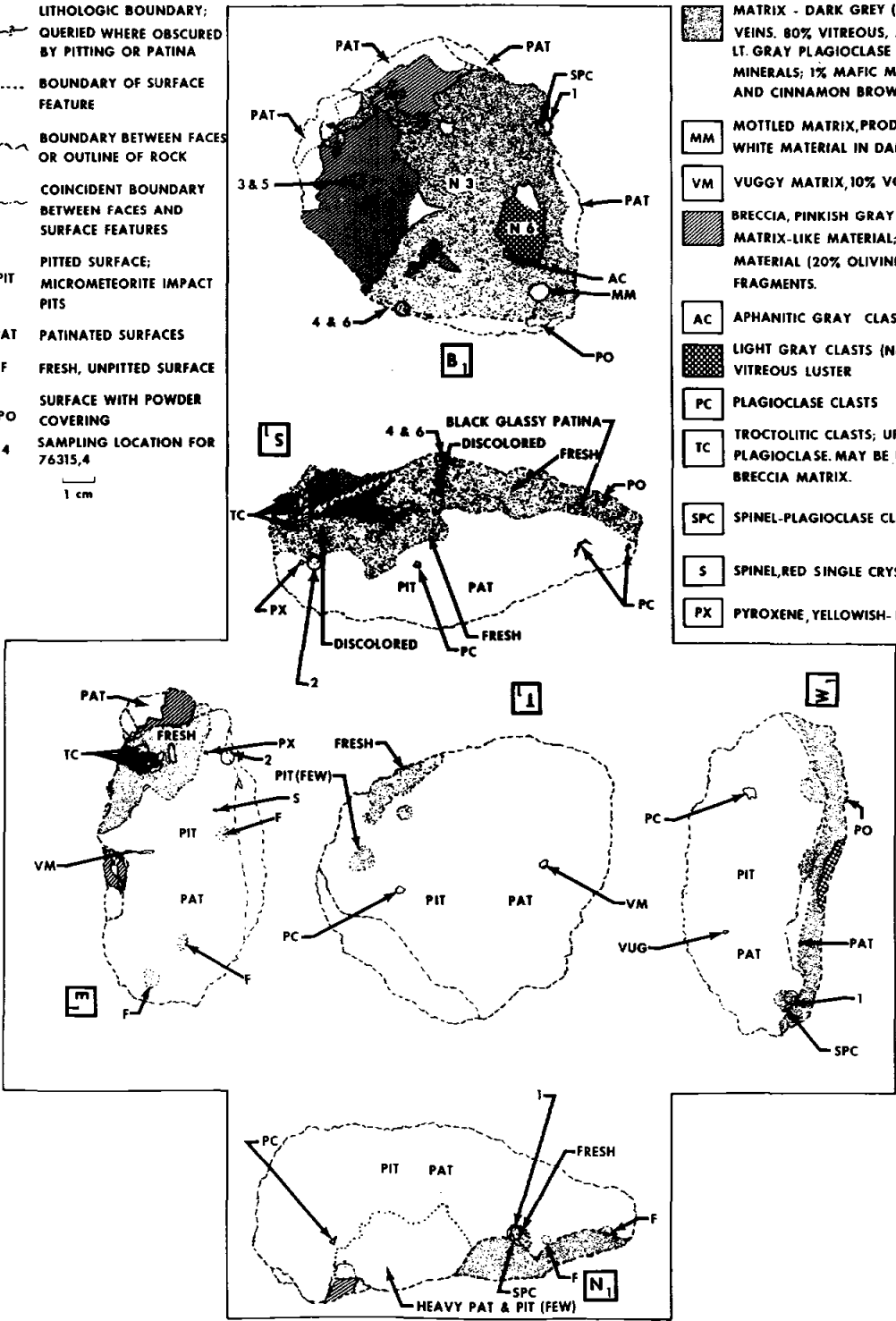


Figure 8. - Map of sample 76315.

76215

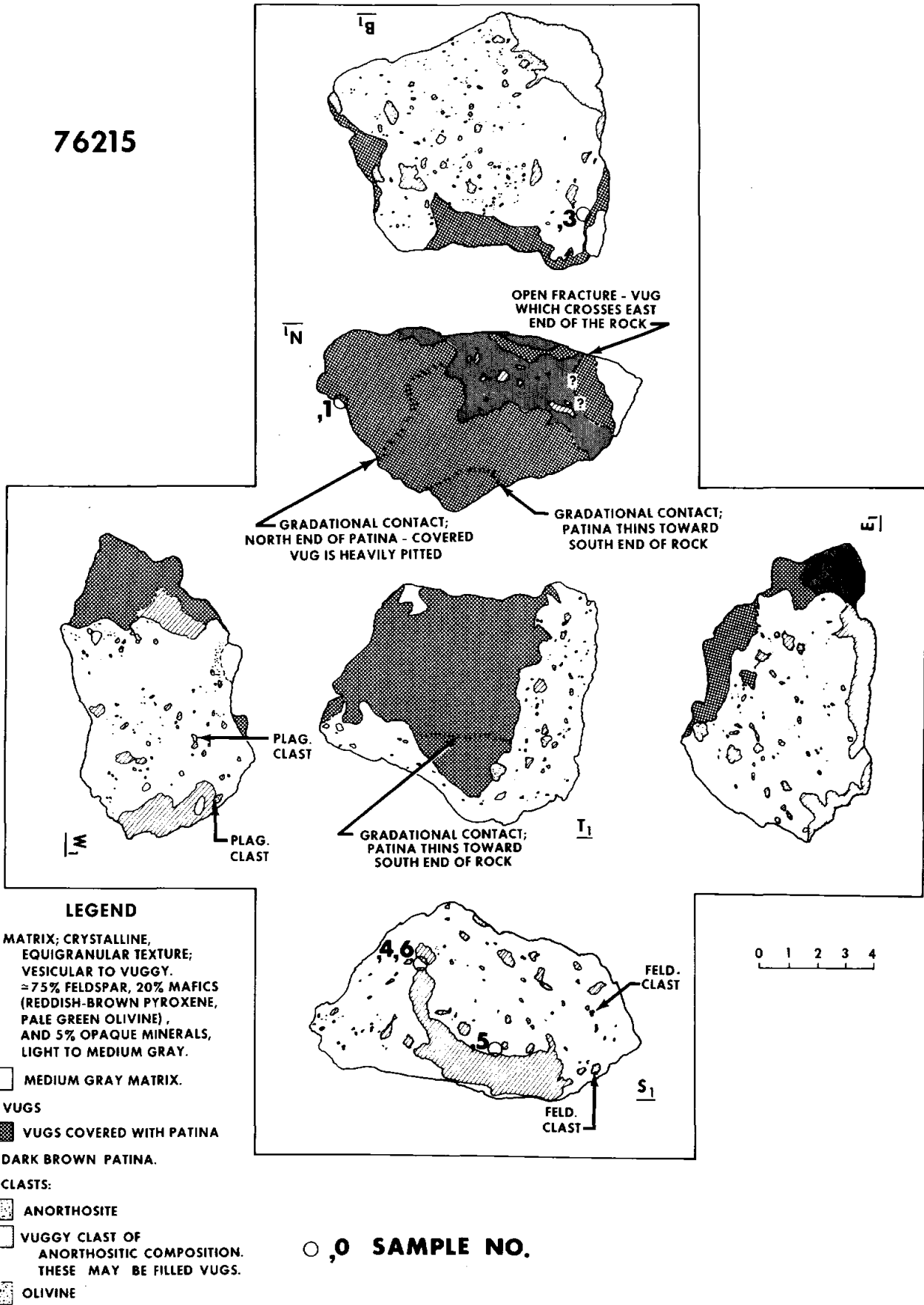


Figure 9. - Map of sample 76215.

The most remarkable feature of the rock is vugs ranging from 25 μm to 8 cm long. One whole side of the rock is a large vug or vesicle wall; rounded and smooth. The vug walls are covered by patches of sugary-textured, pale yellow minerals (1-3.5 mm long), pale gray feldspar crystals, and metal grains. There are traces of gold- and gray-colored metallic crystals, 120-500 μm in diameter. Several of the metallic crystals are tarnished to peacock blue and red colors.

The large vug has a glassy patina, which thins toward one end. The thickest part is heavily pitted by micrometeorite craters. It is possible that the thickest patina and heaviest pitting are located at the former open end of this large vug (prior to its separation from the boulder).

Sample 76015 - Green-Gray Breccia; 2819 gms

This breccia (Figure 10) is a very vesicular rock with <0.1 mm to 5 cm long, irregular vesicles comprising about 20% of the rock by volume. The flattened vesicles define a preferred orientation best seen on the west (W_1) side of the rock.

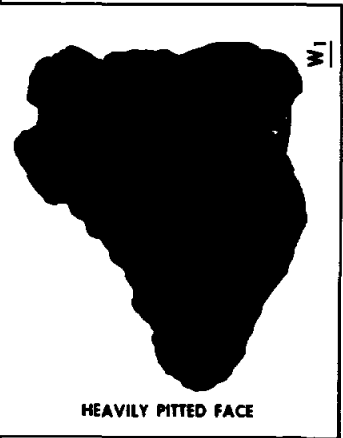
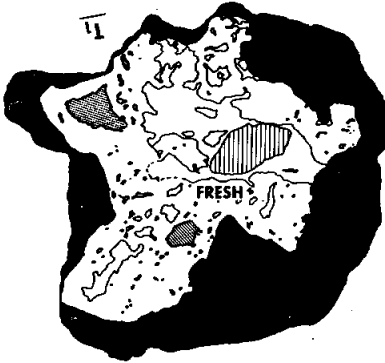
The matrix has an equant, holocrystalline texture and consists of ~40% low Ca pyroxene, ~18% vesicles (<1 mm), ~2% olivine "clasts" and ~40% plagioclase.

Clasts >1 mm in diameter make up less than 2% of the rock. These range up to 1.5 cm and consist of pale green to medium gray, aphanitic lithic types with green and brown phenocrysts or possibly xenocrysts.

Coarse-grained "pseudoclasts," up to 4.5 cm in diameter, consist of matted, interwoven pyroxene and feldspar crystals. These appear to be a coarser version of the matrix lining vesicle walls. The largest "pseudoclast" is surrounded on all sides except one by large vesicles.

Much of the rock surface (including exposed vesicle walls) has been coated with a very thin layer of brown glass (patina).

76015



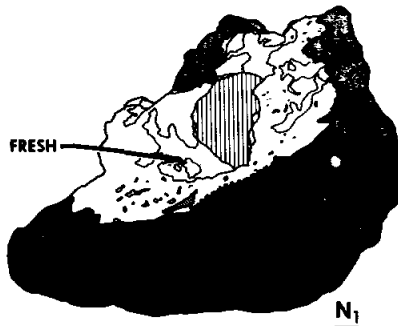
HEAVILY PITTED FACE

0 1 2 3 4
cm

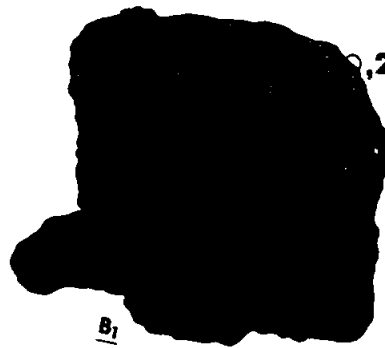
LEGEND

-  VESICLES OR VUGS
-  PALE GREEN TO MED GRAY APHANITIC CLASTS WITH GREEN AND BROWN PHENOCRYSTS (?)
-  COARSE EQUIVALENT TO MATRIX; MAY BE CLAST OR VUG LININGS (THE "CLAST" IS SURROUNDED ON ALL SIDES BY VUGS)
-  MATRIX - LOCA PYX ~40%
- VESICLES (1mm) ~18%
- OLIVINE "CLASTS" ~2%
- PLAG ~40%
- HOLOCRYSTALLINE, EQUIGRANULAR TEXTURE
-  PATINA

0,0 SAMPLE NO.



N₁



B₁

HEAVILY PITTED, PATINATED FACE

Figure 10. - Map of sample 76015.

Sample 76275 - Blue-Gray Breccia; 55.93 gms

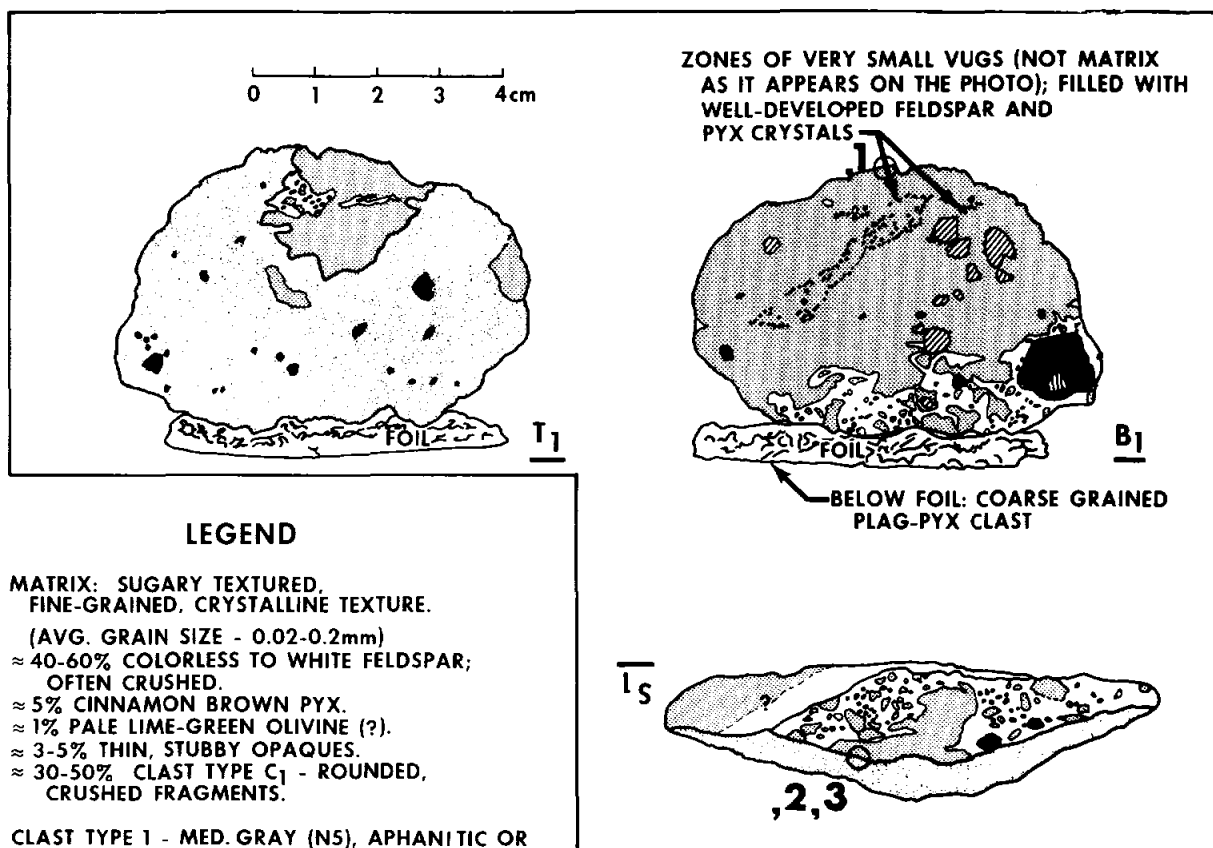
The matrix is brownish-gray, having a fine-grained, equigranular, holocrystalline texture; it consists of ~40-60% colorless to dull white feldspar, ~5% cinnamon brown pyroxene, ~1% pale lime-green olivine, ~3-5% thin, short, opaque minerals, and 30-50% clast type 1. See Figure 11 for clast descriptions. The rock has less than 1% vesicles or vugs; these are concentrated in several elongate zones of <0.5 mm voids and scattered voids up to 0.25 cm in diameter.

Most of the rock is covered by a glassy, dark olivine gray (5Y3/1) patina. Lithic types present on all but two sides are marked by this patina.

Sample 76295 - Blue-Gray Breccia; 26.07 gms

Two lithologic types with complex interrelationships compose most of the rock. See Figure 12. A pale brown breccia is predominant on the best-exposed (N_1-T_1) face where it appears to form a matrix to clasts of the other abundant lithology, gray breccia which is fine-grained and recrystallized. On the other well-exposed surface (one side of the B_1 face), the gray breccia forms nearly all of the rock. Surface features, such as pitting, patina, and powder, obscure the underlying lithology.

A direct relationship of the very fine powder covering much of the S_1-T_1 face and part of the W_1 face to the underlying lithology is suggested by the presence of a white powder coating part of a white clast. If the relationship is consistent, the buff color of most of the powder reflects the presence of underlying light brown breccia.



LEGEND

- MATRIX:** SUGARY TEXTURED, FINE-GRAINED, CRYSTALLINE TEXTURE. (AVG. GRAIN SIZE - 0.02-0.2mm) ≈ 40-60% COLORLESS TO WHITE FELDSPAR; OFTEN CRUSHED. ≈ 5% CINNAMON BROWN PYX. ≈ 1% PALE LIME-GREEN OLIVINE (?). ≈ 3-5% THIN, STUBBY OPAQUES. ≈ 30-50% CLAST TYPE C₁ - ROUNDED, CRUSHED FRAGMENTS.
- CLAST TYPE 1 -** MED. GRAY (N5), APHANITIC OR GLASSY (VITREOUS LUSTER) GROUND MASS, WITH ≈ 30% PLANOCRYSTS? OR CLASTS? "CLASTS" CONSIST OF ≈ 50% PLAG, 25% REDDISH PYX, 15% PALE GREEN OL. AND 10% OPAQUES (ILMEN.). SOME ARE VUGGY.
- CLAST WITHIN CLAST TYPE 1:** 3.6-2.4mm LONG, ROUNDED EQUANT ANORTHOSITE CLASTS.
- CLAST TYPE 2:** - POLYGONAL, ROUNDED, MED. GRAY, APHANITIC BRECCIA. SIMILAR TO CLAST TYPE 1, BUT HAS 20% VESICULARITY.
- ANORTHOSITE CLAST -** WITHIN CLAST TYPE 2.
- PYROXENE CLASTS:** RED-BROWN.
- VESICLES AND VUGS.**
- PATINA:** AND ZAP/PIT COVERED AREAS. - MOST LITHIC TYPES MASKED BY THE DK. OLIVE GRAY, THIN COATING.
- GABBROIC ANORTHOSITE CLAST:** 1mm LONG XLS OF PLAG. AND PYX.

76275

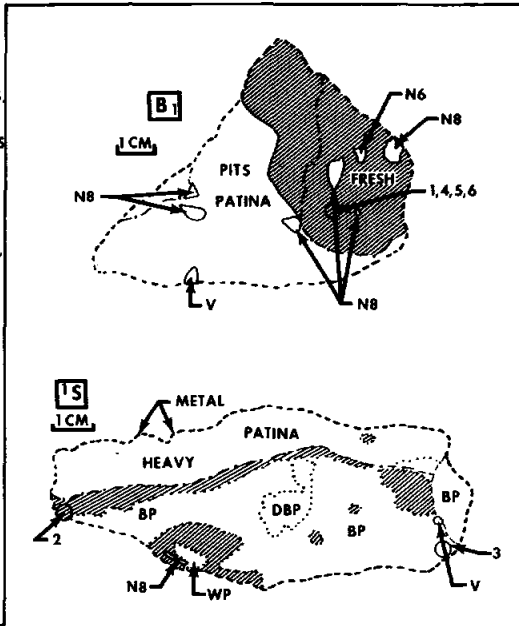
○,0 **SAMPLE NO.**

Figure 11. - Map of sample 76275.

76295

EXPLANATION

- LITHOLOGIC BOUNDARY
- BOUNDARY OF SURFACE FEATURES
- OUTLINE OF ROCK AND BOUNDARY BETWEEN FACES
- COINCIDENT BOUNDARY BETWEEN SURFACE FEATURES AND FACES.
- BP: BUFF POWDER - VERY PALE YELLOWISH BROWN (10YR 7/2).
- DBP: DISCOLORED BUFF POWDER, WHICH IS DIRTY YELLOW AND GLASSY OR PATINA-LIKE.
- WP: WHITE POWDER.
- 2 SAMPLING LOCATION FOR 76295.2



- 'MATRIX' - VERY PALE BROWN (5YR 6/2); COMPOSITION: 50% GRAY (N4) CLASTS (LIKE THE LARGER CLASTS BUT <1MM); 40% WHITE PLAGIOCLASE; 5% CINNAMON BROWN PYROXENE; 1% OLIVINE (BOTTLE GREEN); 1% BLACK (ILMENITE) FLAKED.
- N8 WHITE CLASTS (VERY LIGHT GRAY = N8) WHICH ARE COMPOSED OF COLORLESS TO LIGHT GRAY PLAGIOCLASE GRAINS REACHING 1 MM IN SIZE.
- N6 MEDIUM LIGHT GRAY (N6) CLASTS; FINE GRAINED PLAGIOCLASE TO APHANITIC.
- MEDIUM DARK GRAY (N4) CLASTS AND MATRIX; VITREOUS AND APHANITIC.
- N3 DARK GRAY (N3) CLASTS, APHANITIC.
- V BASALTIC VUGS - COLOR IS MODERATE BROWN (5 YR 3/); COMPOSITION IS: 60% PLAGIOCLASE (PLATY); 35% CINNAMON BROWN PYROXENE; 5% ILMENITE; TRACE OF OLIVINE. UP TO 40% VOID SPACE.

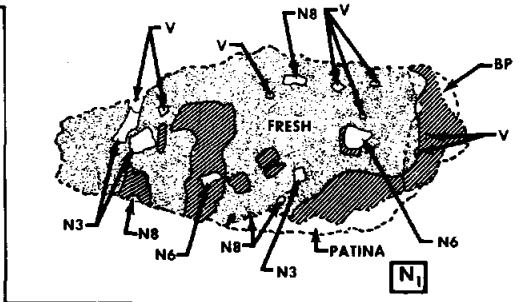
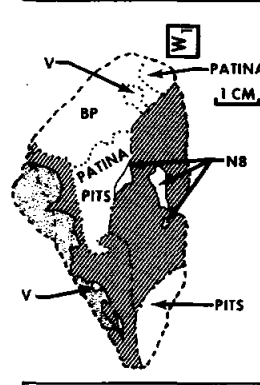
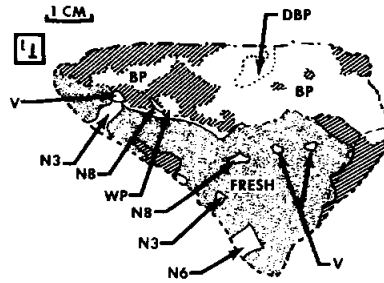
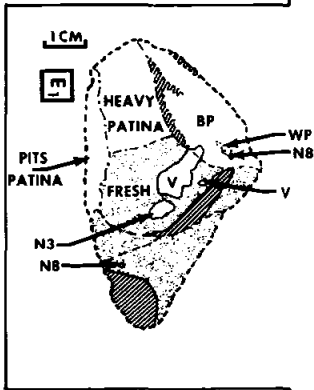


Figure 12. - Map of sample 76295.

Sample 76255 - Banded Tan and Blue-Gray Breccia; 406.6 gms

There are bands of three matrix types interwoven throughout this rock; in some parts of the rock, they are so finely banded that it was mapped as undifferentiated matrix. See Figure 13. The matrix types are: (1) tan matrix: ~40% pale brown pyroxene and 60% feldspar, (2) gray matrix: ~92% colorless feldspar, ~5% pale brown pyroxene, and ~3% opaque minerals. Several varieties of this matrix type contain up to 10% equant, possibly aphanitic vitric fragments, (3) "white" matrix (actually yellowish gray, but white relative to the other matrix types): ~15% 0.5 to 0.8 mm long red-brown pyroxene and colorless and white feldspar, and 65% feldspar plus glass grains less than 0.05 mm in diameter.

The main clast type consists of 0.1 mm to 5.5 cm diameter, rounded clasts of gray (~5%) glass; these consist of 1.0 mm, equant, colorless feldspar crystals in vitreous or aphanitic groundmass. Some of the larger clasts contain feldspar crystals up to 4 mm long. There is a trace of spherical, 0.1 mm diameter vesicles.

Other clasts include a crushed version of the gray clast type, large plagioclase grains (>2 mm), and basalt. The last type may not be clasts but rather vugs completely filled with coarse, well-developed crystals of pale brown pyroxene (40%), plagioclase (50%), and ilmenite (10%).

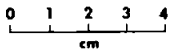
The surface of the rock is covered in part by a dark patina and in part by white powder. The olive gray (5Y 5/1) patina covers most of the T₁ side of the rock, broken only by micrometeorite pits. Along the edges the patina grades into what is definitely a thin glass coating. Several parts of the rock are covered by a 0.1 to 1 mm thick coating of very fine-grained white powder.

The "exposed" face of this sample has been differentially eroded, with the more resistant gray, aphanitic clasts standing 0.1 to 2 mm above the matrix.

76255

LEGEND

- MATRIX; UNIDENTIFIED
- ▨ MATRIX; PREDOMINANTLY TAN (CONTAINS ≈40% PALE BROWN PYROXENE)
- CLAST, UNIDENTIFIED
- GREY APHANITIC CLAST WITH A VITREOUS LUSTER
- GREY CLAST; SHEARED OR CRUSHED
- PLAGIOCLASE CLAST (>2 mm DIAMETER) WITHIN GREY CLAST
- ▨ VUG FILLINGS; OPEN NETWORK OF PLAGIOCLASE, ILMENITE AND PYROXENE CRYSTALS. WHEN VUGS ARE FILLED, THESE RESEMBLE BASALT CLASTS
- ▨ WHITE POWDER (ON SURFACE)



0 SAMPLE NO.

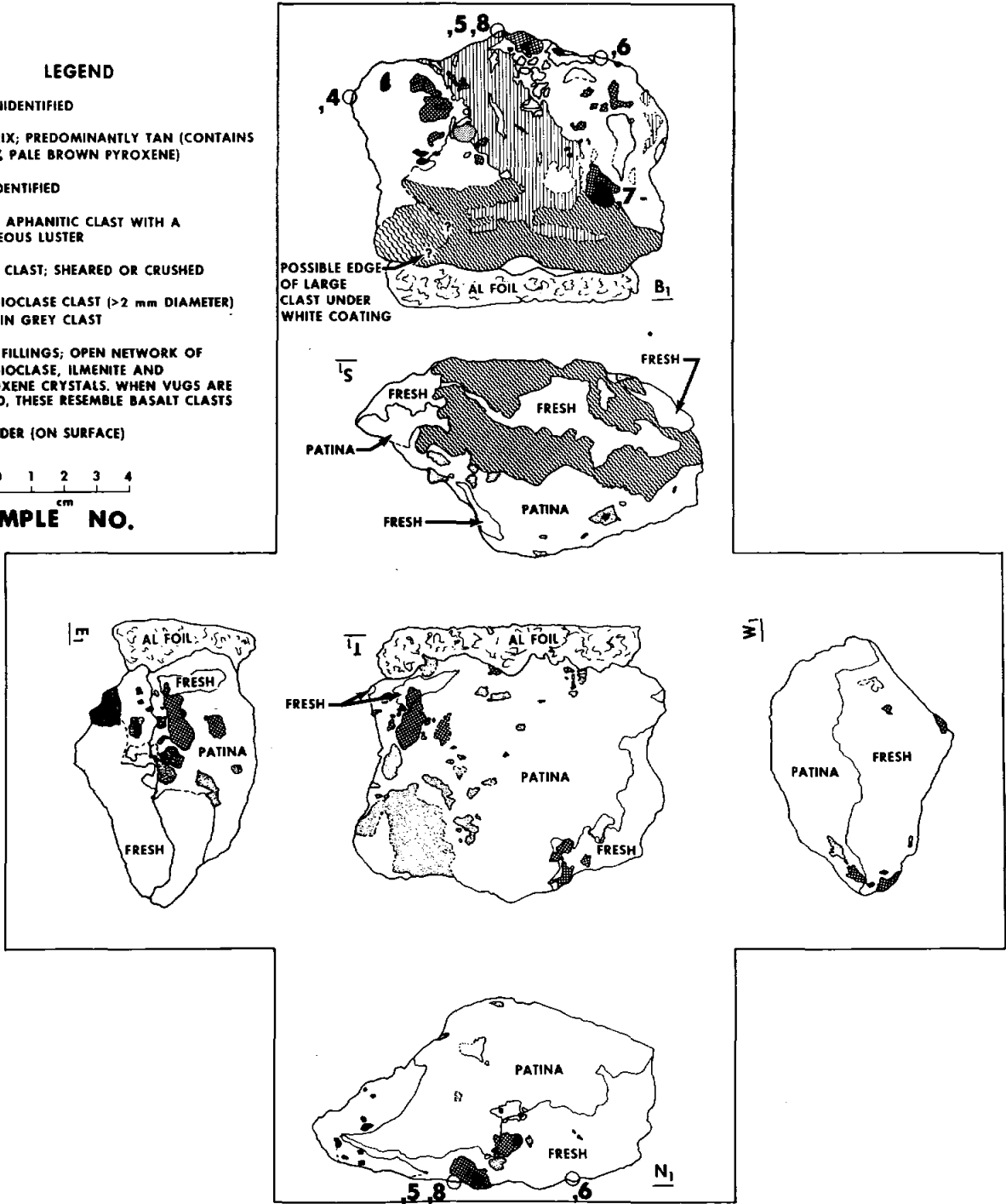


Figure 13. - Map of sample 76255.

76235

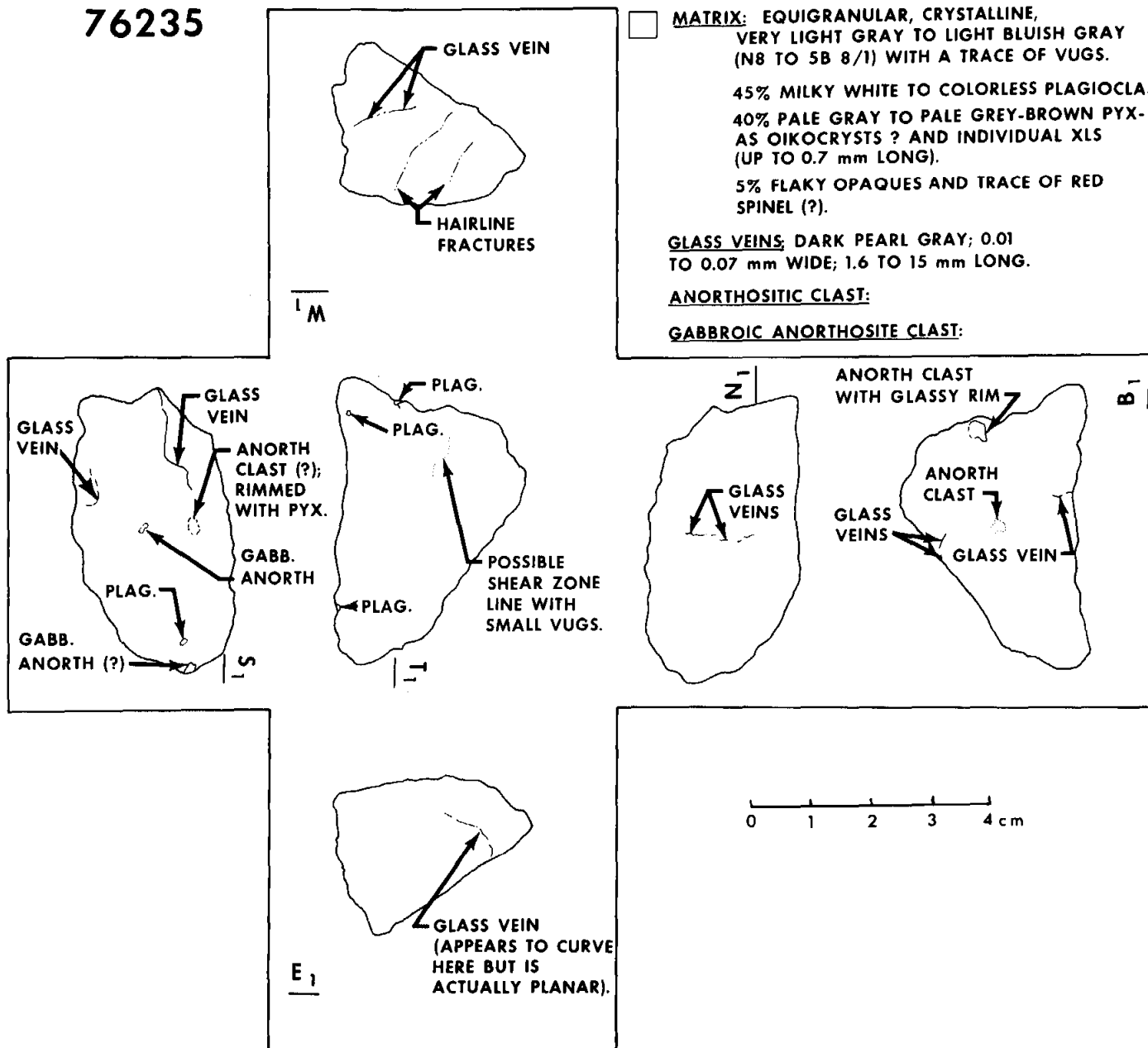
LEGEND

MATRIX: EQUIGRANULAR, CRYSTALLINE, VERY LIGHT GRAY TO LIGHT BLUISH GRAY (N8 TO 5B 8/1) WITH A TRACE OF VUGS.
 45% MILKY WHITE TO COLORLESS PLAGIOCLASE
 40% PALE GRAY TO PALE GREY-BROWN PYX-AS OIKOCRYSTS ? AND INDIVIDUAL XLS (UP TO 0.7 mm LONG).
 5% FLAKY OPAQUES AND TRACE OF RED SPINEL (?).

GLASS VEINS: DARK PEARL GRAY; 0.01 TO 0.07 mm WIDE; 1.6 TO 15 mm LONG.

ANORTHOSITIC CLAST:

GABBROIC ANORTHOSITE CLAST:



0 1 2 3 4 cm

Figure 14. - Map of sample 76235.

Sample 76235 - Brecciated Gabbro; 26.56 gms

Very light gray (N8) to light bluish gray (5B 8/1) breccia with uniform, equigranular, fine-grained texture (see Figure 14). The rock is composed of ~45% plagioclase, ~40% pale gray to pale gray-brown pyroxene present as patchy oikocrysts and tabular crystals up to 0.7 mm long, and ~5% opaque minerals. Vugs are rare, ranging up to 0.35 mm in diameter; they are lined with euhedral crystals of plagioclase, pyroxene and ilmenite. There is also a trace of metal droplets within the vugs. Clasts are rare.

There are several thin (0.01-0.07 mm) glass veins, 1.6 to 13 mm long.

Petrography

In order to plan the detailed allocations for a consortium study of the boulder a preliminary set of chips for polished thin sections was taken from several clasts and each variety of matrix of each rock. Chips were obtained by prying off loose pieces and clipping off corners with dykes. At least two chips were taken from each macroscopically homogeneous matrix to test for petrographic homogeneity.

Each section was examined in both transmitted and reflected light. All comments about the textures of matrices are based on the reflected light observations.

On the basis of modal mineralogy, most materials fell into two groups.

1. Matrices with 50-60% modal feldspar, about 45% orthopyroxene and 1 to 7% Fe-Ti oxide. The chemically analyzed portion of 76315 falls into this category and may indicate that this group of rocks has a composition range known as low-K Fra Mauro, low-K KREEP or High Alumina Basalt. Textures of rocks with this modal mineralogy are either poikilitic, like many Apollo 16 crystalline rocks, or fine-grained and subophitic.

2. Clasts with about 70% feldspar plus orthopyroxene and olivine and relatively few opaque minerals. Sample 76230 falls into this category and its chemical composition falls into the Highland Basalt range which is slightly more aluminous than VHA basalt. All of the rocks with this modal mineralogy have brecciated textures which have been annealed to various degrees.

Slab Descriptions and Allocations

Following the preliminary petrographic study of chips from each matrix and some clasts, the photos of each rock were studied in detail and detailed cutting plans were devised. After completion of sawing to produce a slab the textures on each sawn surface were mapped by means of a binocular microscope. The mapped surfaces are displayed in Figures 15-32 and described below. Detailed allocation plans were then revised to develop a final allocation plan. The allocations that resulted are listed in Table 1 and shown in the maps of Figures 17, 20, 23, 25 and 28,

76015 - Unit B - Figs. 15, 16, 17

Alignment of elongate vesicles or vugs define a foliation on the surface of the slab. Yellow euhedral crystals extend from the walls in some vugs. The slab consists primarily of a matrix which in thin section is poikilitic. Submillimeter metal grains occur throughout the matrix. There are several millimeter-sized clasts of olivine and plagioclase mineral grains. One large, porous, basaltic clast (L3) occurs on the W face of the slab but diminishes greatly in size towards the E face. There are several lithic clasts of dark fine-grained material (L1) up to 5 mm across and a few millimeter sized clasts of troctolitic material (L2).

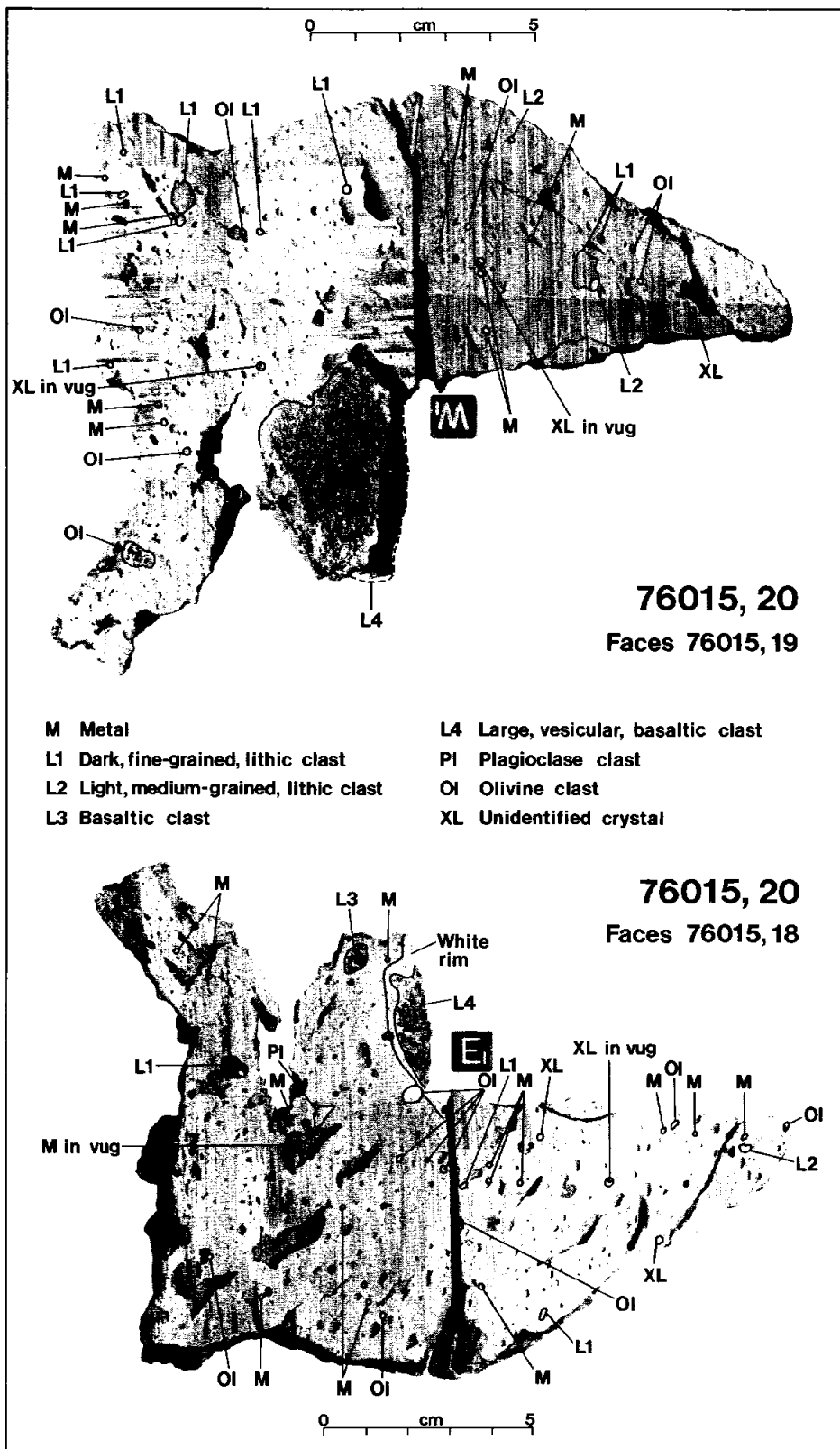
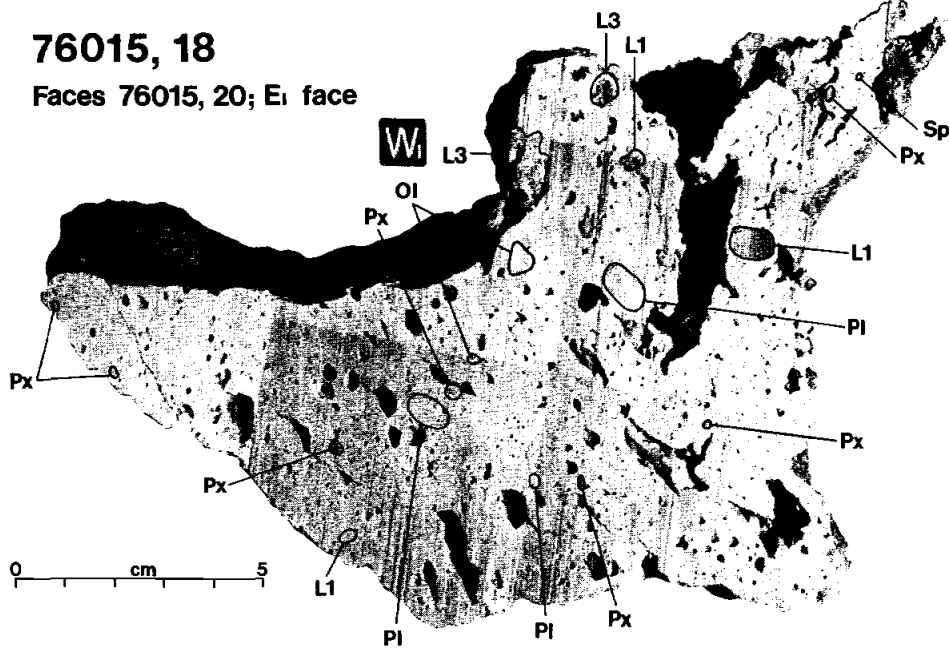


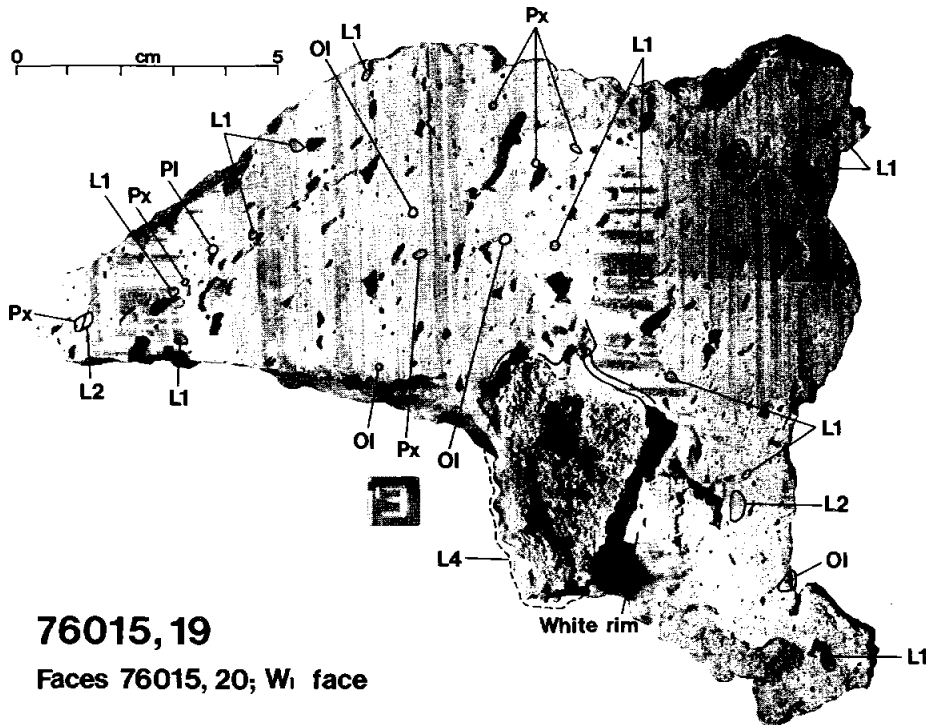
FIGURE 15: Lithologic maps of the two faces on slab 76015,20. Note that the large vesicular, basaltic clast thins significantly from the W to E sides.

76015, 18

Faces 76015, 20; E_i face



- | | |
|--|----------------------|
| L1 Dark, fine-grained, lithic clast | Pl Plagioclase clast |
| L2 Light, medium-grained, lithic clast | Px Pyroxene clast |
| L3 Basaltic clast | OI Olivine clast |
| L4 Large, vesicular, basaltic clast | Sp Pink spinel clast |



76015, 19

Faces 76015, 20; W_i face

FIGURE 16: Lithologic maps of the faces opposing the slab faces of Figure 15.



FIGURE 17: Reconstruction of slab 76015,20 showing the various fragments as prepared for distribution.

76215 - Unit B - Figs. 18, 19, 20

A crude foliation is defined in the slab by the alignment of rounded 5 mm vesicles and the long dimensions of several cavities including one that makes up most of one side on the E face of the slab. There are two matrix textures: unit 1 is a bit more porous, or at least has larger vesicles, and shows more mottling than unit 2. The mottling is a result of development of oikocrysts in unit 1. The contact between the two units is reasonably sharp but very irregular in shape. Petrographic studies indicate an ophitic texture for unit 2 and a poikilitic texture for unit 1. The two textures apparently represent variations within one matrix. Clasts appear to be primarily millimeter-sized mineral grains of olivine and plagioclase with a few more present in the poikilitic unit than in the ophitic unit. The overall occurrence of clasts is very sparse.

76255 - Unit C and large clast - Fig. 21, 22, 23

This sample was taken across the contact between unit C and a large clast. The sample contains mostly crushed material from the clast but from the maps of the sawn surfaces and the descriptions of the five mapped units it is seen that the contact zone may be mixed and more than one clast type occurs.

Unit 1 is medium-dark-gray crystalline breccia with a matrix of less than 0.1 mm grain size. The only resolvable materials under the binocular microscope are two clast types: a fine grained black material and a honey colored mafic mineral similar to that found in unit 4. There are no visible pores. This unit is in sharp contact with unit 2 and appears to be a mixed unit like unit 3 but unit 1 contains a higher proportion of unit 2 than does unit 3.

Unit 2 is a dark gray, fine grained, crystalline breccia similar to the more typical matrix of unit C. Clasts consist of white feldspar and very few honey-colored mafic minerals. There are rare 1 millimeter-sized pores. The contact with unit 3

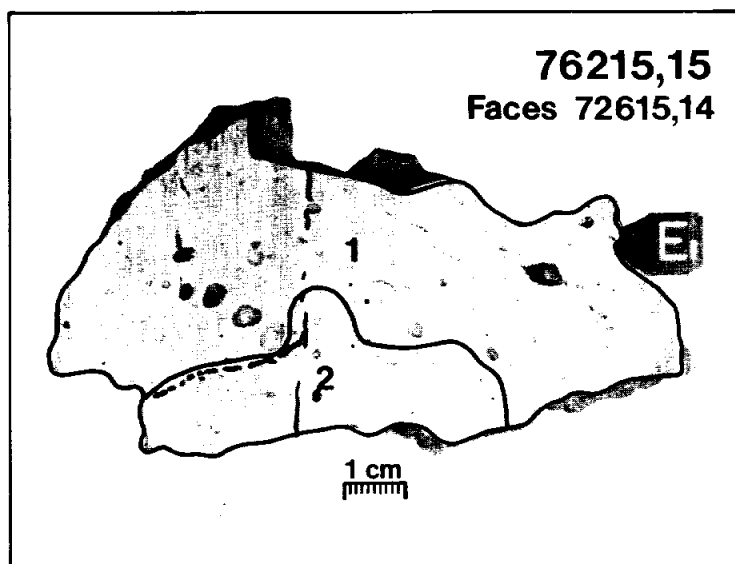
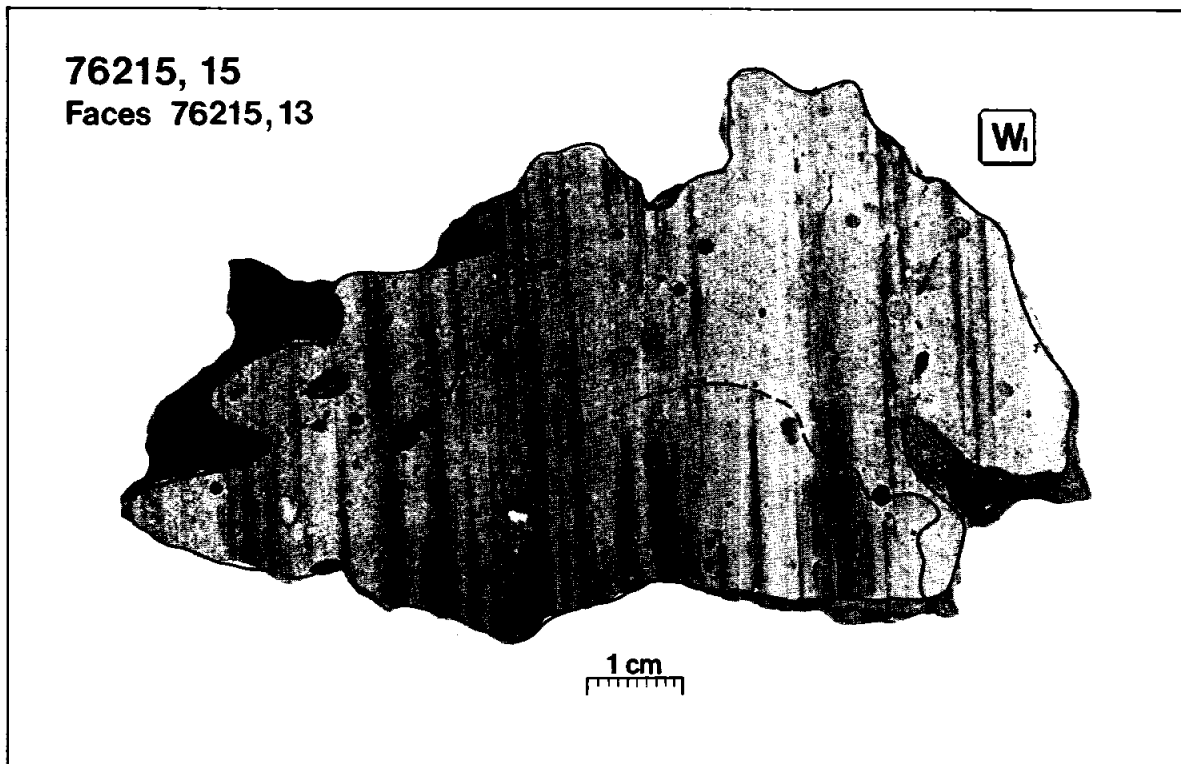


FIGURE 18: Lithologic maps of the two faces on slab 76215,15. See Figure 19 and the text for descriptions of map units.

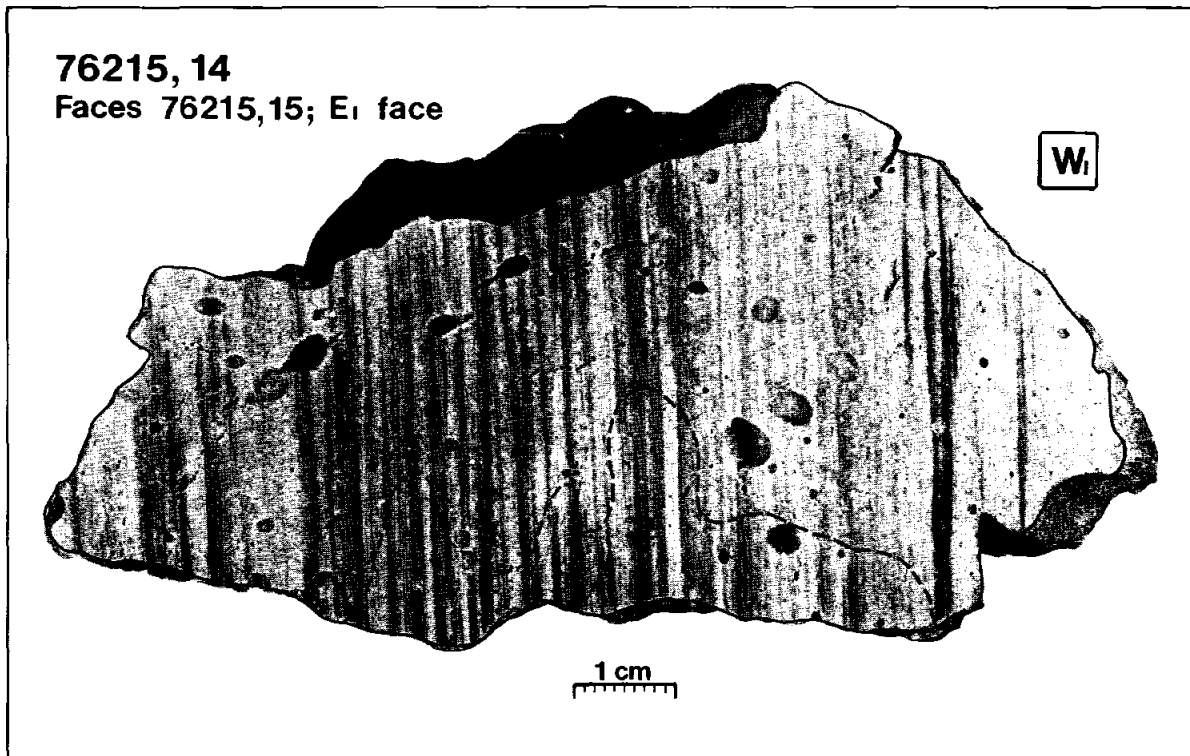
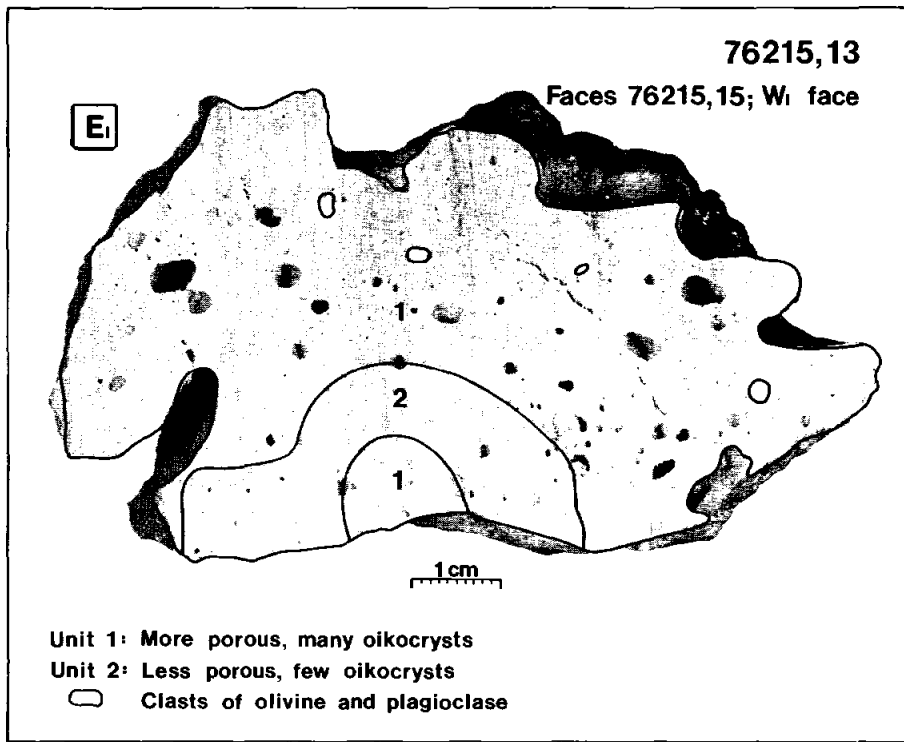


FIGURE 19: Lithologic maps of the faces opposing the slab faces of Figure 18.

76215, SLAB RECONSTRUCTION

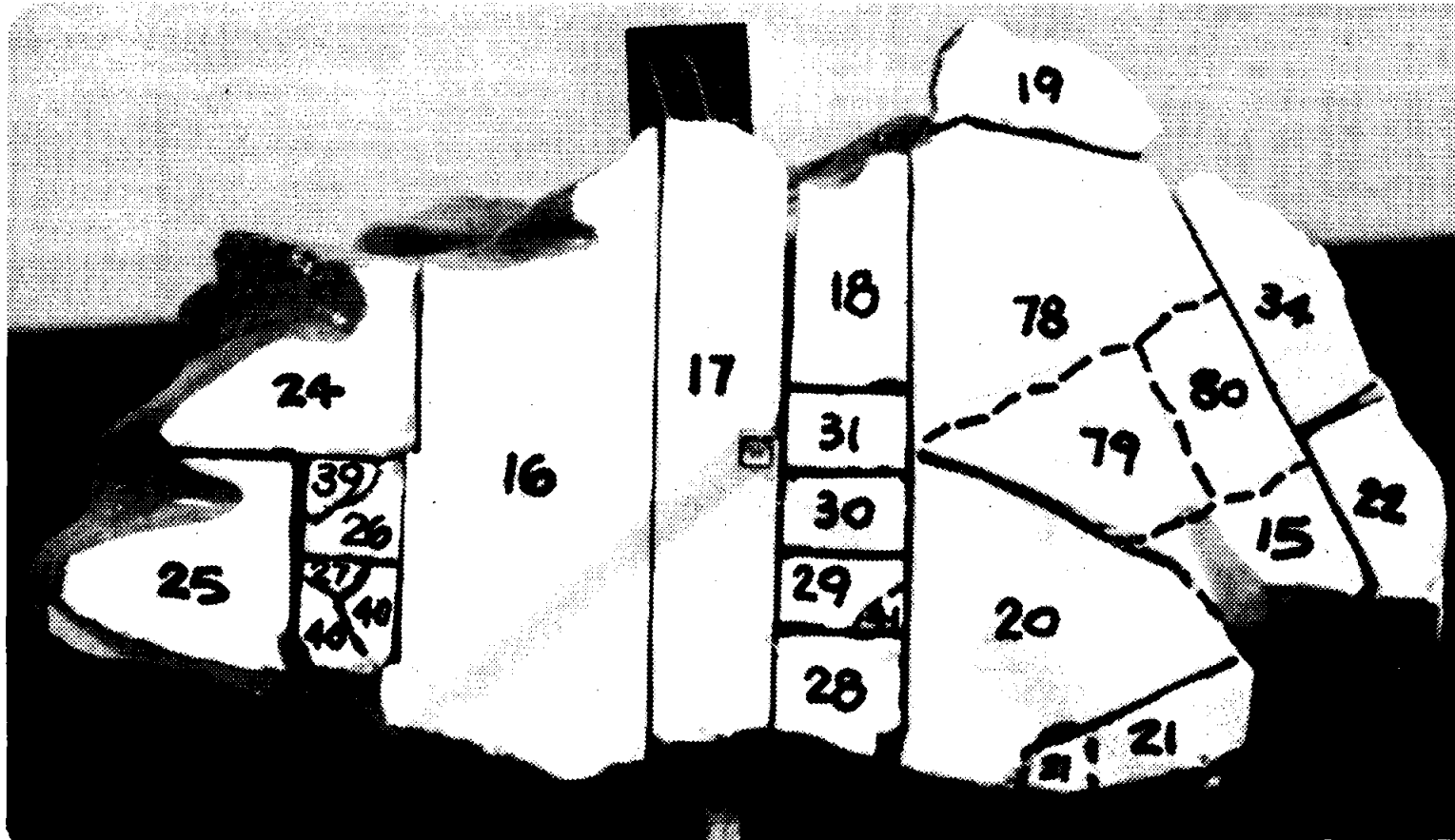


FIGURE 20: Reconstruction of slab 76215,15 showing the various fragments as prepared for distribution.

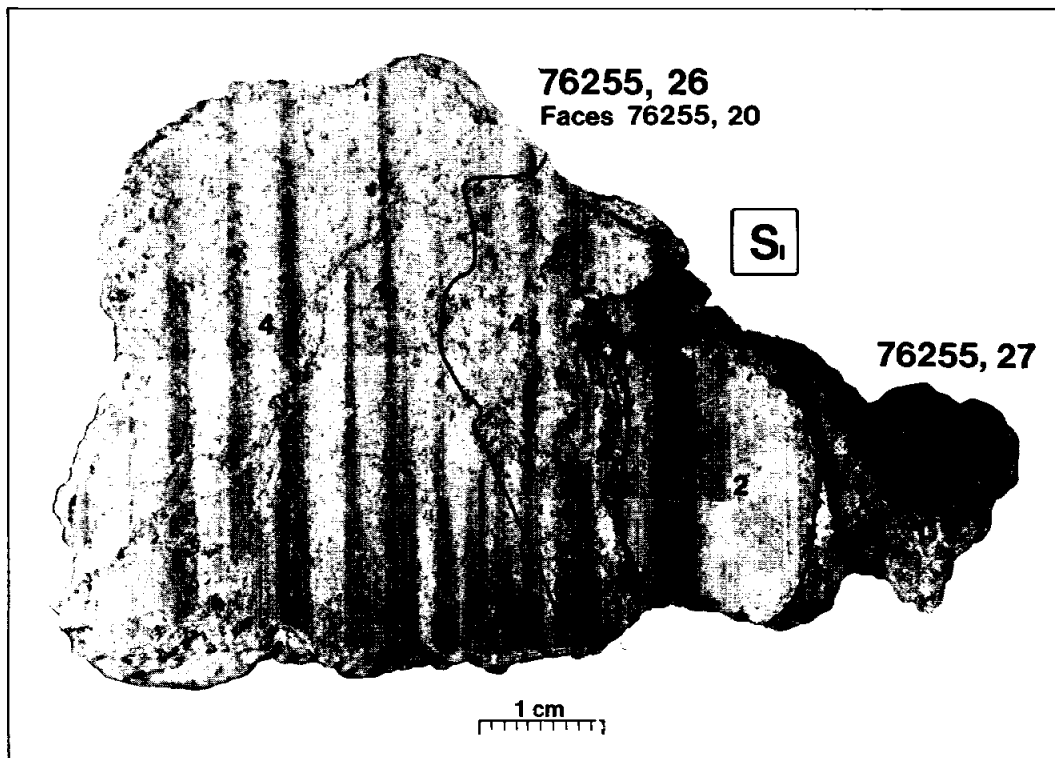
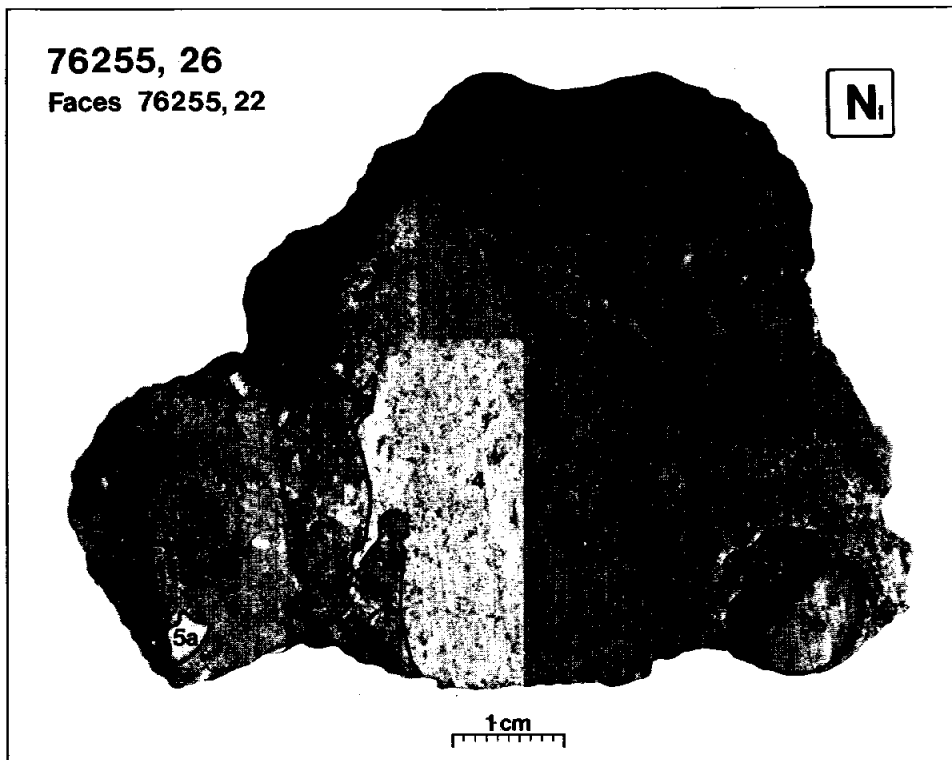
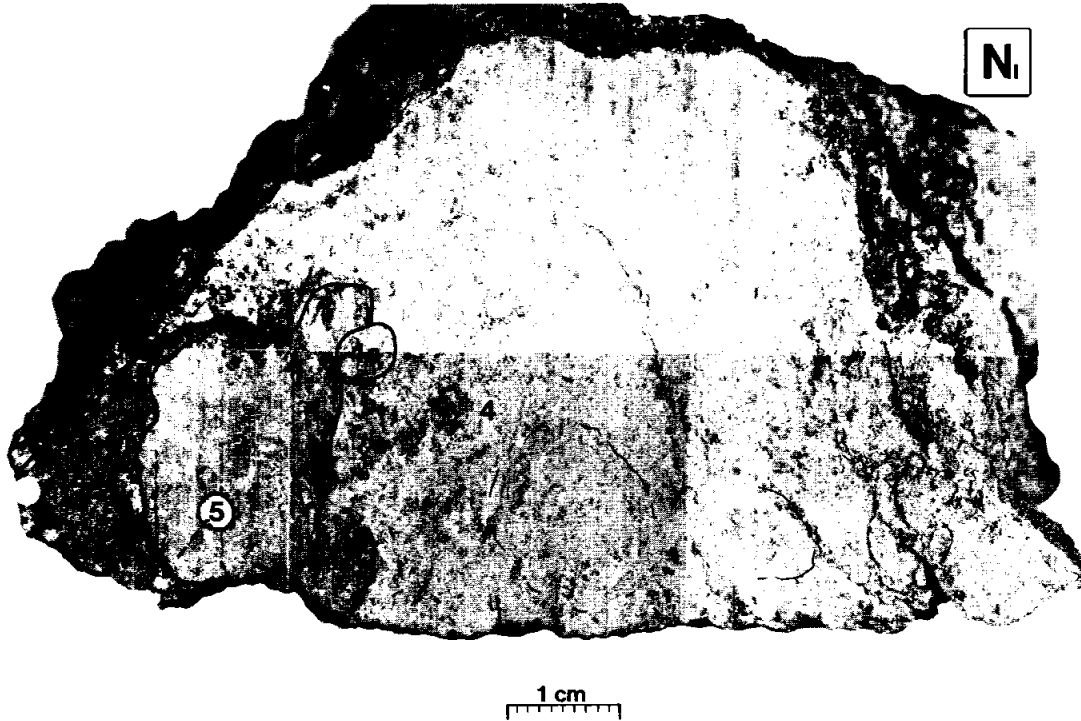


FIGURE 21: Lithologic maps of the two faces on slab 76255,26. See text for descriptions of map units.

76255, 20

Faces 76255, 26; S_i face



76255, 22

Faces 76255, 26; N_i face

S_i

76255, 23

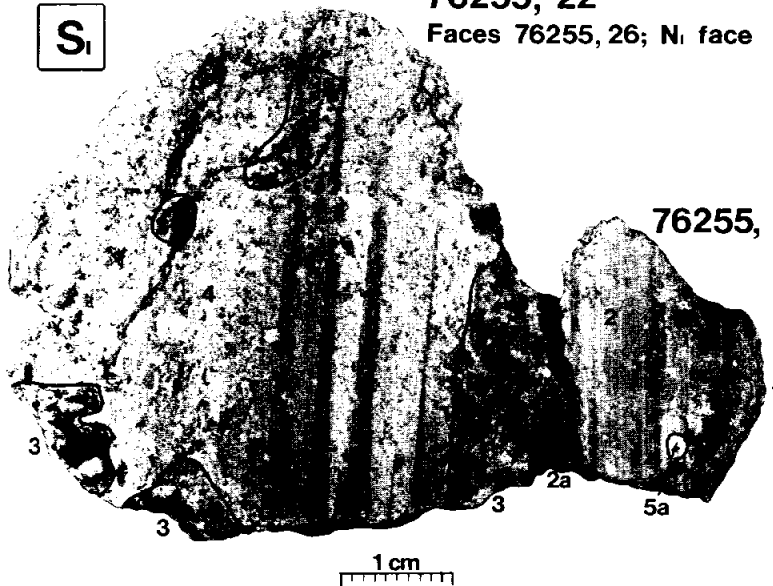


FIGURE 22: Lithologic maps of the faces opposing the slab faces of Figure 21.

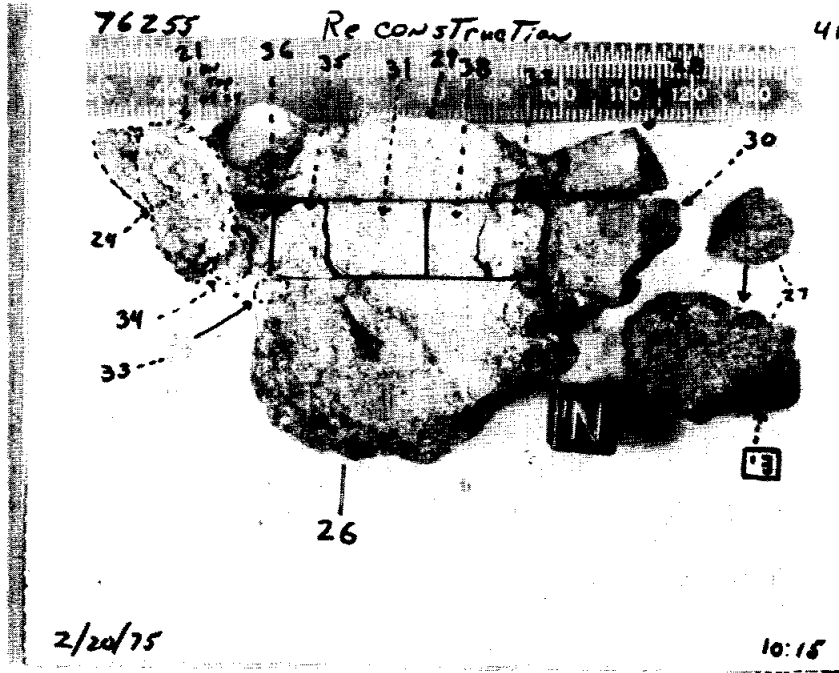


FIGURE 23: Reconstruction of slab 76255,26 showing the various fragments as prepared for distribution.

is quite irregular. A subunit, 2a, is found on the S_1 surface of 76255,22. It appears to be identical to 2 except for a distinct increase in the content of vugs some of which have minerals protruding into them. On the S_1 surface of 76255,26 and the N_1 surface of 76255,20 the clastic material seems to be more stringy or vein-like than on the other two mapped surfaces where the clasts are more discrete fragments. The vein-like appearance is reminiscent of 76275 and 76295.

Unit 3 contains isolated patches of unit 2 mixed with the brecciated clast of unit 4. The 3-dimensional relations are difficult to discern but it appears as though small dikes or apophyses of unit 2 have penetrated and permeated into the porous brecciated material of unit 4. Unit 3 is present on the N_1 face of 76255,26 and the S_1 face of 76255,22 but is practically nonexistent on the other two mapped surfaces.

Unit 4 is a massive clastic breccia (not a melt rock) with four major components: (1) White, very fine grained ($<50 \mu\text{m}$), sugary matrix that makes up 50% of the unit; (2) honey-brown, angular, mafic silicate clasts generally less than 1/4 mm make up 20%; (3) white, angular plagioclase clasts generally $<1/4$ mm make up 20%; and (4) black, irregularly shaped fragments of unit 2 1 mm and less in size, make up $<10\%$. A coarser-grained, more mafic subdivision, 4a, of this unit occurs on the S_1 surface of 76255,26 and the N_1 surface of 76255,20. Petrographically unit 4 has been described as a cataclastic norite (Ref. 11).

Unit 5 consists of a variety of light colored lithic clasts. 5a is a gabbro clast. 5b is a troctolite clast.

76275 - Unit C - Similar to 76295 as in Fig. 24, 25

This rock is essentially identical to 76295. No slab was cut; three notch cuts were made to obtain the three major types of material: the bluish-gray

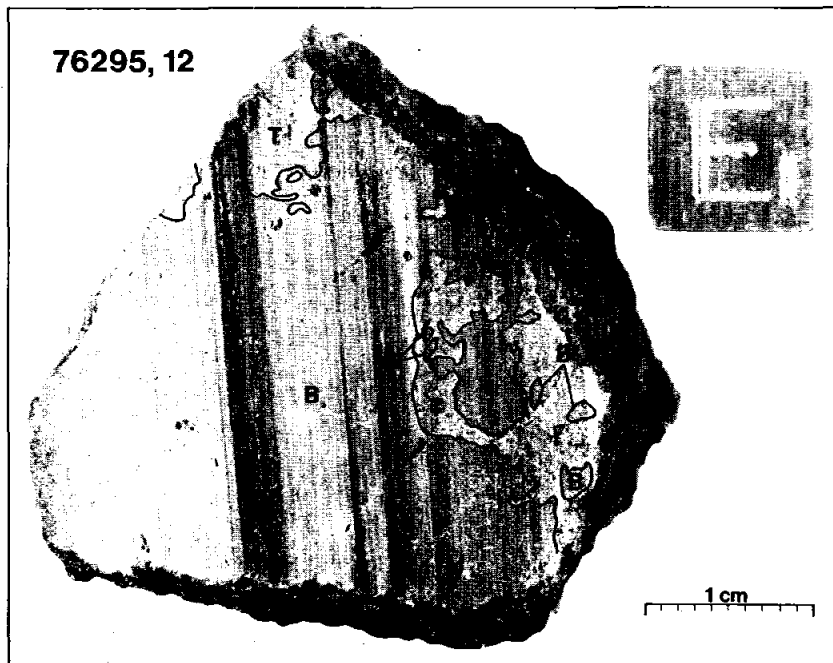
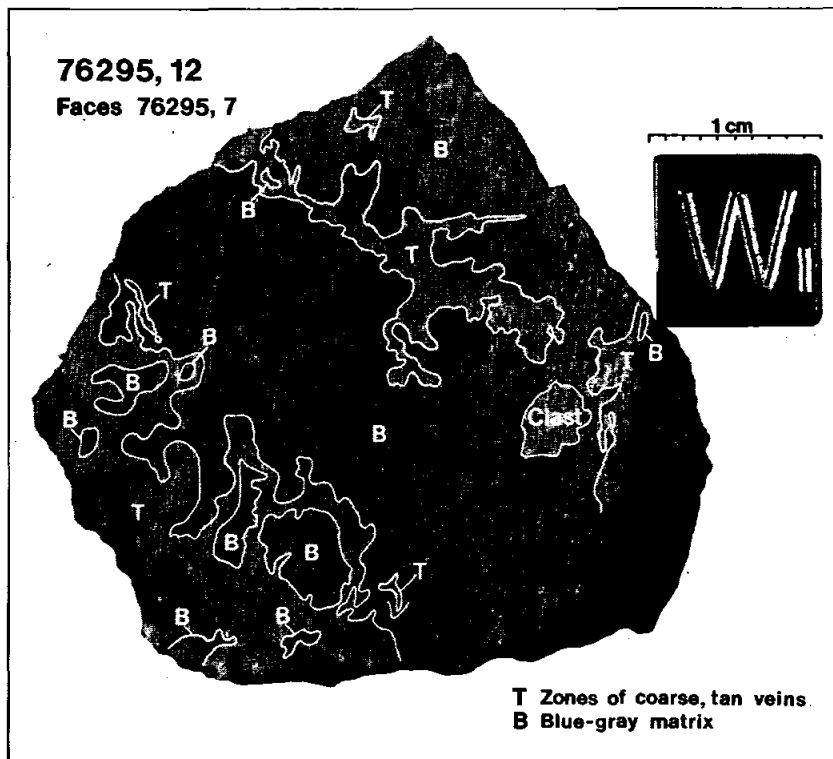


FIGURE 24: Lithologic maps of the two faces on slab 76295,12 showing the interfingers of coarse, light-colored, clast-rich veins in darker melt-rock.

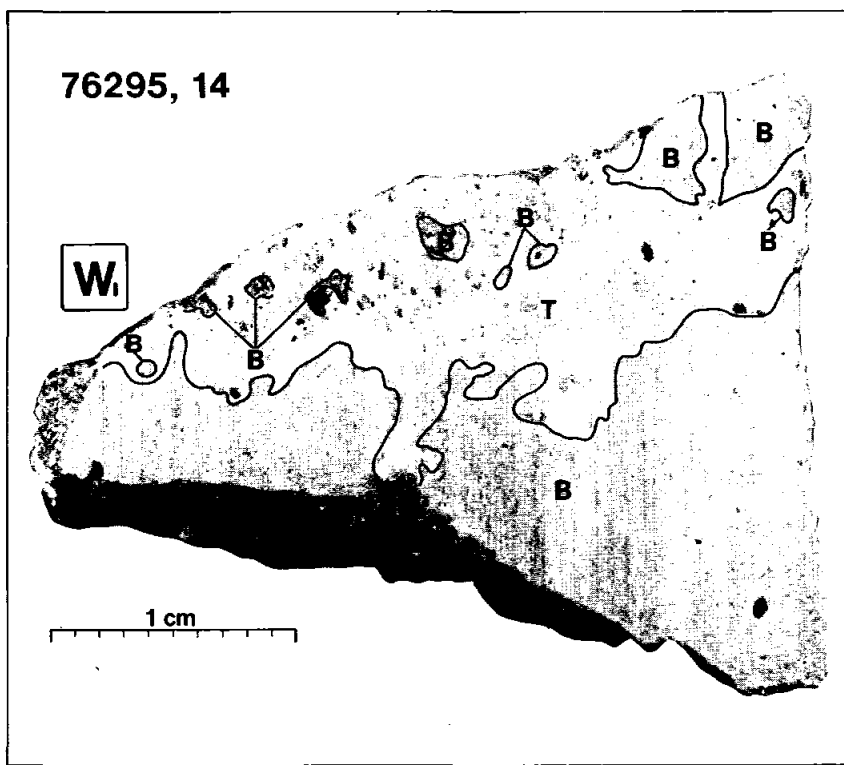
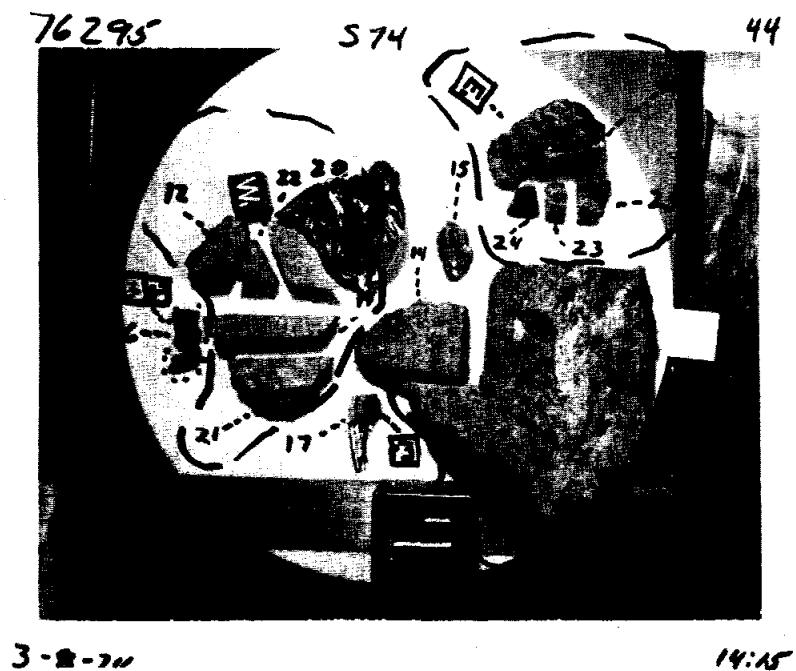


FIGURE 25: Lithologic map of a third face from 76295 and a reconstruction of slab 76295,12 showing fragments as prepared for distribution.

matrix, the tan, vein-like material, and a porous basaltic clast. All three materials are the same as found in 76295 which was studied in greater detail.

76295 - Unit C - Fig. 24, 25

A foliation is defined on the slab by trains of vesicles and, in a crude fashion, color variations. Most of the slab consists of matrix with a bluish-gray hue. Tan, more porous, coarser-grained material occurs throughout the slab as irregular vein-like masses up to a few millimeters across. The tan veins are less coherent than the remainder of the rock and serve as weak surfaces when the rock breaks, resulting in samples whose external surfaces display misleading proportions of tan material. Mineral clasts occur throughout the matrix. Although one lithic clast occurs in the slab several types were sampled throughout the rock including a dark gray type, light gray type, and a basaltic type that is rather porous and gives the impression of being vug-fillings. The basalt is similar to that found in 76015.

76315 - A-B Transition Unit - Fig. 26, 27, 28

A distinct foliation is defined in the slab by variations in matrix color and by trains of <1 mm vesicles throughout the matrix. Along one edge of the slab and parallel to the trend of foliation are white patches referred to as clast 1. Because this white material covers a large area on the external surface of the rock it was thought initially that the clast would extend throughout a larger volume than is the actual case. In fact it is only a 1 to 2 mm thick coating or rind and probably represents a brecciated clast that was squeezed along the direction of foliation in a vein-like fashion as in the case with similar material in 76275 and 76295. Such clastic veins serve as weak surfaces along which the rock is fractured easily when breaking off a specimen. The vein-like material then forms much of the exposed surface area suggesting a deceptively large estimate for the volume of such material.

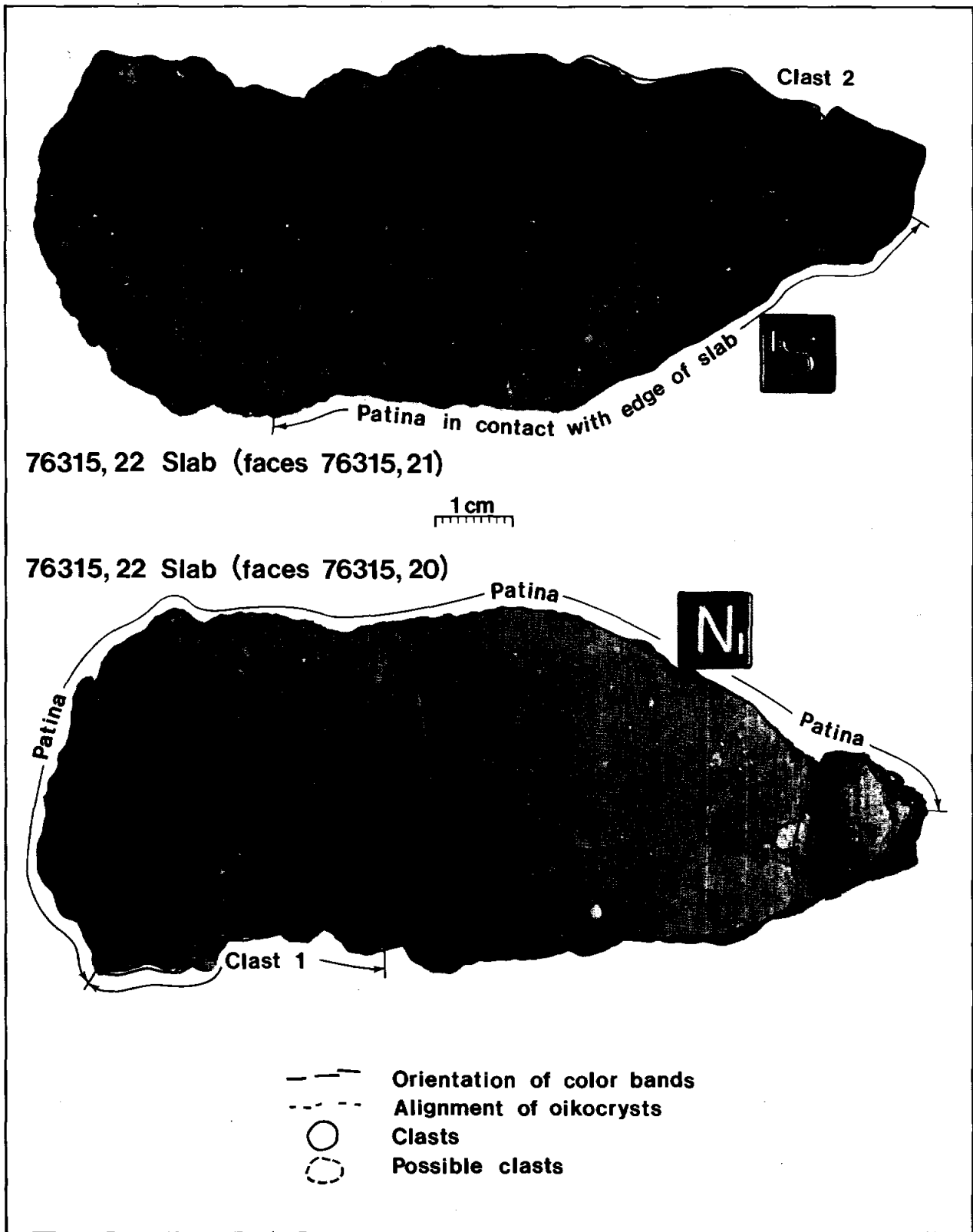


FIGURE 26: Lithologic maps of the two faces on slab 76315,22.

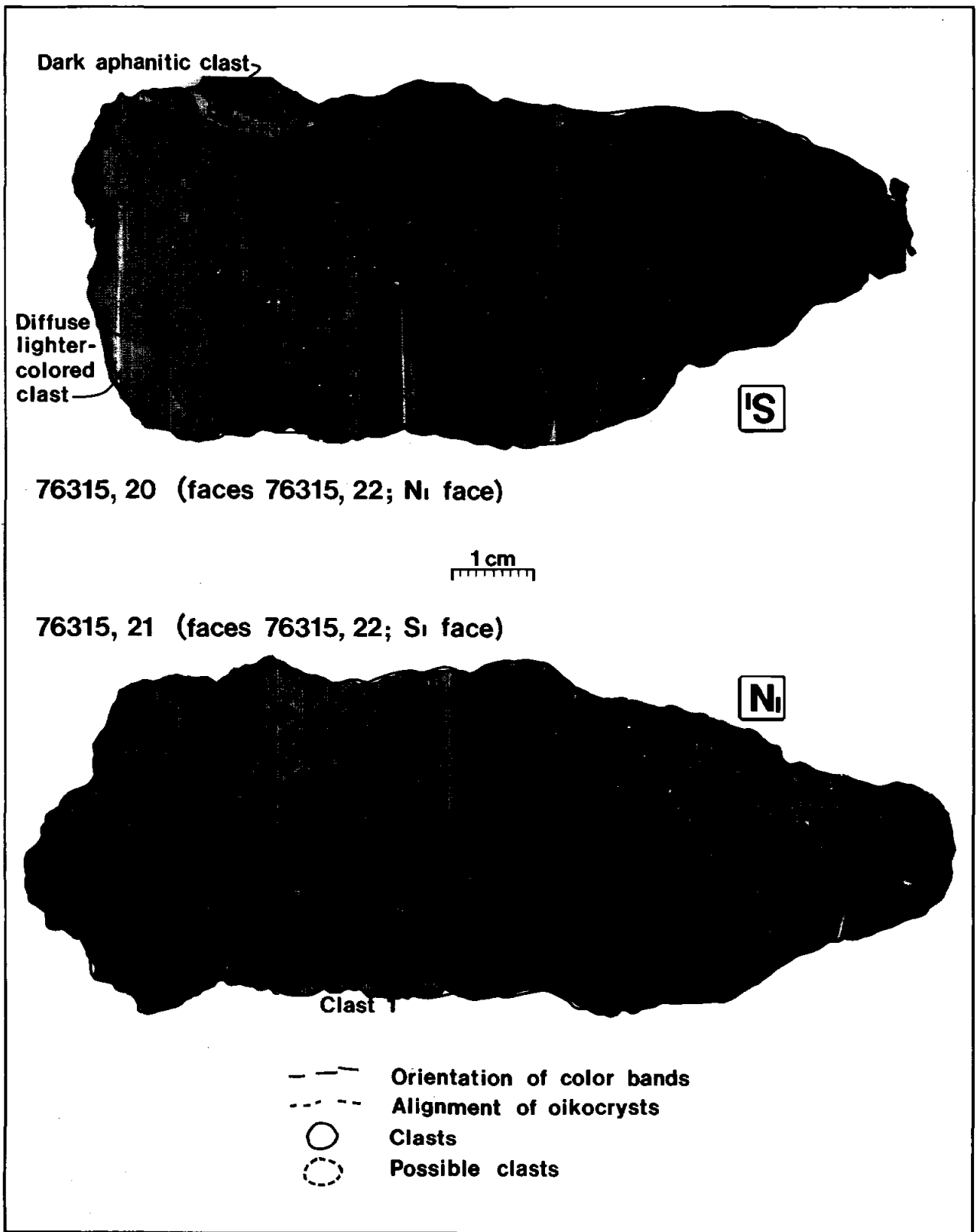


FIGURE 27: Lithologic maps of the faces opposing the slab faces of Figure 26.

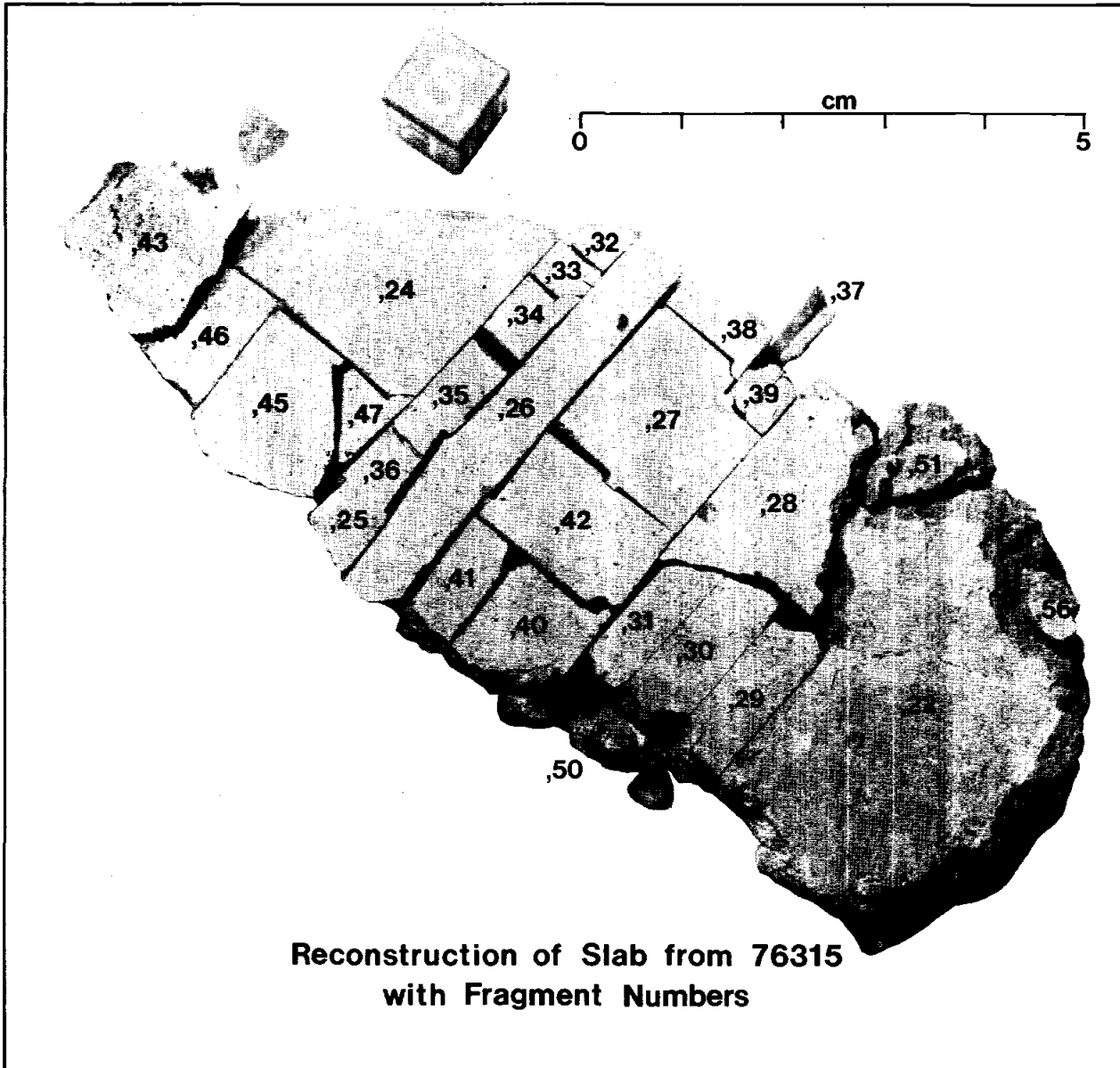


FIGURE 28: Reconstruction of slab 76315,22 showing the various fragments as prepared for distribution.

Table 1: Allocations

<u>76015</u> (2819 gms) Unit B		
Anders	,77	matrix
Bogard	,60	matrix
	,61	matrix
	,71	porous clast
Smyth-Brett	,63	green euhedral crystals from vug
Gibson	,32	matrix
	,58	matrix
	,59	matrix
	,65	matrix
	,70	porous clast
Rhodes-Nyquist-Hubbard	,22	matrix
	,37	matrix
	,41	matrix
	,64	matrix
	,68	porous clast
Morrison	,23	} chips along surface of interior fracture extending to surface
	,25	
	,26	
	,27	
	,34	
	,35	} two halves of a vug on exposed surface
	,24	
	,40	} exposed end of track column from freshly spalled crater surface
	,28	
	,66	
Silver	,53	matrix
Strangway	,28	porous clast
	,29	matrix
	,30	matrix
	,33	matrix
	,48	matrix
	,50	porous clast and matrix
	,69	porous clast

Table 1 (continued)

76015 (continued)

Turner	,36	matrix near surface
	,38	matrix a few centimeters deep
Walker	,39	matrix for noble gas study
	,67	porous clast for noble gas study
	,29	matrix for track column
	,30	matrix for track column
	,23	} same as Morrison, to Walker after Morrison finishes
	,24	
	,25	
	,26	
	,27	
	,28	
	,34	
	,35	
	,40	
	,66	
Clanton	,81	
McKay	,84	crystals in vugs
Phinney	,1 ,8	matrix
	,3 ,13	matrix
	,4 ,15	porous clast
	,5 ,17	matrix
	,48 ,86	} matrix with small clast
	,48 ,87	
	,48 ,88	
	,48 ,89	
	,50 ,90	} contact of porous clast and matrix
	,50 ,91	
	,50 ,92	
	,50 ,93	
	,69 ,94	} porous clast and matrix
	,69 ,95	
	,69 ,96	
	,29 ,97	} matrix
	,29 ,98	
	,29 ,99	
	,29 ,100	

Table 1 (continued)

76015 (continued)

Phinney (cont'd)

,30 ,101	}	matrix
,30 ,102		
,30 ,103		
,28 ,108	}	across contact of porous clast and matrix
,28 ,109		
,28 ,110		

N.B. On the Phinney allocations, in the cases where there are two daughter numbers, the first is the chip and the second is the polished thin section. In the cases where there are three numbers, the first is the parent chip, the second is the daughter chip, and the third is the polished thin section.

Table 1 (continued)

76215 (642.8 gms) Unit B

Anders	,48	matrix
Bogard	,39	porous, mottled matrix
	,41	more massive matrix
Gibson	,26	porous, mottled matrix
	,29	more massive matrix
Rhodes- Hubbard- Nyquist	,27	porous, mottled matrix
	,28	more massive matrix
Morrison	,17	intermediately patinated surface at end of track column
	,19	surface with least patination along gradient
	,22	surface from fresh spall
	,23	same as 22
	,24	surface from most patinated area along gradient
	,34	surface from spall surface
	,38	same as 22
	,32	vug surface from E spall face
	,33	vug surface from W spall face
Silver	,47	matrix
Strangway	,17	
	,21	
	,40	
Turner	,30	matrix
Walker	,17	track column
	,31	matrix for Kr age
	,19	} to Walker after completion by Morrison
	,22	
	,23	
	,24	
	,34	
	,38	
	,32	
	,33	

Table 1 (continued)

76215 (Continued)

Phinney

,3 ,8		matrix
,4 ,10		matrix
,5 ,12		matrix
,17 ,55		more massive matrix
,17 ,56		more massive matrix
,21 ,57	}	more massive matrix
,21 ,58		
,21 ,59		
,21 ,60		
,40 ,62	}	porous, mottled matrix
,40 ,63		
,17 ,53 ,67		porous, mottled matrix
,17 ,53 ,68		porous, mottled matrix
,19 ,69 ,70		coarse clast
,19 ,69 ,71		coarse clast

Table 1 (continued)

76235 (26.56 gms) Clast in Unit C

Anders	,9
Bogard	,2
Gibson	,8
Phinney	,4
Silver	,7
Strangway	,4
Turner	,3
Walker	,13

76235 through 76239 and 76305 through 76307 provide a total of about 80 gms of chips all derived from one large clast. All of 76235 is a cataclastic anorthositic norite clast from Unit C of the boulder. Samples 76275 and 76295 are matrix samples of Unit C.

76230 (Residue of 76235)

Hubbard- Rhodes	,4
Phinney	,3 ,12

Table 1 (continued)

76255 (393.2 gms) Clast in Unit C

Anders	,47	Unit 2, gray crystalline breccia melt rock, matrix
	,52	Unit 1, breccia
	,56	Unit 4, clastic breccia
	,57	Unit 5, white clast
Bogard	,39	Unit 4
	,48	Unit 2
	,53	Unit 1
Gibson	,36	Unit 4
	,45	Unit 2
	,54	Unit 1
Haskin	,58	Unit 5
Hörz	,25	Zap pit
Phinney	,28 (77, 78)	Unit 2
	,29 (68, 69, 70)	Unit 3, 4, 4a
	,62 (74, 75, 76)	Unit 4, 5
	,50 (71, 72, 73)	Unit 1 + gabbro clast
	,61	Unit 4
Rhodes	,38	Unit 4a
Hubbard	,44	Unit 2
Nyquist	,51	Unit 1
	,55	Unit 4
Silver	,60	Unit 4
Strangway	,28	See Phinney
	,29	" "
	,62	" "
Turney	,42	Unit 4
	,56	Unit 2
Walker	,35	Unit 4
Takeda	,61	Unit 4 pyroxene crystals

76250

Phinney	,3 (4 and 5)	2 fragments from residue in bag
Takeda	,5	

Table 1 (continued)

76275 (55.9 gms) Unit C

Anders	,23	tan breccia
	,33	vesicular clast
	,36	blue-gray breccia
Hubbard	,24	tan
Nyquist	,32	vesicular clast
	,38	blue-gray
Turner	,34	vesicular clast
	,39	blue-gray
Strangway	,12	vesicular clast + matrix
Phinney	,12 (54, 55, 56, 57, 58)	vesicular clast + matrix
	,21 (44, 45)	tan
	,37 (48, 49)	blue gray

Table 1 (continued)

76295 (260.7 gms) Unit C

Anders	,31	light gray clast
	,34	tan matrix
	,37	blue matrix
	,49	basaltic vug
	,52	dark gray clast
Bogard	, ⁵ ,36	tan matrix
	,39	blue matrix
Gibson	,40	blue matrix
Haskin	,30	light gray clast
	,35	tan matrix
	,48	basaltic vug
	,51	dark gray clast
Rhodes- Hubbard- Nyquist	,14	blue matrix
	,46	basaltic vug
Silver	,28	blue and tan matrix
Strangway	,19	track column
	,43	tan matrix
	,32	light gray clast and tan matrix
	,38	blue matrix
	,45	basaltic vug
	,50	dark gray clast
Turner	,29	blue matrix
	,41	blue matrix
Walker	,19	track column
	,53	blue matrix for Kr age
Phinney	,1 ,11	blue matrix
	,2 ,13	blue and tan matrices
	,19 ,78	blue and tan matrices
	,32 ,79	light gray clast and tan matrix
	,32 ,80	light gray clast and tan matrix
	,38 ,81	blue matrix
	,38 ,82	blue matrix
	,43 ,83	tan matrix
,43 ,84	tan matrix	

Table 1 (continued)

76295 (Continued)

Phinney	,45 ,85	basaltic vug
	,45 ,86	basaltic vug
	,50 ,87	dark gray clast
	,50 ,88	dark gray clast
	,43 ,74 ,89	tan matrix
	,43 ,74 ,90	tan matrix
	,19 ,91	blue and tan matrices

Table 1 (continued)

76315 (669.2 gms) Unit A-B

Anders	,73		matrix
	,74		dark, smeared-out clast
Bogard	, ^b ,34		matrix
	,63		light gray clast
	,66		dark, smeared-out clast
Hubbard-Nyquist-Rhodes	,2		
	,30		1/2 matrix and 1/2 dark, smeared-out clast
	,35		matrix
	,52		white rind
	,62		light gray clast
Gibson	,33		matrix
	,65		dark, smeared-out clast
Silver	,71		matrix
	,72		dark, smeared-out clast
Turner	,36		matrix
	,61		1/2 matrix and 1/2 light gray clast
	,67		dark, smeared-out clast
Walker	,41		matrix and dark, smeared-out clast for Kr age
	,26		track column
Strangway	,26	,104	matrix
		,105	matrix
	,29		contact of matrix and dark, smeared-out clast
	,46	,60	contact of light clast and matrix
Phinney	,1	,12	matrix plus some dark, smeared-out clast
	,3	,14	white rind
	,4	,16	
	,29	,90	
	,29	,91	} orthogonal of dark, smeared-out clast and matrix
	,29	,92	
	,46	,96	
	,60	,98	} fragments of white rind
	,60	,99	
	,60	,100	
	,26	,105	,108
,26	,104	,111	matrix

A light gray clast designated clast 2 has an intercept of 1/2 cm by 2 cm on the S face of the slab and enlarges slightly towards the N face. Both clast 1 and clast 2 are anorthositic gabbros but clast 1 has a granulitic texture and clast 2 is poikilitic. Most of the matrix is medium gray but within it there are several smeared out, darker gray areas referred to originally as clast 3. There do not appear to be any significant differences chemically or petrographically between the dark gray material of clast 3 and the typical matrix. There are several mineral and lithic clasts of about 1 mm diameter throughout the slab surface but they make up only a few percent of the exposed surface.

Detailed Studies

Petrography

Detailed petrographic studies of the boulder samples were completed (Refs. 4 and 11) and provided the impetus for detailed studies of impact melt sheets in terrestrial impact craters (Ref. 25 and the first 8 papers in Jour. Geophys. Res. for June 1978, vol. 83, p. 2729-2816). In general the boulder consists of 4 units (A, B, C, and the A-B transition), 3 of which were sampled; all are similar, consisting of crystalline matrix polymict breccias of the type that have been interpreted as impact melts. The breccia matrices are fine-grained, noritic in composition, and consist of about 50% calcic plagioclase, 45% low-Ca pyroxene, 3% olivine and 1% ilmenite. Chemical analyses of sample matrices display very minor variations between boulder units. The breccias from these units contain angular to subrounded mineral and lithic clasts. The two most widely spaced units both contain clasts of a porous, almost vuggy coarse-grained basalt consisting of abundant augite in addition to orthopyroxene, plagioclase, olivine, and distinctive, radially-aligned K-feldspar intergrowths located at margins of the plagioclase and pyroxene crystals. The presence of this unique

clast type in two widely separated units, combined with the similar textures, mineralogy and chemistry of all units suggests that the section represented in this boulder is the product of a single impact event.

The sequence of matrix textures and clast populations may be explained in terms of a model in which superheated impact melt is mechanically mixed with cold clasts and deposited between masses of cold fragmental debris.

76275 and 76295 - Unit C

According to the above model unit C forms the base of the sequence. The unit is mainly massive and dark gray with vesicles that are all less than 5 cm across. A network of porous, clast-rich, tan veins criss-crosses the dark gray material (Fig. 29). These samples have the finest-grained matrices and a subophitic texture; plagioclase laths are less than 20 μm long and individual pyroxene crystals enclose only a few plagioclase crystals. Within separate 5 mm^2 areas of 76295 over half the matrix, pyroxenes define tight compositional clusters ($\text{Wo}_{3-5}\text{En}_{60-74}\text{Fs}_{23-31}$), with differences in the cluster-centers all within the area of 3-5% En. The remaining matrix pyroxenes are low-Ca (total range $\text{Wo}_{3-9}\text{En}_{63-75}\text{Fs}_{21-10}$) and augite. Plagioclase ranges from An_{80} to An_{97} with a peak at An_{85} . Olivine (Fo_{61-69}) forms small grains. Mineral clasts make up about 15% of the samples and include not only similar olivine and plagioclase as found in other impact-melt polymict breccias, but also abundant low- and high-Ca pyroxene. Most clasts in these rocks are concentrated within discrete, tan-colored bands that form a network with curving surfaces. All of these observations are consistent with very rapid chilling and crystallization of a clast-laden melt that did not have sufficient time to digest included pyroxene clasts.

76015 and 76215 - Unit B

Well-foliated and coarsely vesicular unit B is the next higher unit in the boulder stratigraphy. The samples are coarser-grained than those from unit A, and display a poikilitic matrix texture (Fig. 30). However, sporadic zones in 76215 have an

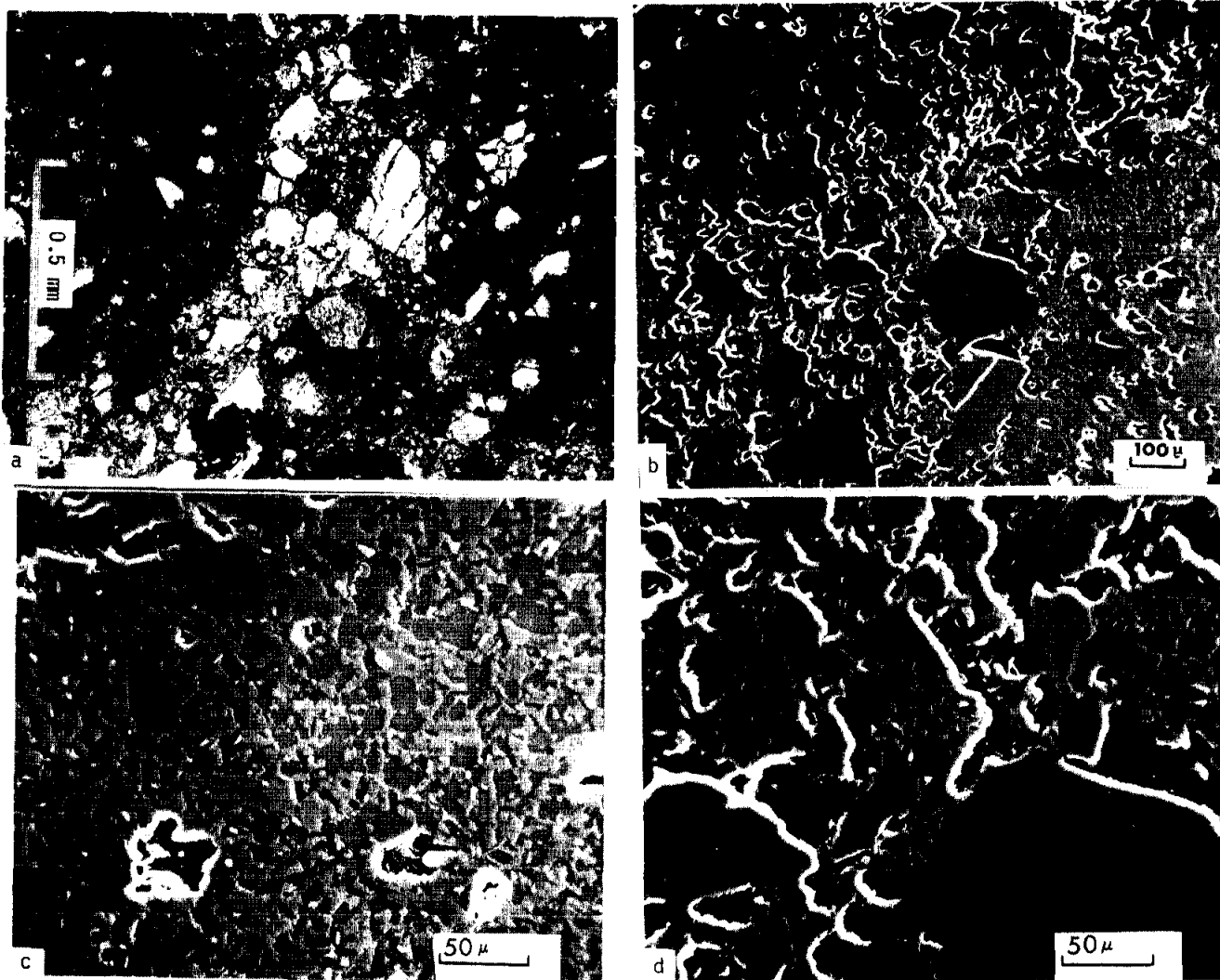


FIGURE 29: (a) General view (single polarizer) of 76295. Dark gray area is very fine-grained subophitic melt-rock. Lighter gray area is a porous, clast-rich, tan vein. Clasts consist of plagioclase, olivine and pyroxene. (b) SEM photo of ion-etched surface of 76295,79 showing a porous, clast-rich tan vein through the more massive subophitic matrix. Lightest gray shades in upper right are opaque minerals, medium gray are pyroxenes, gray are plagioclases, and irregular black patches with white rims are vugs and vesicles. (c) Further magnified SEM photo of subophitic texture in (b). Note the very fine grained opaque minerals scattered through the matrix and the euhedral, lathy nature of many plagioclase grains. (d) Further magnified SEM photo of porous vein in center of (b).

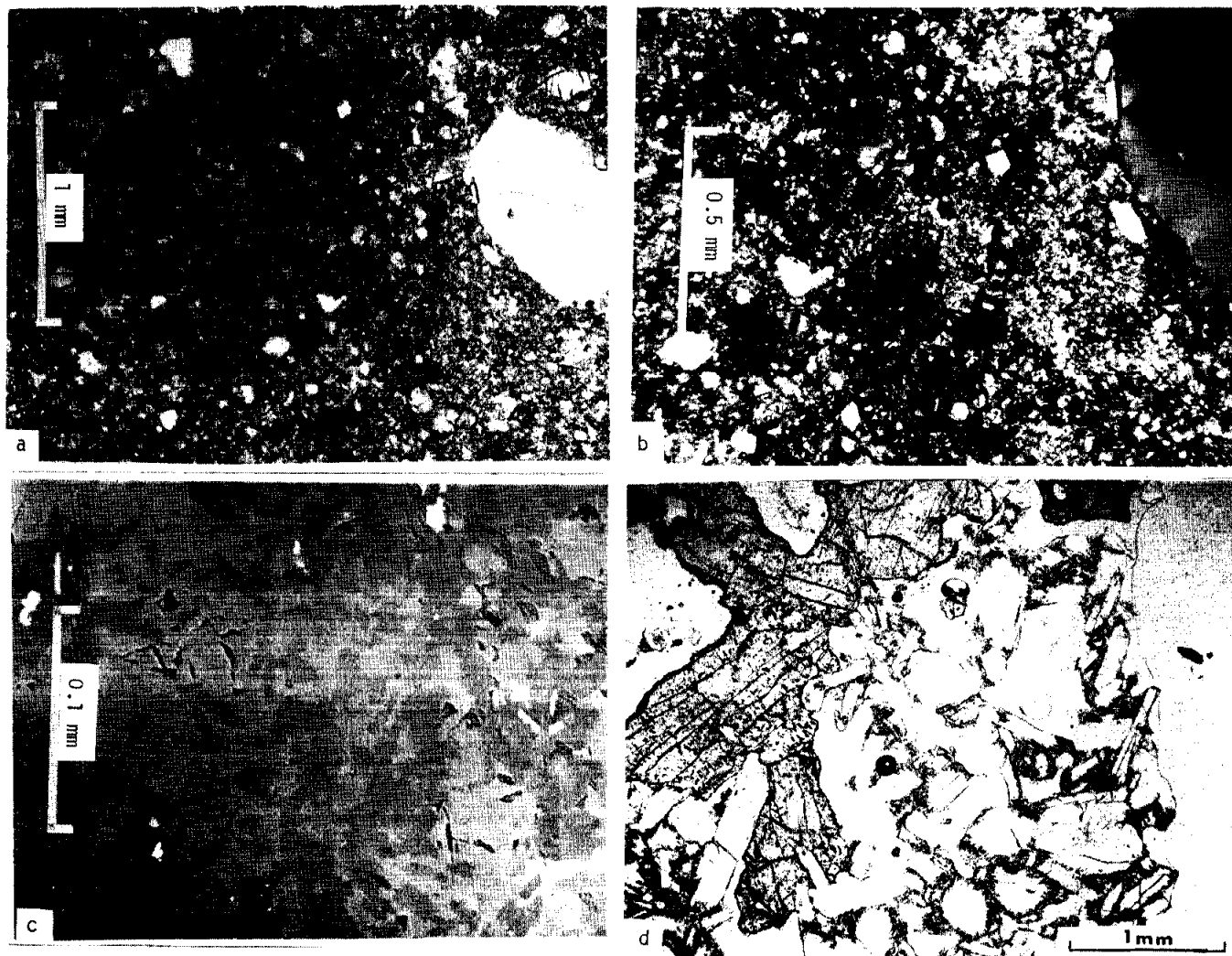


FIGURE 30: (a) General view (single polarizer) of poikilitic melt-rock 76015. The light colored clasts are plagioclase, the darker gray clasts are olivine. (b) Magnified view (crossed polarizers) of matrix in right center of (a) showing optically continuous oikocrysts at varying degrees of extinction. (c) Reflected light view of an oikocryst in 76015. Darkest gray mineral is plagioclase, commonly as euhedral laths; medium gray is pyroxene; white is ilmenite. Note the concentration of ilmenite and plagioclase around the oikocryst. (d) Porous basaltic clast in 76015,91. Large dark mineral is clinopyroxene, smaller white minerals, commonly lathy, are plagioclase with a small amount of fine-grained mesostasis (gray) in very porous surroundings.

ophitic texture that grades into the normal poikilitic regions (Fig. 31). Within the poikilitic regions the mineralogy is plagioclase (averaging An_{89}), orthopyroxene ($Wo_{4-6}En_{72-78}Fs_{17-24}$), minor Mg-rich augite, and little or no olivine. In contrast, the ophitic regions contain pigeonite ($Wo_{60-66}En_{67-76}Fs_{16-20}$) and abundant olivine (Fa_{26-31}). Individual 5 mm^2 areas in both rocks do not display differences in pyroxene compositions, except for the ophitic vs. poikilitic distinction. Mineral clasts are evenly distributed throughout the rocks. They consist of plagioclase (more calcic than in the matrix) and olivine (more magnesian than in the matrix). All of these observations are consistent with slow (relative to unit C) crystallization from a clast-laden melt. The slower crystallization rate allowed time for the melt to digest all but a trace of relic pyroxene and for the matrix pyroxenes to fractionate as they crystallized.

76315 - Contact Zone Between Units A and B

This sample comes from the transition unit between the poikilitic unit B and the most vesicular (unsampled) unit A. Both the contact unit A-B and sample 76315 are moderately foliated. The matrix texture of 76315 displays coarser-grained and more euhedral plagioclase and pyroxene crystals than unit C, and is finer-grained and less euhedral than unit B (Fig. 32). The composition of the matrix orthopyroxene is more magnesian than unit C and less magnesian than unit B. The clast population is intermediate in that there are a lower percentage of pyroxene clasts than in unit C, but a higher percentage than in unit B, and clast segregations such as are found in unit C are not found. These observations suggest that the thermal history is also intermediate, crystallizing less rapidly than unit C and more rapidly than unit B.

The range in textures in the boulder samples is similar to that observed in the much thicker melt sheets at Manicouagan, West Clearwater Lake, and Mistastin Lake Impact Craters in Canada. The base of all three sheets contains an abundance of

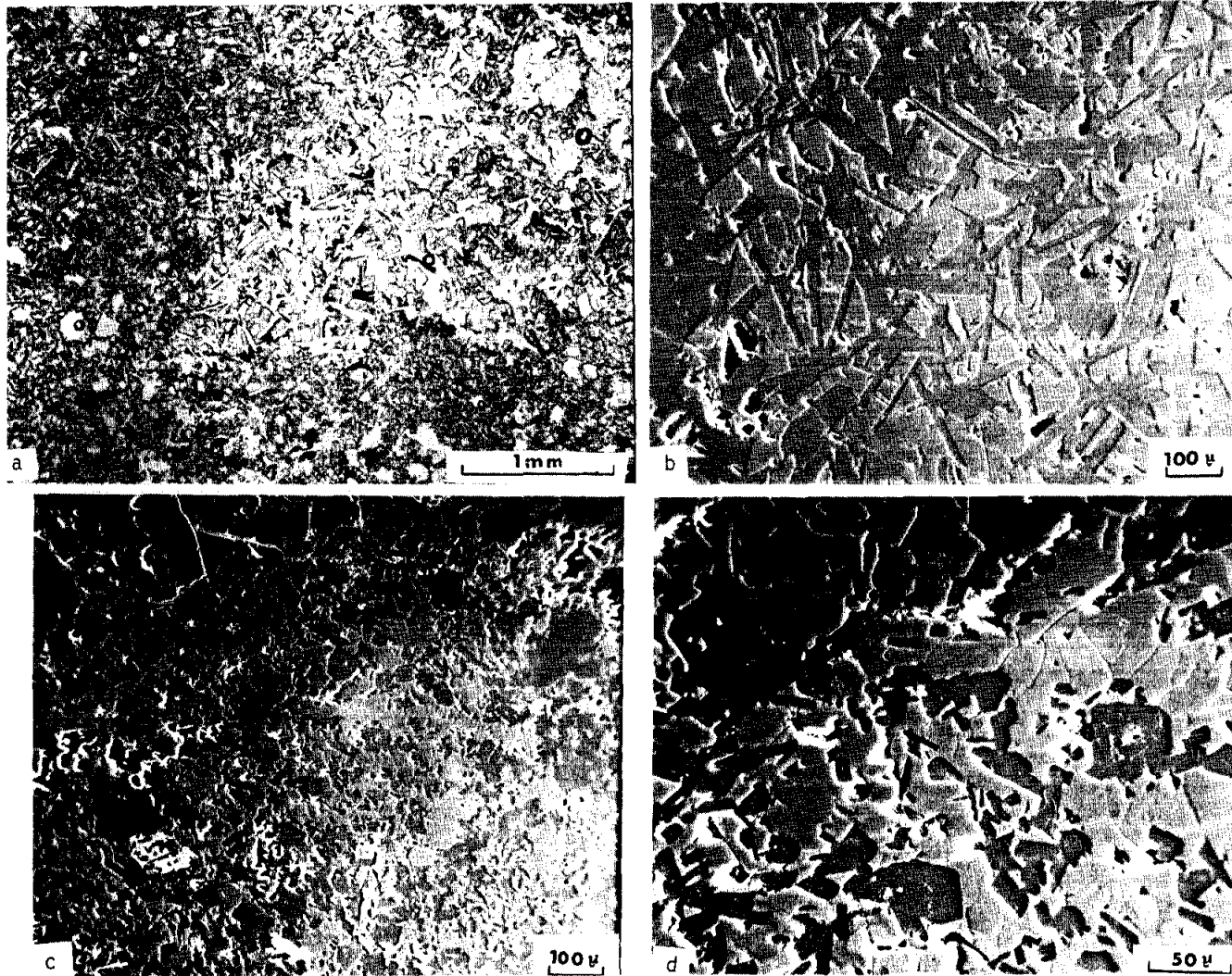


FIGURE 31: (a) General view (single polarizer) of a zone in 76215,60 where coarser grained ophitic texture interfingers with finer grained poikilitic texture. (b) SEM photo of ion-etched surface of 76215,57 showing coarse subophitic texture. Darker gray is plagioclase, mostly lathy; lighter gray is pyroxene. (c) SEM photo of poikilitic zone in 76215,67. One large oikocryst of pyroxene occurs in the center. Lightest gray minerals in lower left and lower center are opaque minerals that concentrate in zones outside the oikocrysts. (d) Further magnified view of part of oikocryst in center of (c).

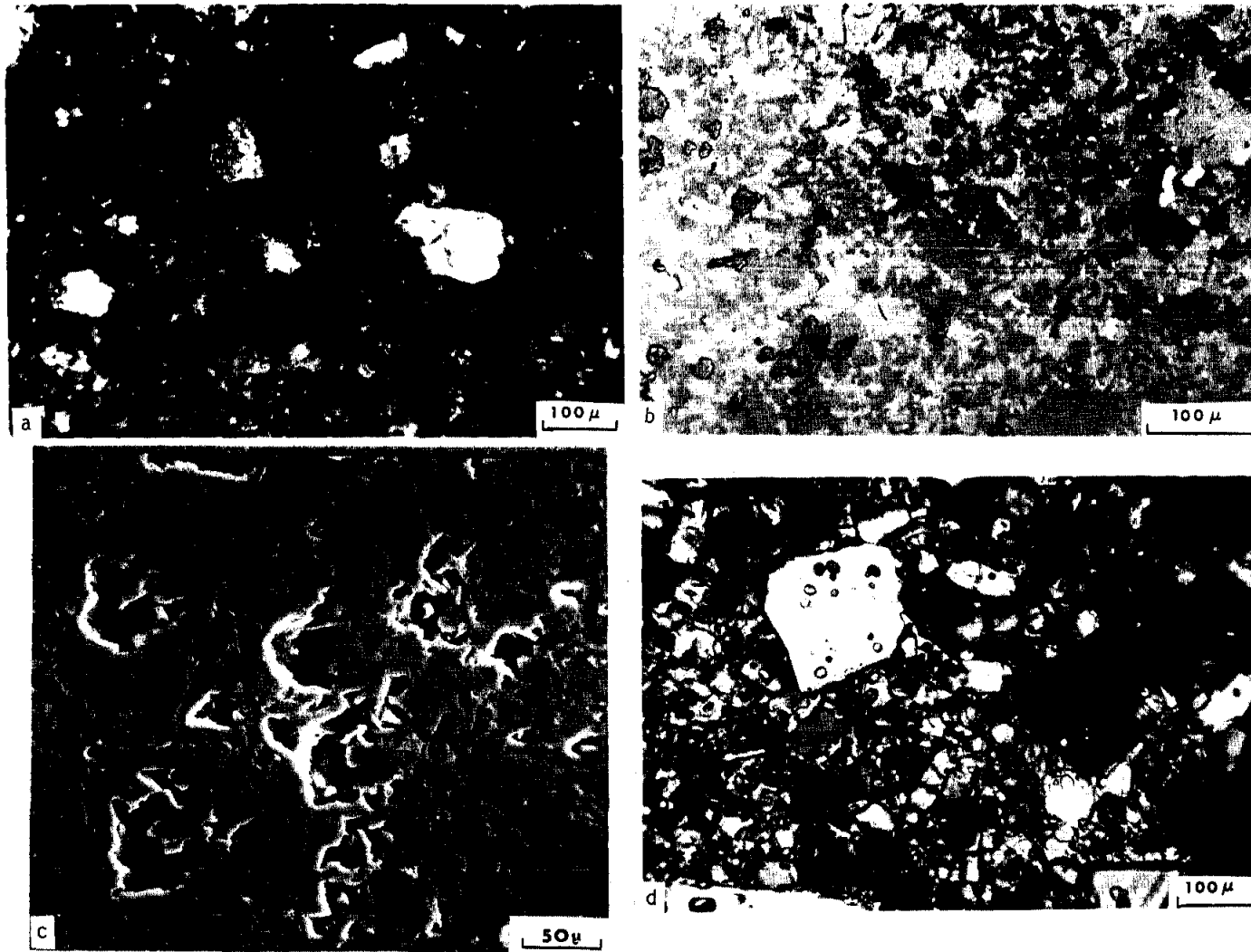


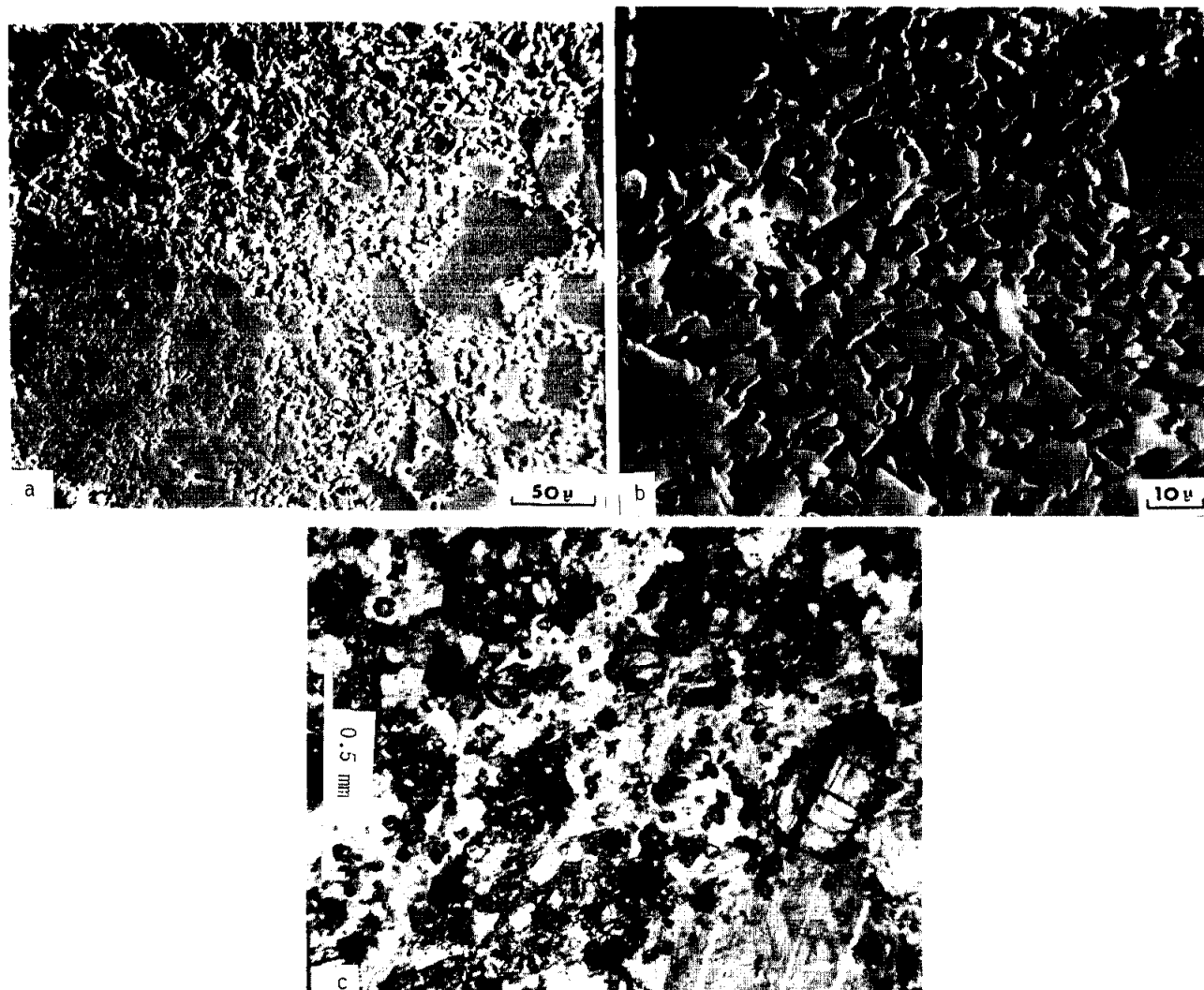
FIGURE 32: (a) General view (single polarizer) of 76315,92 showing fine-grained matrix and clasts. (b) Further magnified view of matrix in (a) showing subophitic texture. Dark gray minerals, commonly euhedral, are plagioclase; light gray minerals are pyroxene; and white minerals are ilmenite. Irregularly shaped gray areas with dark outlines are vugs. (c) SEM photo of ion-etched surface of subophitic matrix of 76315,111. Darker gray areas are plagioclase, commonly as euhedral laths; lighter gray areas are pyroxene; the few small white spots are ilmenite. One plagioclase clast at lower center contains several small olivine grains that form a crude triangular pattern. (d) General view (crossed polarizers) of granular, olivine-bearing, feldspathic norite that occurs as a light gray clast in 76315,96.

clasts of all mineral and lithic types and the matrix is very fine-grained with anhedral to subhedral feldspar. Higher in the section the texture is coarser feldspar is the dominant clast material. There is no doubt that even the basal units had the rheology of a liquid as they contain smooth bubble-like cavities and intrude both basement and clasts.

The loss of heat to material both surrounding and within the melt offers a partial explanation for the systematic variation in texture of both the terrestrial and lunar melt rocks. The more slowly cooled melts in both cases had time to digest the easily fused pyroxene and lithic clasts, whereas the more rapidly cooled units digested few clasts. In the terrestrial cases unshocked clasts were clearly colder than the melt as evidenced by chilled textures of melt-rock against the larger clasts at Manicouagan. The cool, included clasts which make up from 10 to 30% of the melt rocks form a significant thermal sink. Thus the cooling of initially superheated masses of impact melt to solidus temperatures can take place in a fraction of the time expected for the cooling of a slab of a normal igneous magma of identical thickness.

Clasts

Several clasts were examined. 76235 (or 76230) is an olivine bearing feldspathic norite containing equant plagioclase (An_{95-96}) with grain sizes ranging from 20 to 600 μm in poikilitic low-Ca pyroxene (Fig. 33c). The plagioclase lacks the polygonal outlines of a well-annealed rock. The light gray clast of 76315 has a similar mineral mode and texture. The white clast or rind of 76315 has similar mineralogy but has more polygonal plagioclase and lacks poikilitic pyroxene (Fig. 32d). 76255 is primarily a clast of cataclastic norite with some adhering matrix (Fig. 33a, b) of unit C (Ref. 11). The norite has been crushed to a seriate texture with grains ranging in size from 2 μm to over 2 mm. This clastic aggregate is permeated with sub-millimeter to centimeter pods and septa of the impact-melt matrix of unit C making clean separations of bulk norite samples difficult to impossible. The cataclastic norite contains plagioclase



62.

FIGURE 33: (a) SEM photo of ion-etch surface of fine grained matrix (Unit 2) of 76255,78 showing the clast-rich nature of even the finest grained part of the rock. Dark gray areas are mainly plagioclase; medium gray areas are mostly pyroxene with some olivine. (b) SEM photo of further magnified matrix in 76255,78. Note that the subophitic texture is less developed than in 76315 or 76295: The plagioclase is less euhedral. Some of the dark gray areas contain higher contents of potassium than occurs in the other rocks. (c) General view (partially crossed polarizers) of granular, olivine-bearing, feldspathic norite. Light colored grains are complexly twinned and laminated feldspar. The large feldspar clast in the lower right is a clast as is the olivine in the right center. The irregular dark gray patches are pyroxene oikocrysts and the smaller, isolated, lighter gray grains in plagioclase are olivine.

(An₈₇₋₈₈), pigeonite (Wo₈En₆₁Fs₃₁), and augite (Wo₃₇En₄₅Fs₁₇). Many of the pyroxenes display coarse exsolved lamellae (Fig. 34d) that are typical of slowly cooled plutonic rocks. The augite also contains a second set of much finer exsolution lamellae. Within the adhering matrix on 76255 are (1) a gabbro clast with oscillatory-zoned plagioclase tablets (An₈₂₋₈₉) and euhedral augite and interstitial pigeonite both of the latter having exsolution lamellae (Fig. 34b), (2) a troctolite clast with euhedral but shock metamorphosed plagioclase (An₉₅₋₉₆) and crushed olivine (Fo₈₉₋₉₀) (Fig. 34c) and (3) two basalt clasts whose mineralogy and texture display mare basalt affinities (Fig. 34d). In 76295 a dark gray and a light gray clast are subophitic and poikilitic melt rocks, respectively, quite similar to the melt rocks that form the matrices of the boulder. An unusual vuggy basaltic material occurs as a large clast in 76015 (Fig. 30d) and as 4 small clasts in 76295. Because of its high porosity this material, particularly the smaller clasts in 76295 appear to be to vug fillings: in fact the initial descriptions contained the term "basaltic vug." The basic texture of the material is that of an intersertal basalt but with pore space in place of mesostasis. Plagioclase occurs as subhedral grains up to 300 μm long with inclusions of pyroxene, K-feldspar, opques, and a silica phase concentrated at their rims. Small, 10 μm or less, euhedral plagioclase grains protrude into the pore spaces and may contain several percent K₂O.

Major element compositions of pyroxenes, olivines, and feldspars from the Apollo 17, Station 6 Boulder Samples are plotted in Figures 35-47. Symbols used are:

Pyroxene: dots-matrix; triangles-mineral clasts

Olivine: open-matrix; filled-mineral clasts

Feldspars: solid-matrix; dashed-mineral clasts

The following scheme was used in generating the mineral chemistry data:

(1) For each petrographically distinct lithology, one to five 1 mm² area(s) are arbitrarily selected from each available thin section. These areas form the basis for analyses of matrix minerals. Within each area, about 50 randomly selected feldspar crystals and about 50 randomly selected mafic crystals (pyroxene plus olivine) are analyzed.

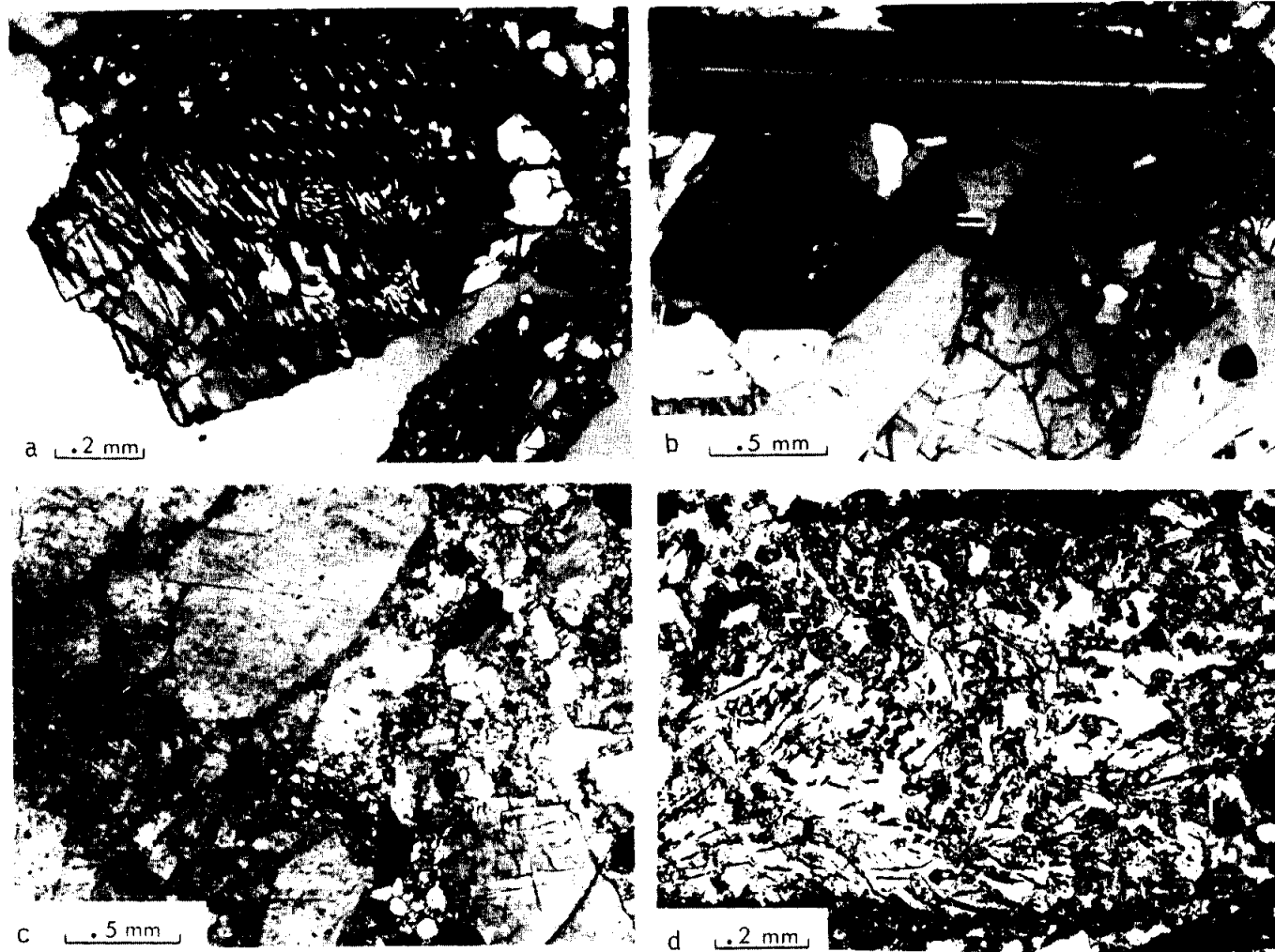


FIGURE 34: (a) Pigeonite crystal (partially crossed polarizers) with exsolution lamellae in crushed norite clast of 76255. (b) Gabbro clast (crossed polarizers) with plagioclase tablets and augite in 76255. (c) Troctolite clast (partially crossed polarizers) in 76255. Larger grains are plagioclase. Finer grained region on right is crushed olivine. (d) Basalt clast (single polarizer) in 76255. White is plagioclase, gray is mostly subcalcic augite, and black lines are ilmenite.

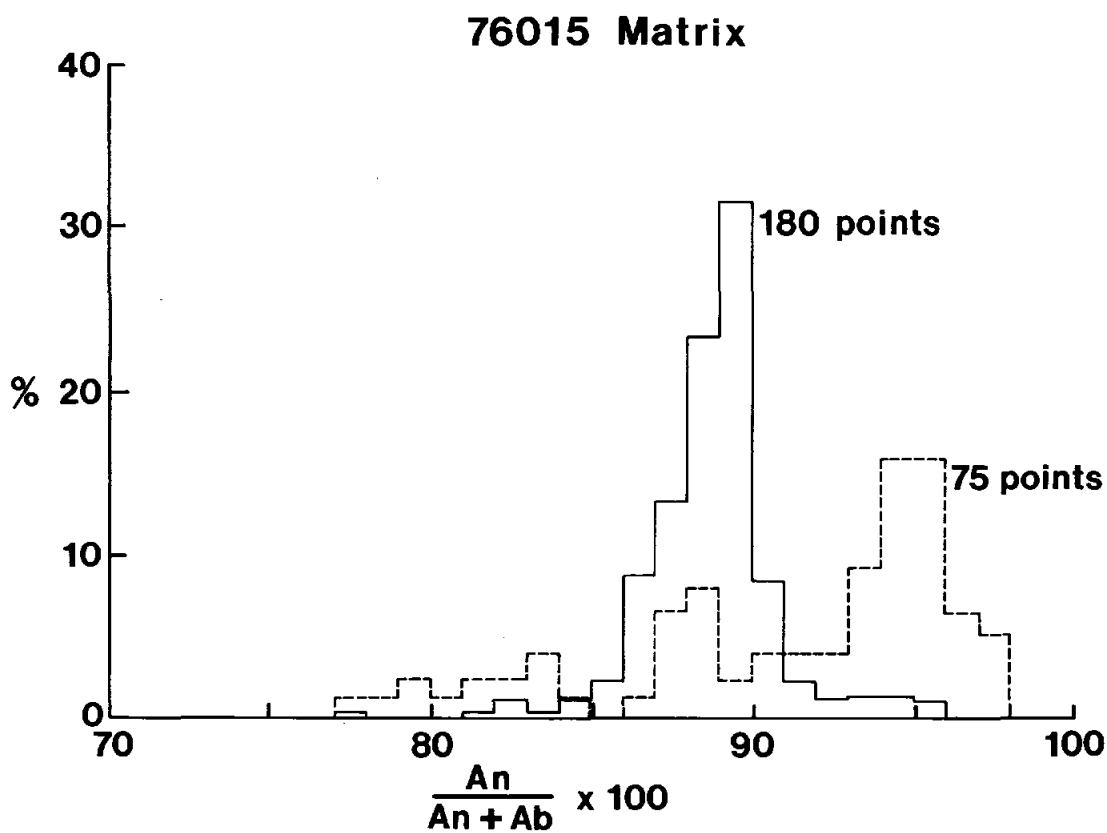
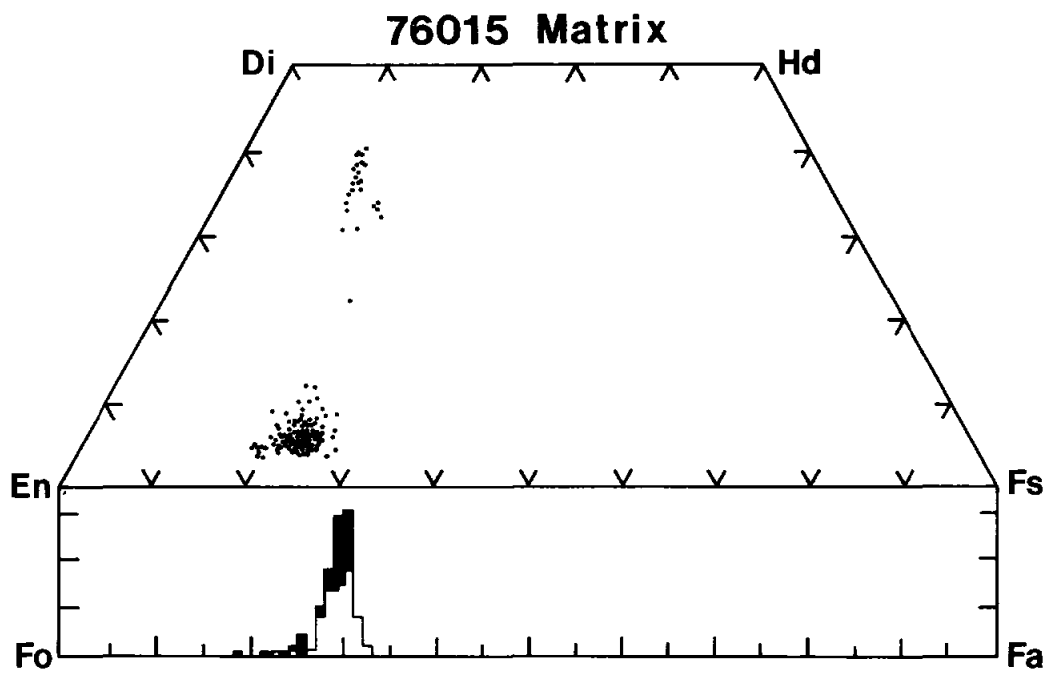


FIGURE 35: Electron microprobe analyses of minerals in matrix of 76015.

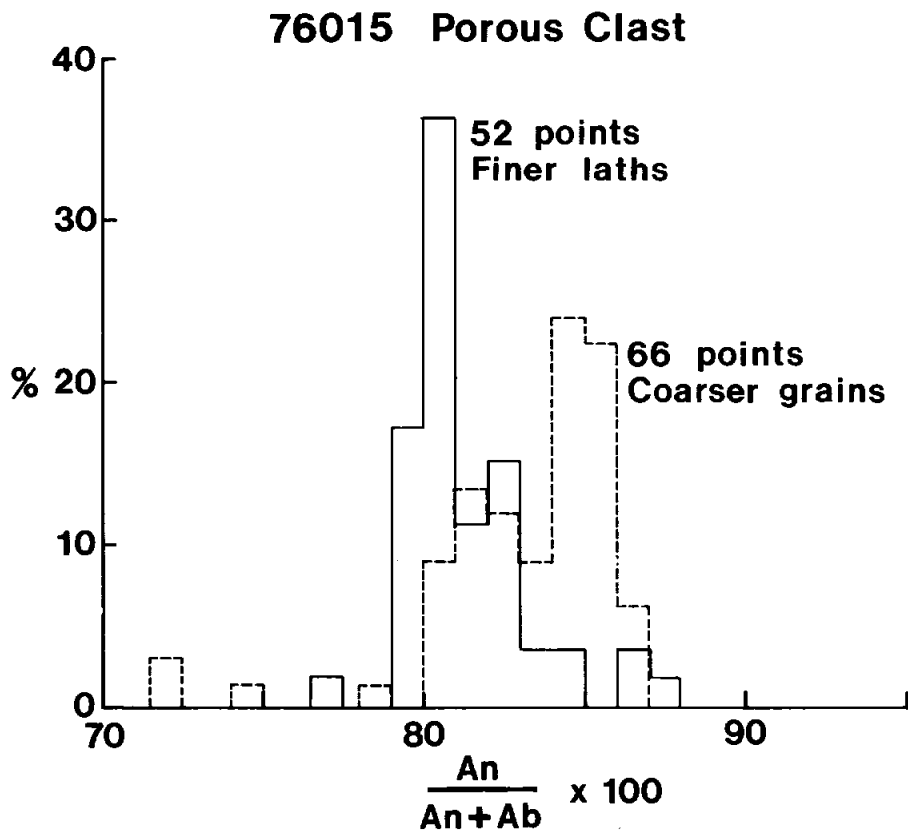
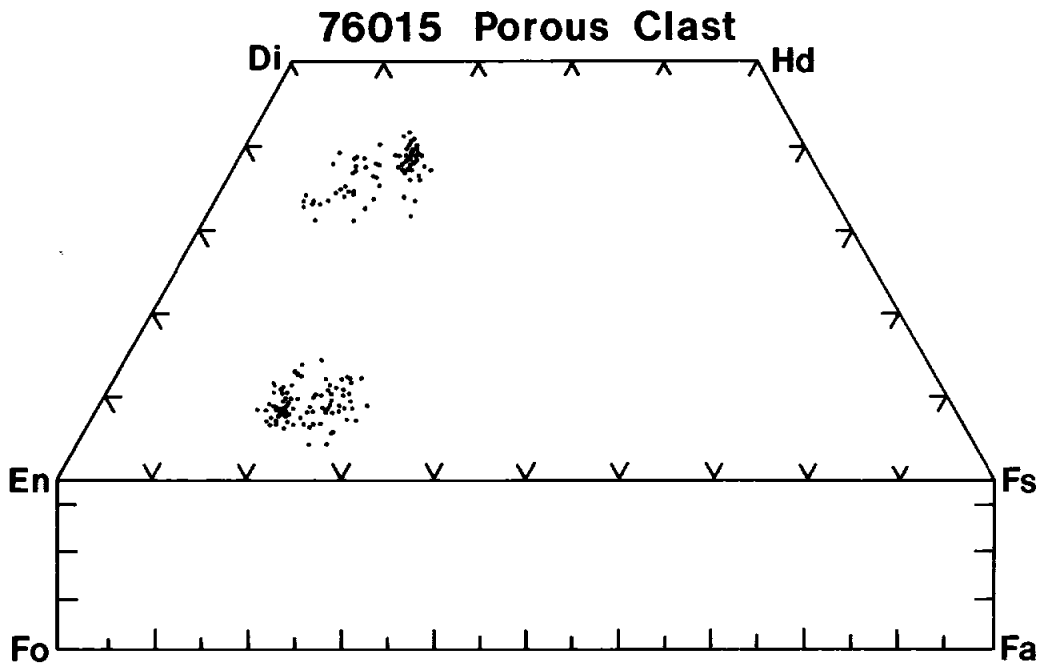


FIGURE 36: Electron microprobe analyses of minerals in porous basaltic clast of 76015.

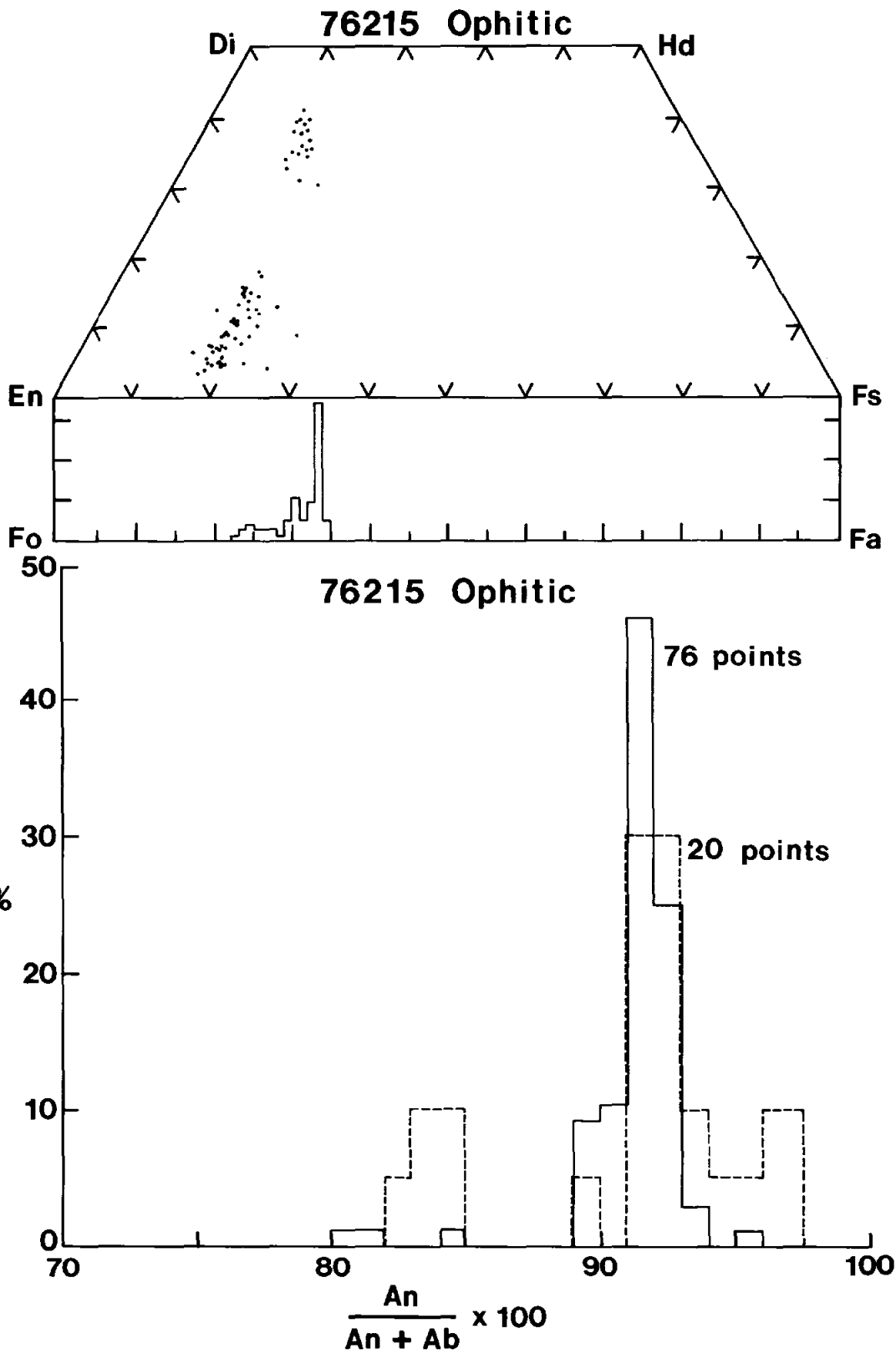


FIGURE 37: Electron microprobe analyses of minerals in ophitic portion of matrix in 76215.

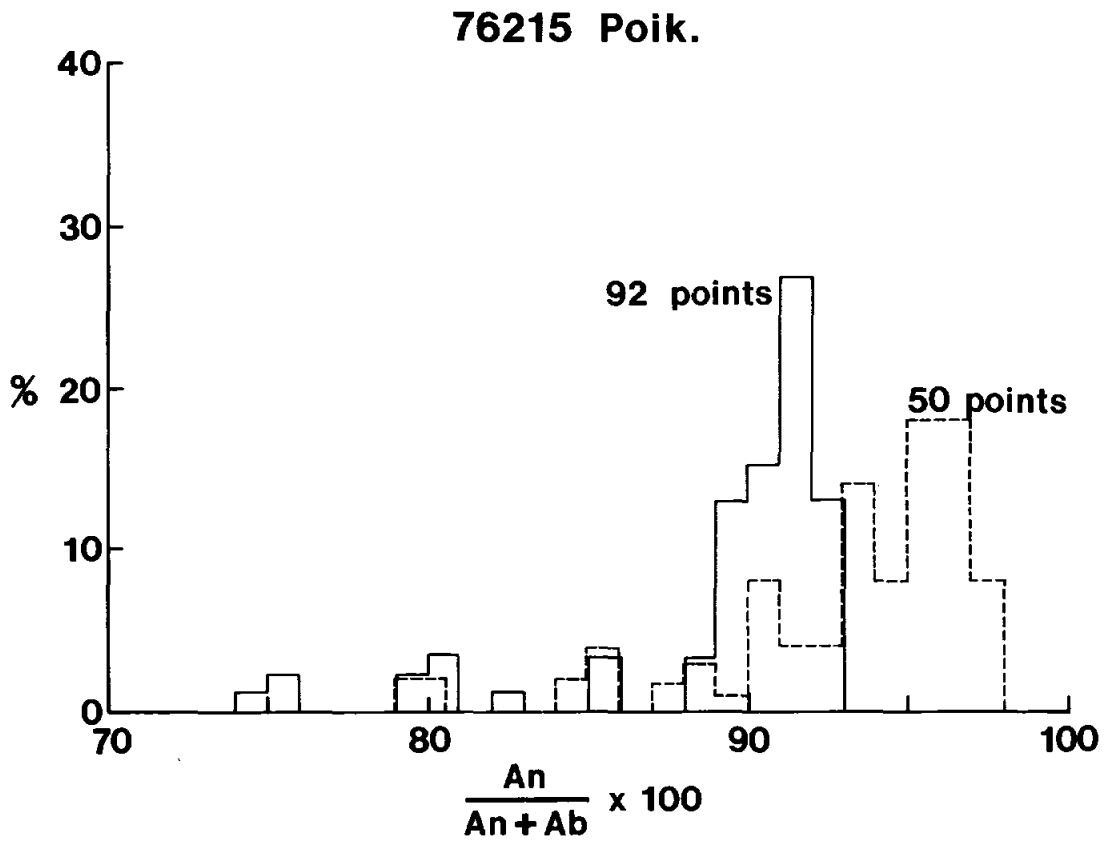
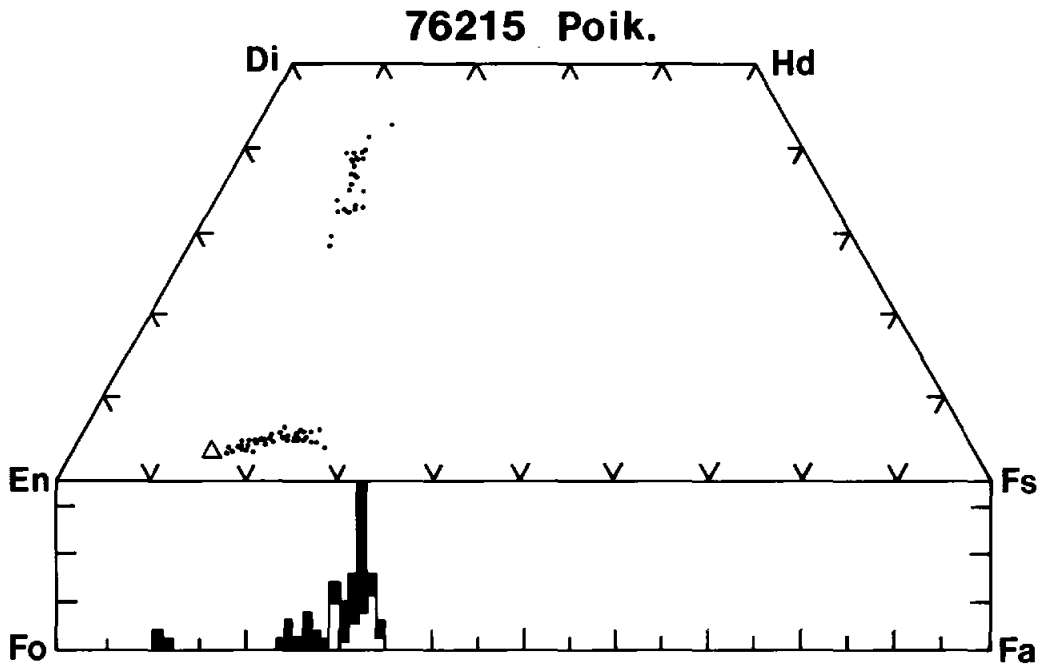


FIGURE 38: Electron microprobe analyses of minerals in poikilitic portion of matrix in 76215.

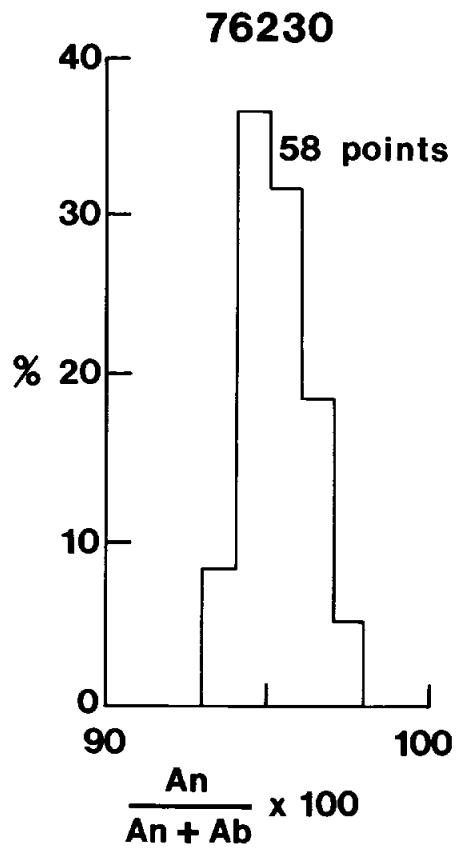
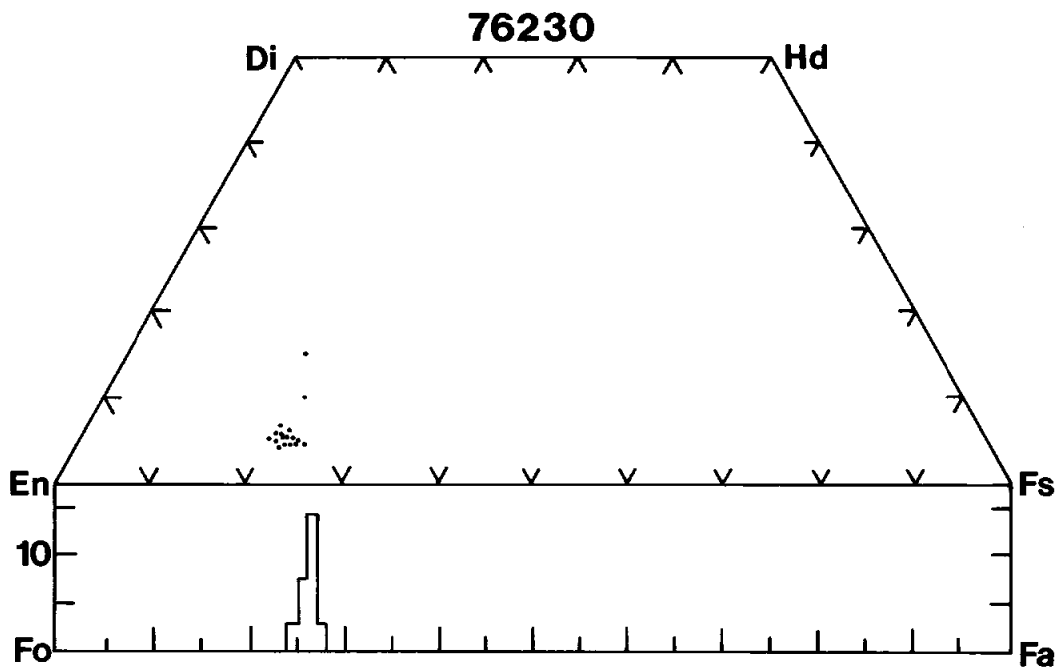


FIGURE 39: Electron microprobe analyses of minerals in 76230.

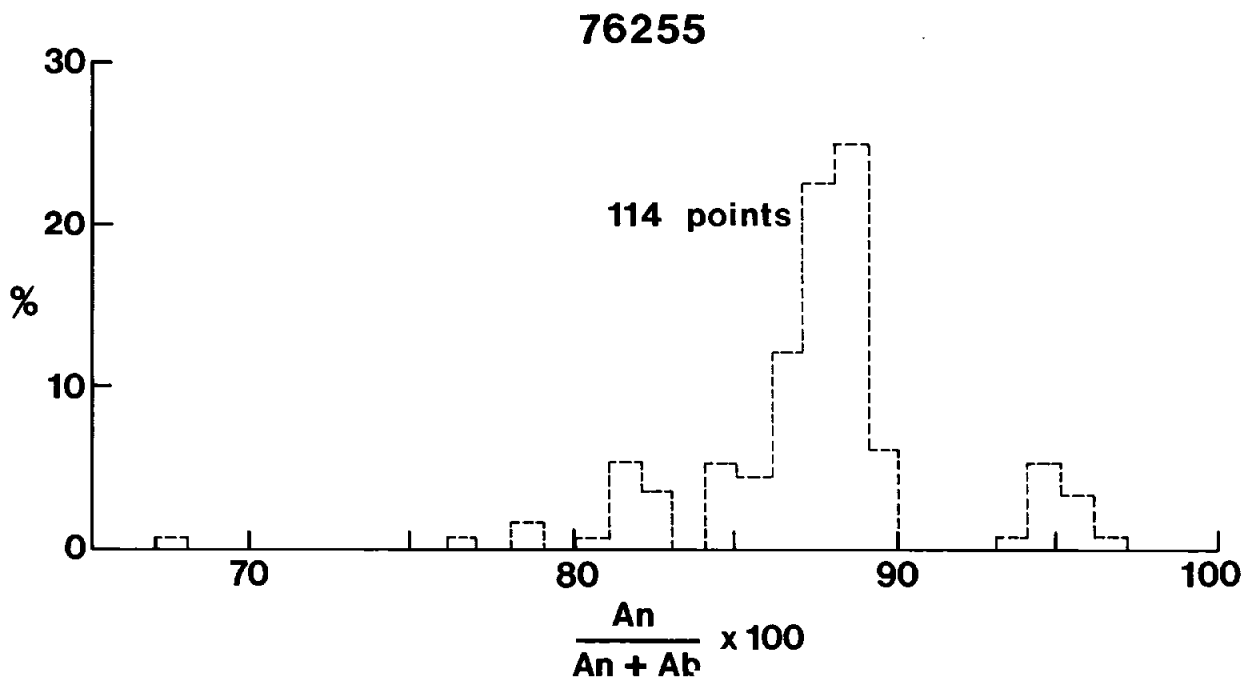
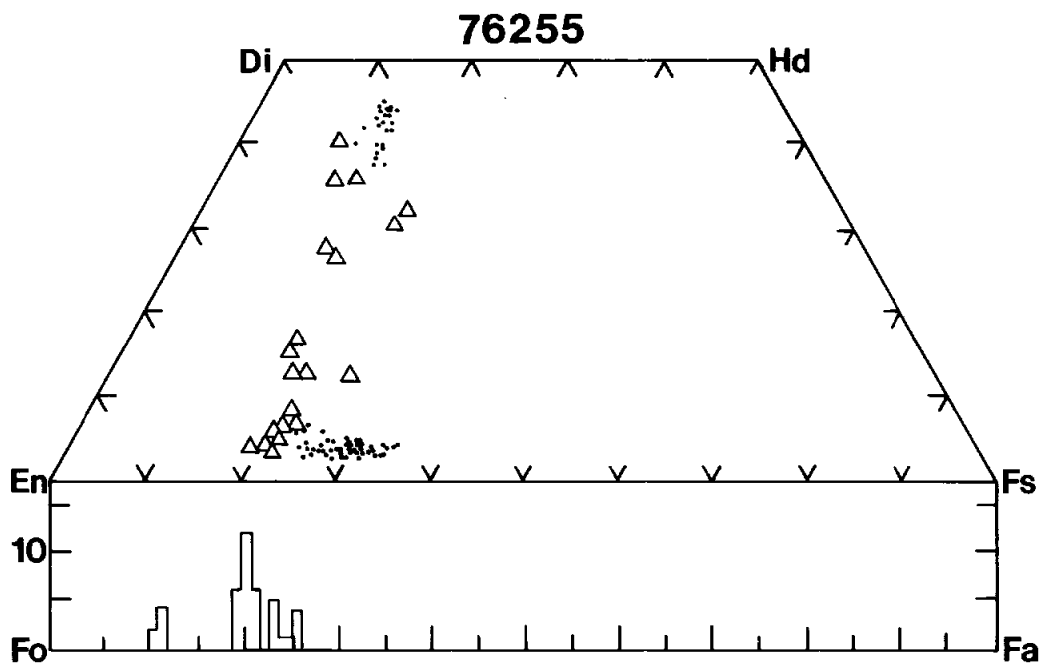


FIGURE 40: Electron microprobe analyses of minerals in matrix of 76255.

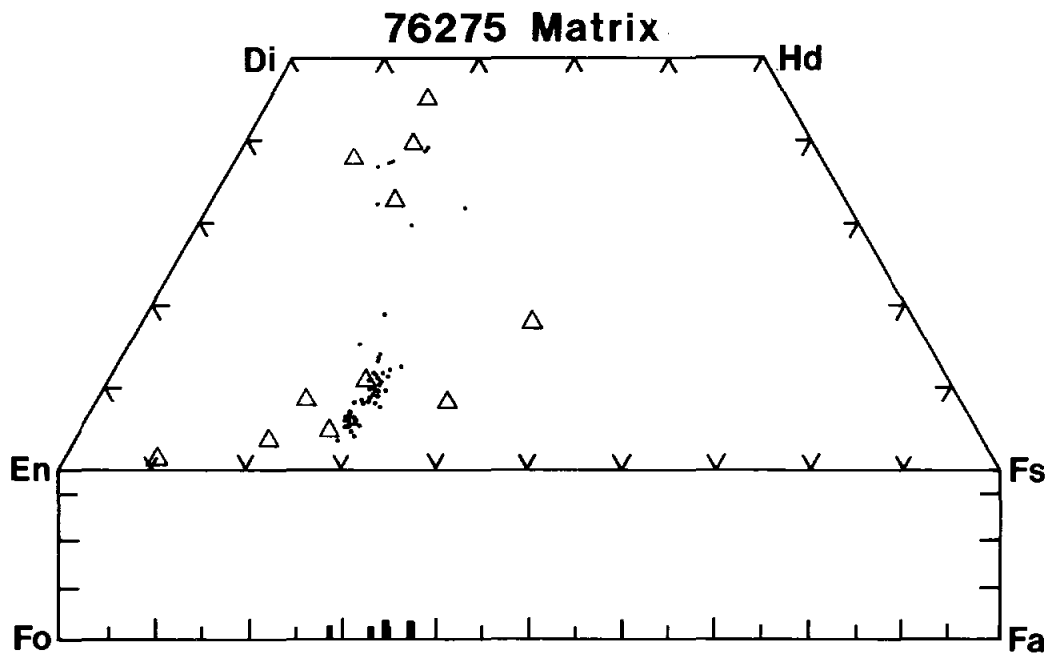


FIGURE 41: Electron microprobe analyses of minerals in matrix of 76275.

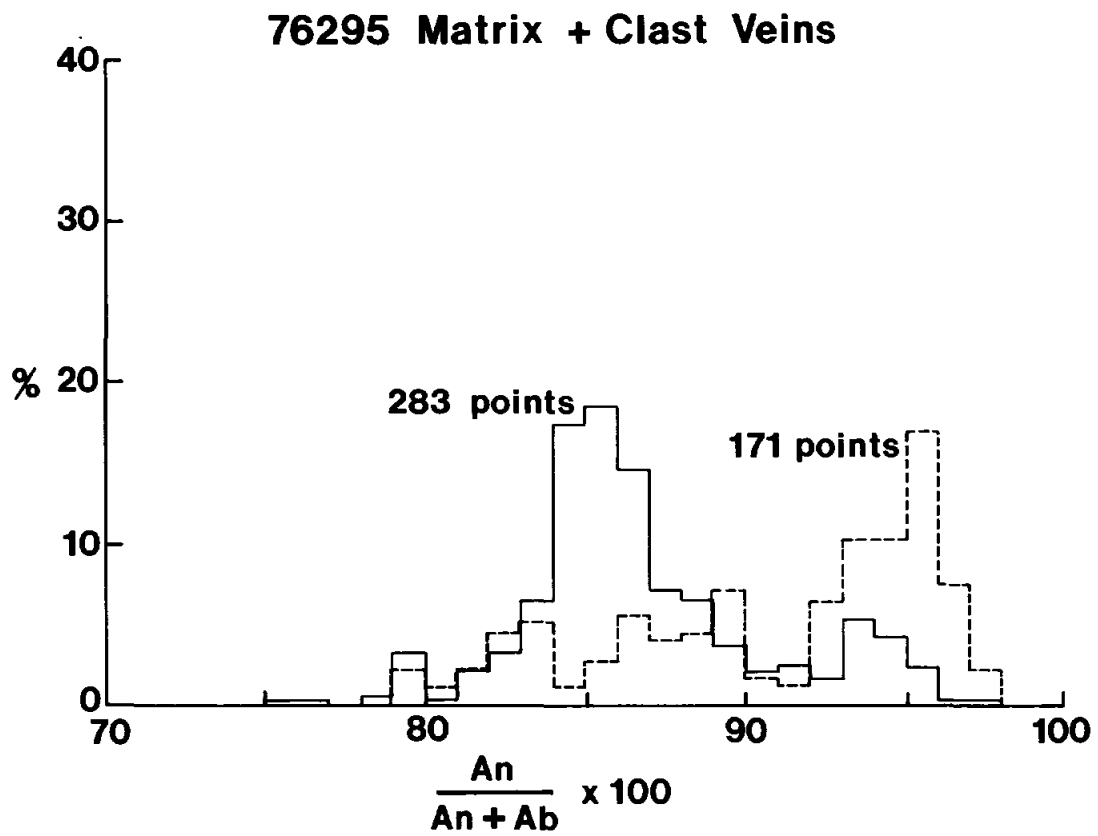
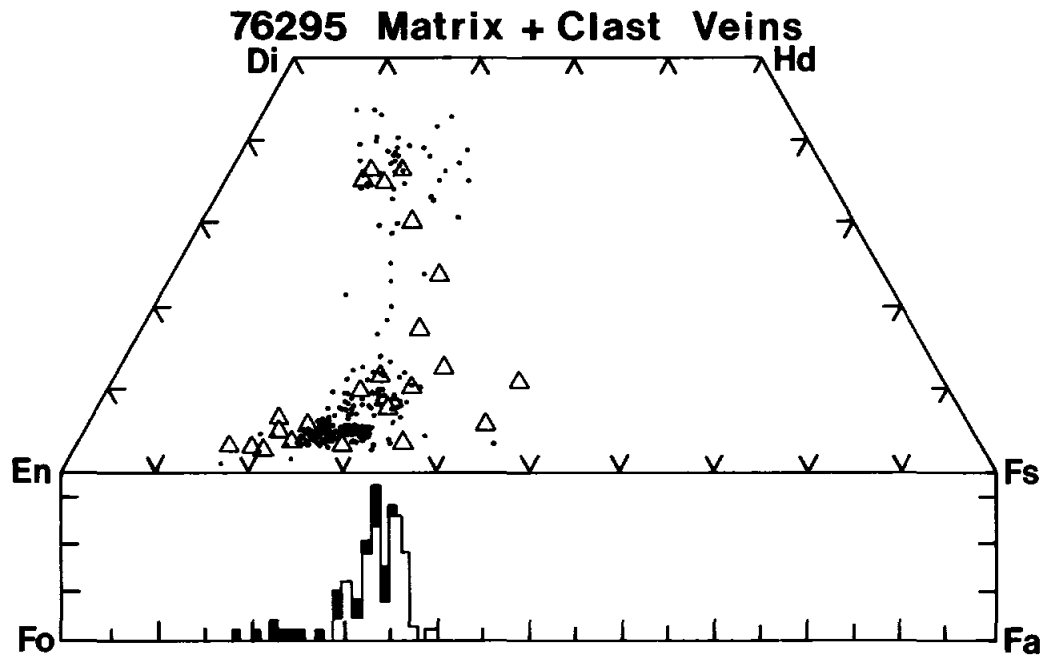


FIGURE 42: Electron microprobe analyses of minerals in matrix and clast-veins of 76295.

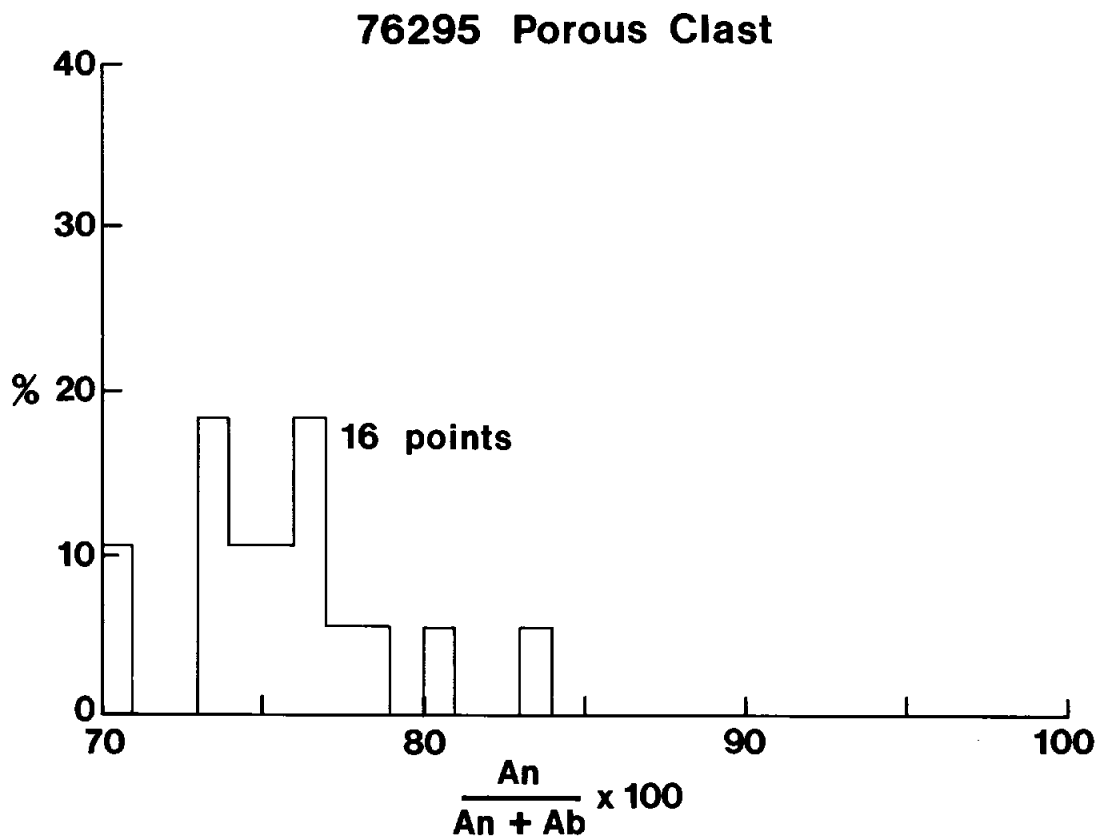
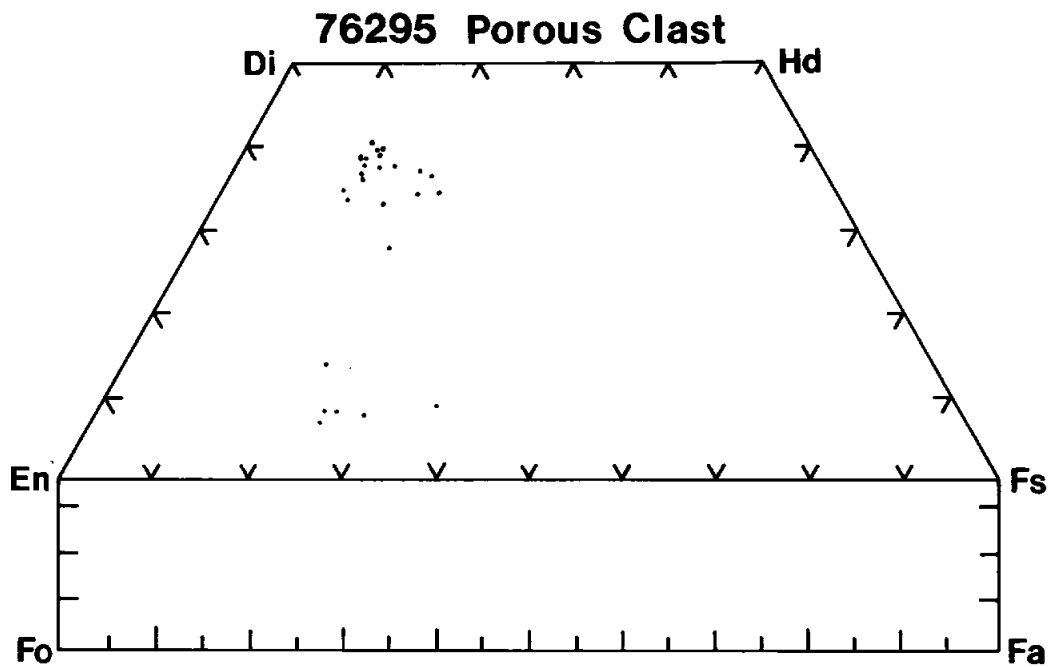


FIGURE 43: Electron microprobe analyses of minerals in porous basaltic clast of 76295.

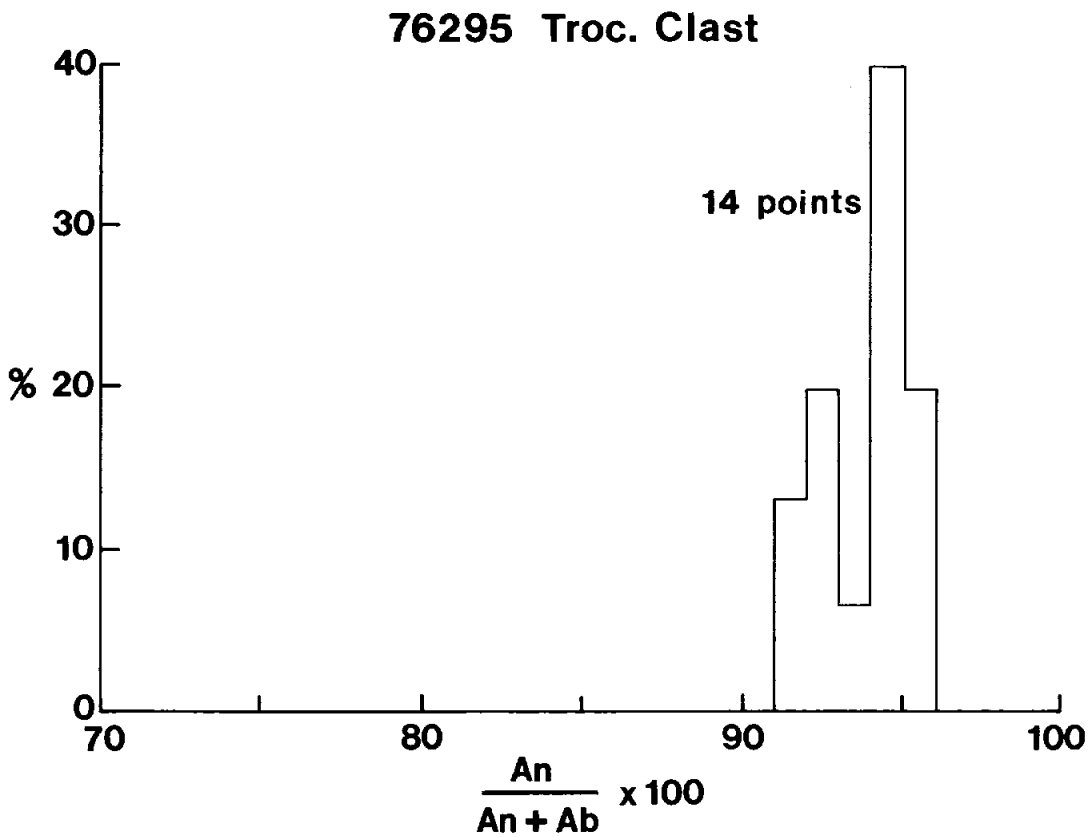
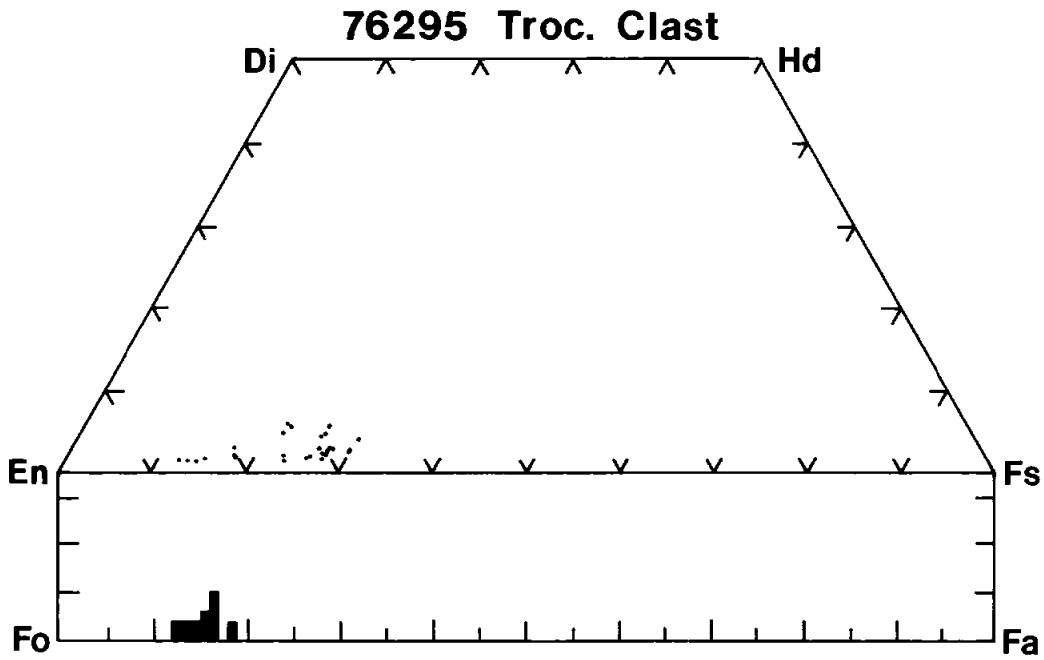


FIGURE 44: Electron microprobe analyses of minerals in troctolite clast of 76295.

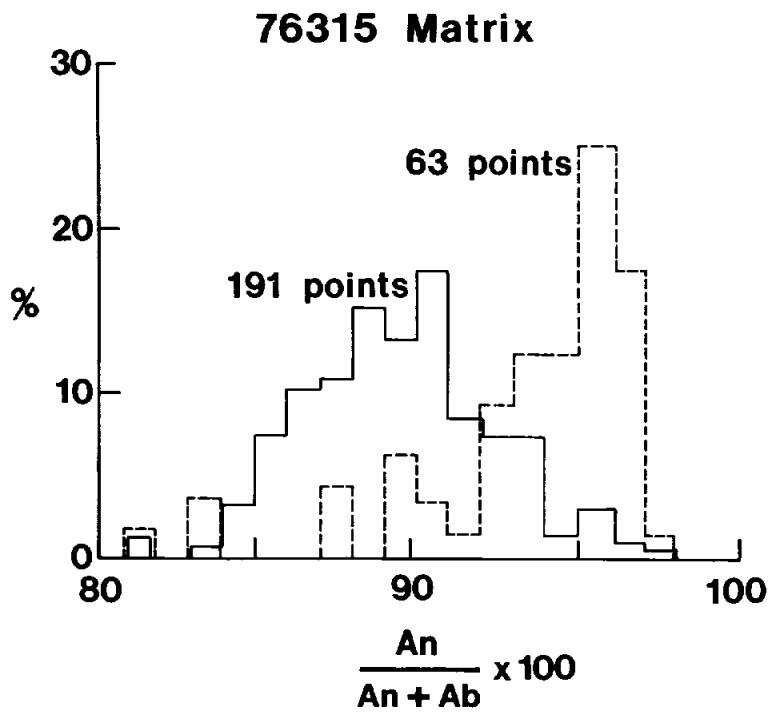
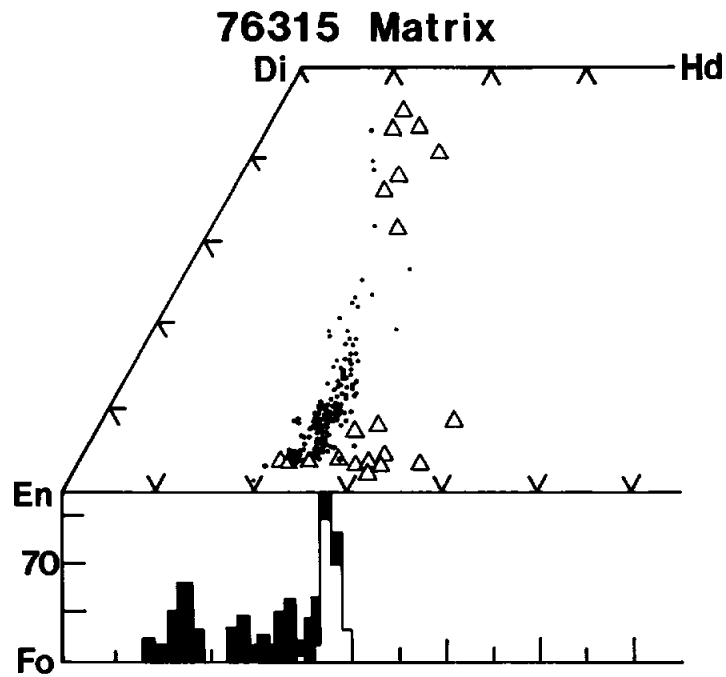


FIGURE 45: Electron microprobe analyses of minerals in matrix of 76315.

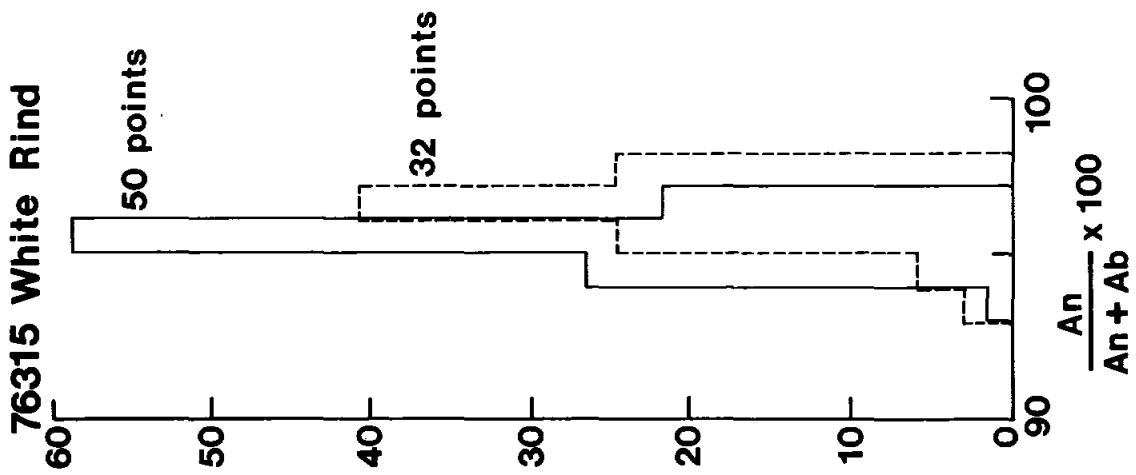
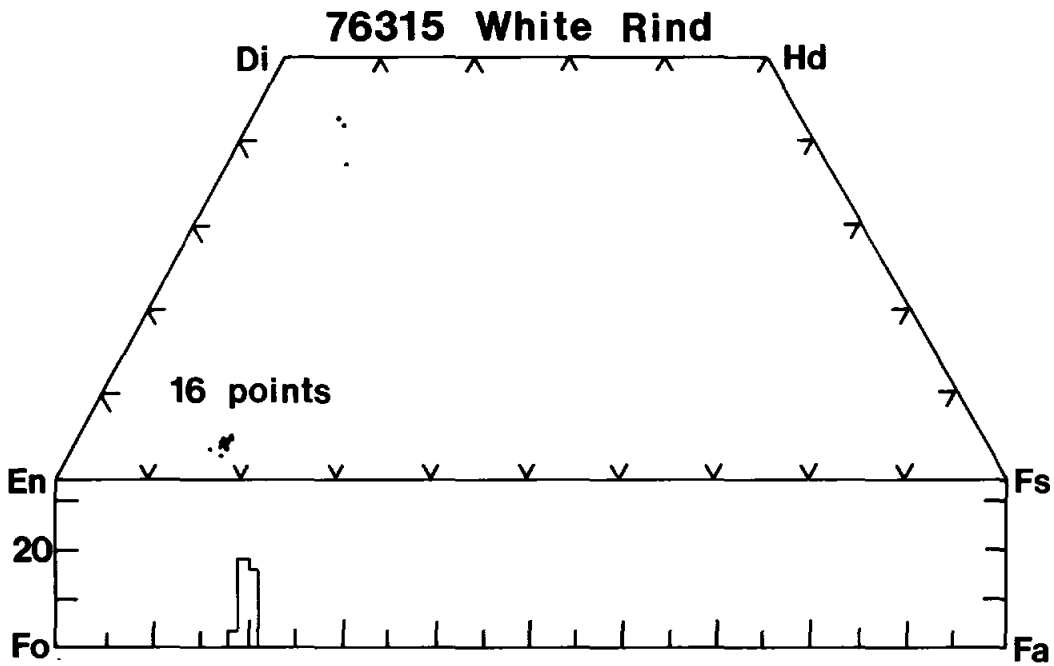


FIGURE 46: Electron microprobe analyses of minerals in white rind (clast 1) of 76315.

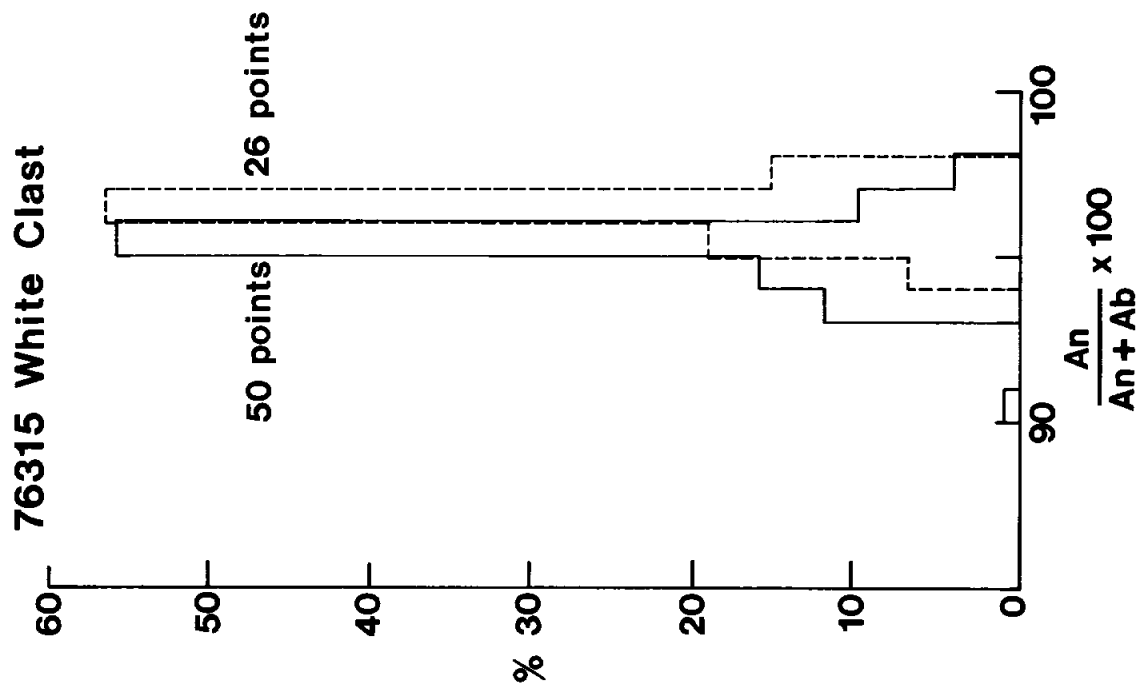
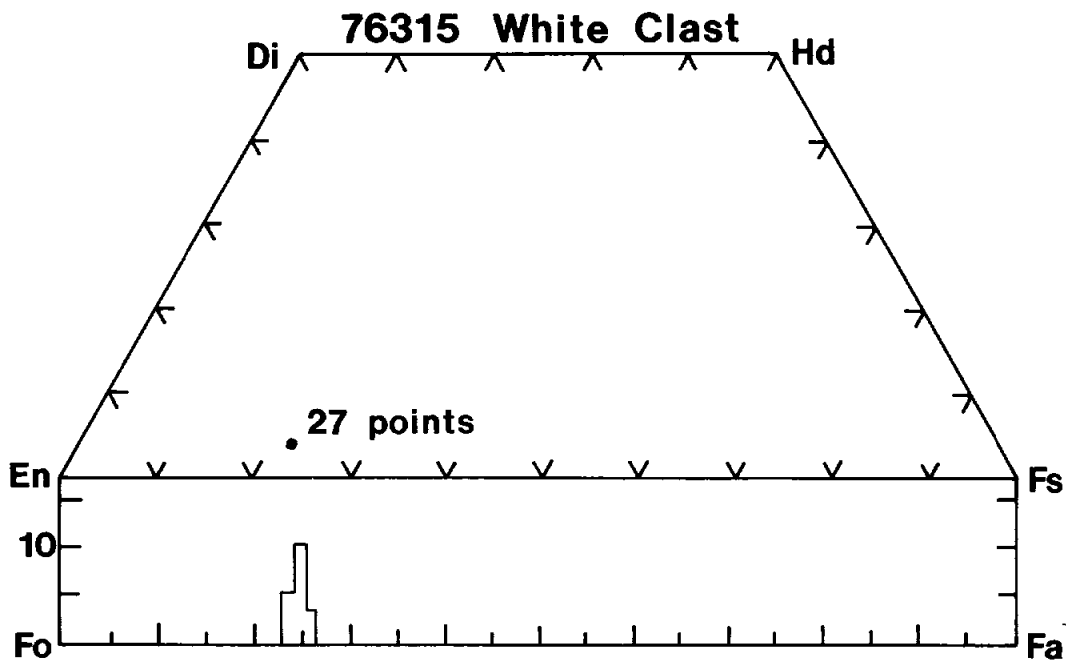


FIGURE 47: Electron microprobe analyses of minerals in light gray or white clast (clast 2) of 76315.

(2) The core of every feldspar, pyroxene, and olivine mineral clast, where the size of the clast is greater than a predetermined value, is analyzed. The threshold size is set such that for each sample there are at least 50 feldspar clasts analyzed and at least 50 pyroxene plus olivine clasts analyzed.

Petrographic data are summarized in the following table where the samples are listed in order of decreasing cooling rate. The correlation between mineral chemistry and matrix texture are in support of the model of breccia evolution as presented in Refs. 7 and 25.

Table 2: Petrographic Summary

Sample Number	Matrix Texture	Matrix Feldspar		Matrix Pyroxene En/(En+Fs)		Matrix Clasts: pyrox/(pyrox+oliv)
		Length (µm)	Peak An/(An+Ab)	Cluster Center	Normative	
76215	ophitic	100-300	.91	.806	.747	0
76215	poikilitic	10-25	.91	.779	.761	.02
76015	poikilitic	5-15	.89	.757	.740	0
76315	micro-poikilitic	5-25	.88-90	.750	.73-.74	.25
76295	fine subophitic	5-15	.85	.715	.709	.36
76275	fine subophitic	5-10	.84	.705	-	.80

Crystallography

Numerous vugs occur in 76015 and 76215. The vugs are lined with a variety of crystals and, in some cases, there are well formed crystals protruding into the vugs or lying loosely in the vugs.

In the vugs of 76015 apatite occurs as honey-yellow, transparent single crystals up to 1 mm in greatest dimension. The crystals were found to be doubly-terminated and loose or very weakly adhering to the cavity walls. Crystal forms present are hexagonal prism and hexagonal bipyramid. Single-crystal precession photographs were taken of one crystal and yielded cell dimensions $a = 9.39(1)\text{\AA}$ and $c = 6.85(1)\text{\AA}$ and space group $C6_3/m$ consistent with fluor-apatite.

β -cristobalite also occurs in 76015 vugs as honey-yellow, transparent single crystals up to 0.5 mm in greatest dimension. Crystals were singly-terminated octahedra (111) forming encrustations in smaller cavities (1 to 2 mm in size). These crystals were firmly adhered to the cavity walls. Single crystal precession photographs were taken of one such crystal. Cell dimensions were measured from the film were $a = 5.02(1)\text{\AA}$, $c = 7.11(1)\text{\AA}$. The space group was determined as $P4_12_1$ or its enantiomorph $P4_32_1$ (tetragonal). The octahedral habit indicates that the material crystallized as high cristobalite (space group $Fd3m$) above 220°C.

Vugs from 76015 and 76215 are lined with euhedral crystals of plagioclase, pyroxene, ilmenite, Ni-Fe, and troilite. Smaller crystals of chromite, pentlandite, and chalcopyrite occur on the surface of the troilite in 76015 (Ref. 13). Wiry Cu and dendritic-metallic Cu occur with metallic Ni-Fe and troilite in some vugs of 76215. Troilite in both samples may have crystallized from an immiscible sulfide liquid. With falling temperature, chalcopyrite, and pentlandite may have exsolved from the troilite in 76015. By contrast, metallic Cu may have formed in 76215 by thermal breakdown of a bornite, troilite, and Ni-Fe assemblage which originally crystallized from a low-Ni immiscible sulfide liquid.

Single crystal x-ray diffraction studies and electron microprobe analyses of pyroxenes in breccia 76255 indicate that they are inverted pigeonites with exsolution lamellae of augite about 15 μm thick and developed in a primary pigeonite with (001) in common (Ref. 24). The host orthopyroxene contains blebby augite inclusions similar

to those found in the most magnesian eucrite, Binda. The orientation of orthopyroxenes with respect to the (001) augite differs from grain to grain in 76255 but retains some geometrical relationships. Compositional relations within this very Mg-rich Stillwater-type inverted pigeonite indicate a crystallization temperature of about 1140°C and a final exsolution equilibrium at about 970°C. A simple computer simulation of the growth rates of lamellae in this pyroxene suggests that the observed texture was developed at a depth of a few kilometers in the lunar crust.

Major Element Chemistry

In Table 3 are listed the **major element analyses for the Station 6 boulder samples.** The remarkable compositional uniformity of all the matrix samples is noteworthy and suggests a rather thorough mixing of the target material during formation of the impact melt. Some of the clasts are anorthositic with over 25% Al_2O_3 . However, the cataclastic norite clast of 76255 contains less Al_2O_3 than the matrix, it also contains less MgO but considerably more SiO_2 . Three gray clasts in unit C have compositions similar to the matrix suggesting an origin similar to the impact melt rocks of the boulder.

Lithophile Trace Elements

The chemical compositions of the matrices (Table 4 and Figure 48) are generally the Apollo 17 variety of KREEP. All of the fine grained subophitic and poikilitic matrices contain similar rare earth concentrations. The very fine grained subophitic matrices of unit C appear to be slightly more enriched in rare earth elements than the other matrix units. The more massive and coarser ophitic matrix of 76215 has the lowest concentration of rare earth elements. The vuggy basaltic material,

Table 3. Major Element Chemistry

	76015				76215		76230	76255			
	Unit B Matrix	Unit B Matrix, Porous	Unit B Matrix	In Unit C Anorthositic Clast	In Unit C Brecciated Norite Clast Very Coarse	Unit C Matrix	In Unit C Mixture Matrix + Norite Clast				
	,12	22	37	41	64	27	28	4	38	44	51
SiO ₂	46.57	46.16	46.38	46.38	46.59	46.02	46.13	44.52	50.61	45.45	46.94
TiO ₂	1.52	1.52	1.55	1.53	1.48	1.52	1.24	0.20	0.75	1.60	1.66
Al ₂ O ₃	17.73	17.17	17.78	17.77	18.00	17.83	18.73	27.01	15.37	18.91	19.04
FeO	8.81	9.81	9.65	9.07	9.10	8.70	8.08	5.14	9.80	7.40	7.21
MnO	0.12	0.13	0.13	0.12	0.12	NA	NA	0.06	0.19	0.11	0.13
MgO	12.75	13.03	12.40	12.67	12.43	12.21	12.43	7.63	11.14	13.88	11.86
CaO	10.88	10.77	11.13	11.11	11.10	11.10	11.50	15.17	11.05	11.78	12.47
Na ₂ O	0.69	0.70	0.72	0.69	0.75	NA	0.70	0.35	0.74	0.68	0.76
K ₂ O	0.27	0.26	0.26	0.26	0.29	0.27	0.25	0.06	0.37	0.17	0.18
P ₂ O ₅	0.28	0.27	0.29	0.29	0.28	0.28	0.24	0.05	0.03	0.24	0.22
S	0.39	0.09	0.06	0.08	0.08	0.05	0.06	0.03	0.09	0.03	0.03
Cr ₂ O ₃	0.20	-	-	-	-	-	-	0.11	-	-	-
Total	100.19	99.91	100.35	99.97	100.22			100.33	100.14	100.25	100.51

Ref. 43

Ref. 29

Ref. 29

Ref. 29

Ref. 29

Ref. 7

Ref. 7

Ref. 31

*

*

*

* Unpublished data from M. Rhodes

**Unpublished preliminary fused bead analyses from R. Brown. Analyses are tentative but satisfactory for comparative or grouping purposes.

Table 3. (continued)

	76255		76275				76295			
	In Unit C Brecciated Norite Clast	In Unit C Troctolite Clast	Unit C Tan Matrix	In Unit C Vesicular Clast	Unit C Blue Gray Matrix	Unit C Blue Gray Matrix	In Unit C Light Gray Clast	Unit C Tan Matrix	In Unit C Basaltic Vug	In Unit C Dark Gray Clast
	55	58	24	32	38	14	30	35	48	51
SiO ₂	59.68	43.84	47.14	47.16	46.67	47.03	47.04	47.55	48.11	46.89
TiO ₂	1.37	0.25	1.65	1.43	1.36	1.39	1.36	1.64	1.80	1.50
Al ₂ O ₃	15.89	25.15	18.70	17.68	18.63	18.25	18.98	17.67	16.95	18.67
FeO	9.36	4.23	8.54	8.91	8.41	9.09	8.44	9.05	9.17	8.79
MnO	0.17					NA				
MgO	11.23	11.02	9.22	11.20	10.85	10.78	9.64	9.78	9.72	9.66
CaO	11.17	14.20	12.06	11.30	11.37	11.54	11.95	11.49	11.22	11.69
Na ₂ O	0.73	0.40	0.72	0.70	0.70	0.76	0.66	0.74	0.75	0.71
F ₂ O	0.32	0.08	0.34	0.22	0.28	0.26	0.28	0.29	0.60	0.23
P ₂ O ₅	0.01					0.32				
S	0.03					0.06				
Cr ₂ O ₃	-	0.04	0.15	0.19	0.19	-	0.16	0.17	0.17	0.17
Total	99.96	99.21								
	*	**	**	**	**	Ref. 7	**	**	**	**

* Unpublished data from M. Rhodes

**Unpublished preliminary fused bead analyses from R. Brown. Analyses are tentative but satisfactory for comparative or grouping purposes.

Table 3. (Continued)

	76315						76315			
	Unit A-B Matrix	Unit A-B Matrix	In Unit A-B Dark Clast	Unit A-B Matrix	In Unit A-B White Rind (impure)	In Unit A-B Light Gray Clast	Unit A-B Matrix	In Unit A-B Dark Clast	Unit A-B Matrix	
	2	30	30,3	35	42	62	30	30,3	35	
SiO ₂	45.82	45.64	46.45	46.21	48.57	45.10	Sr	174	172	177
TiO ₂	1.47	1.50	1.43	1.50	0.32	0.36	Rb	6.7	3.6	6.2
Al ₂ O ₃	18.01	17.53	18.18	18.14	17.91	26.37	Y	113	107	111
FeO	8.94	9.53	8.83	8.95	7.66	5.29	Zr	506	478	522
MnO	0.11	0.13	0.13	0.12	0.13	0.07	Nb	33	32	33
MgO	12.41	12.50	12.34	12.02	13.84	7.46	Zn	3	2	4
CaO	11.06	10.97	11.30	11.32	10.36	15.12	Ni	77	82	74
Na ₂ O	0.57	0.70	0.66	0.60	0.47	0.47				
K ₂ O	0.27	0.26	0.22	0.26	0.15	0.10				
P ₂ O ₅	0.29	0.30	0.29	0.29	0.12	0.06				
S	0.08	0.08	0.07	0.07	0.00	0.04				
Cr ₂ O ₃	0.19	0.19	0.20	0.19	-	-				
Total	99.22	99.33	100.08	99.67	99.53	100.44				
	Ref. 2	Ref. 29	Ref. 29	Ref. 29	Ref. 29	Ref. 29				

* Unpublished data from M. Rhodes

** Unpublished preliminary fused bead analyses from R. Brown. Analyses are tentative but satisfactory for comparative or grouping purposes

Table 4. Lithophile and Other Trace Elements

Sample No.	Unit B Matrix	Unit B Matrix	Unit B Matrix	Unit B Matrix	Unit B Nonporous Matrix	Unit B Less Porous Matrix	In Unit C Anorthositic Clast	Unit C Blue-Gray Matrix	In Unit C Basaltic Yug	Unit A-B Matrix
	76015,22M	76015,37M	76015,41M	76015,64M	76215,27	76215,28	76230,4	76230,4	76295,46	76315,2
Li ppm	18.3	19.8	21.6	18.5	19.6	22.6	11.0	19.4	20.5	14.6
K ppm	2223	2304	2279	2414	2336	2008	440	2192	5247	2252
Rb ppm	6.41	6.67	6.57	7.46	6.89	6.10	0.448	5.43	20.47	5.88
Sr ppm	172	178	177	174			146		191	180
Ba ppm	348	362	358	354	352	294	50.2	376	334	359
La ppm	-	34.3	33.4	29.9	33.4	27.3	3.04	37.8	18.2	30.1
Ce ppm	83.3	85.9	84.9	78.4	83.6	68.9	7.54	95.7	46.6	84.6
Nd ppm	52.8	54.4	54.0	49.3	52.2	43.7	4.64	60.0	31.1	53.5
Sm ppm	14.9	15.3	15.2	14.0	14.9	12.3	1.34	16.9	9.22	15.1
Eu ppm	1.94	2.02	1.99	1.97	1.99	1.70	0.805	1.91	2.08	2.00
Gd ppm	18.7	19.0	18.9	17.6	19.3	15.9	1.70	21.3	12.4	18.9
Tb ppm										
Dy ppm	19.5	20.0	19.9	18.3	19.7	16.5	2.02	22.3	13.3	19.9
Ho ppm										
Er ppm	11.5	11.8	11.7	10.9	11.8	9.90	1.31	13.2	8.06	11.7
Tm ppm										
Yb ppm	10.6	11.0	10.8	10.0	10.9	9.00	1.37	12.0	7.60	11.0
Lu ppm	1.58	-	1.30	1.50	-	-	0.202	-	1.07	-
Cr ppm	1316	1099	1188	1226	-	-	685	-	1364	1228
Th ppm	5.44	5.64	5.56	5.41	5.20	4.61	0.72	6.12	2.01	5.20
U ppm	1.46	1.59	1.96	1.48	1.50	1.26	0.20	1.83	0.66	1.52
Zr ppm	490	515	507	484	495	459	-	541	232	477
Hf ppm	12.4	12.7	-	-	-	-	-	-	-	12.5
Cs ppm	-	-	-	-	-	-	-	-	-	-
Ni ppm	-	-	-	-	-	-	-	-	-	-
Sc ppm	-	-	-	-	-	-	-	-	-	-
Co ppm	-	-	-	-	-	-	-	-	-	-
Ta ppm	-	-	-	-	-	-	-	-	-	-
Zn ppm	-	-	-	-	-	-	-	-	-	-
Na ₂ O %	.70	.71	.70	.71	-	-	.39	-	-	.61
TiO ₂ %	-	-	-	-	-	-	.193	-	1.85	-
FeO ^{87/87} %										
Sr ^{87/87}	0.70589±9	0.70605±5	0.70589±11	0.70696±6			0.69979±10		0.71717±5	0.70515±5
	Ref. 31	Ref. 2	Ref. 2	Ref. 2	Ref. 7	Ref. 7	Ref. 31	Ref. 7	Ref. 7	Ref. 31

Table 4 (continued)

Sample No.	Unit A-B Matrix	In Unit A-B Dark Clast ³	Unit A-B Matrix	In Unit A-B White Clast	In Unit A-B Light Gray Clast ²	Unit B Troctolite Clast	Unit C Tan Matrix	Unit C Dark Gray Clast	Unit C Basaltic Vug	Unit C Light Gray Clast	Unit B Matrix
	76315,30M	76315,30,C3	76315,35M	76315,52	76315,62	76255,58	76295,31	76295,51	76295,48	76295,30	
Li ppm	15.6	14.1	13.9	11.8	9.5						17.7
K ppm	2262	1847	2144	1244	809						
Rb ppm	6.56	3.85	5.78	3.73	2.336						
Sr ppm	175	172	174	115	153						180
Ba ppm	349	366	337	129	72.8	240					340
La ppm	32.9	24.7	31.6	7.33	5.41	16.1	37.5 ± .2	44.2 ± .5	22.0 ± .2	31.8 ± .2	33.8
Ce ppm	84.0	78.6	82.3	18.4	13.7	38	102 ± 1	127 ± 1	59.0 ± .4	95.8 ± .6	89.2
Nd ppm	53.5	50.2	52.7	11.5	8.60	24					54
Sm ppm	15.1	14.1	14.8	3.20	2.42	5.4	17.0 ± .1	20.4 ± .1	10.9 ± .1	14.3 ± .1	14.11
Eu ppm	1.97	1.88	1.95	0.971	0.940	1.77	2.11 ± .01	2.01 ± .02	2.15 ± .02	1.77 ± .01	1.99
Gd ppm	18.5	17.6	18.8	3.93	2.99						18.1
Tb ppm						0.94	3.91 ± .04	4.56 ± .06	2.72 ± .07	3.56 ± .04	3.04
Dy ppm	19.7	18.3	19.1	4.59	3.39						19.9
Ho ppm											4.70
Er ppm	11.5	11.0	11.4	2.91	2.14						
Tm ppm											1.92
Yb ppm	10.6	10.0	10.4	2.98	2.07	3.4	12.2 ± .1	14.1 ± 1	8.80 ± .07	10.8 ± .1	11.43
Lu ppm	-	-	-	0.455	0.30	0.46	1.71 ± .01	1.95 ± .02	1.31 ± .01	1.49 ± .01	1.55
Cr ppm	1302	1257	1389	813	770	461	1382 ± 5	1440 ± 20	1440 ± 10	1360 ± 30	
Th ppm	5.36	5.23	5.69	1.34	1.23	1.30	5.6 ± .2	7.6 ± .1	2.2 ± .2	5.2 ± .1	4.18
U ppm	1.47	1.36	2.52	0.34	0.34	.38					1.20
Zr ppm	485	465	-	105	95	150					480
Hf ppm	-	11.9	-	-	5.3	3.0	13.2 ± .1	16.3 ± .2	7.9 ± .2	12.4 ± .1	11.81
Cs ppm								.23 ± .08	1.32 ± .2	.17 ± .06	0.20
Ni ppm						70	160 ± 10	220 ± 20	230 ± 30	170 ± 10	1140
Sc ppm						4.7	17.8 ± .1	18.2 ± .1	21.0 ± .1	16.7 ± .1	16.7
Co ppm						19.4	19.9 ± .2	28.0 ± .3	24.9 ± .2	23.1 ± .2	90.2
Ta ppm						0.27	1.9 ± .1	2.4 ± .1	1.4 ± .1	1.7 ± .1	1.62
Zn ppm						53.2	20 ± 10	30 ± 10			
Na ₂ O %							.824 ± .003	.800 ± .004	.847 ± .004	.725 ± .002	
TiO ₂ %											
FeO %							9.05 ± .04	9.54 ± .05	10.1 ± .1	8.95 ± .04	
Sr ^{87/87}	0.70595 5	0.70351 10	0.70521 7	0.70491 6	0.70185 5						
	Ref. 2	Ref. 2	Ref. 2	Ref. 2	Ref. 31	Ref. 31A	Unpub. data D. Blanchard	Unpub. data D. Blanchard	Unpub. data D. Blanchard	Unpub. Data D. Blanchard	Ref. 43

Rare Earth Element Patterns for Station 6 Boulder

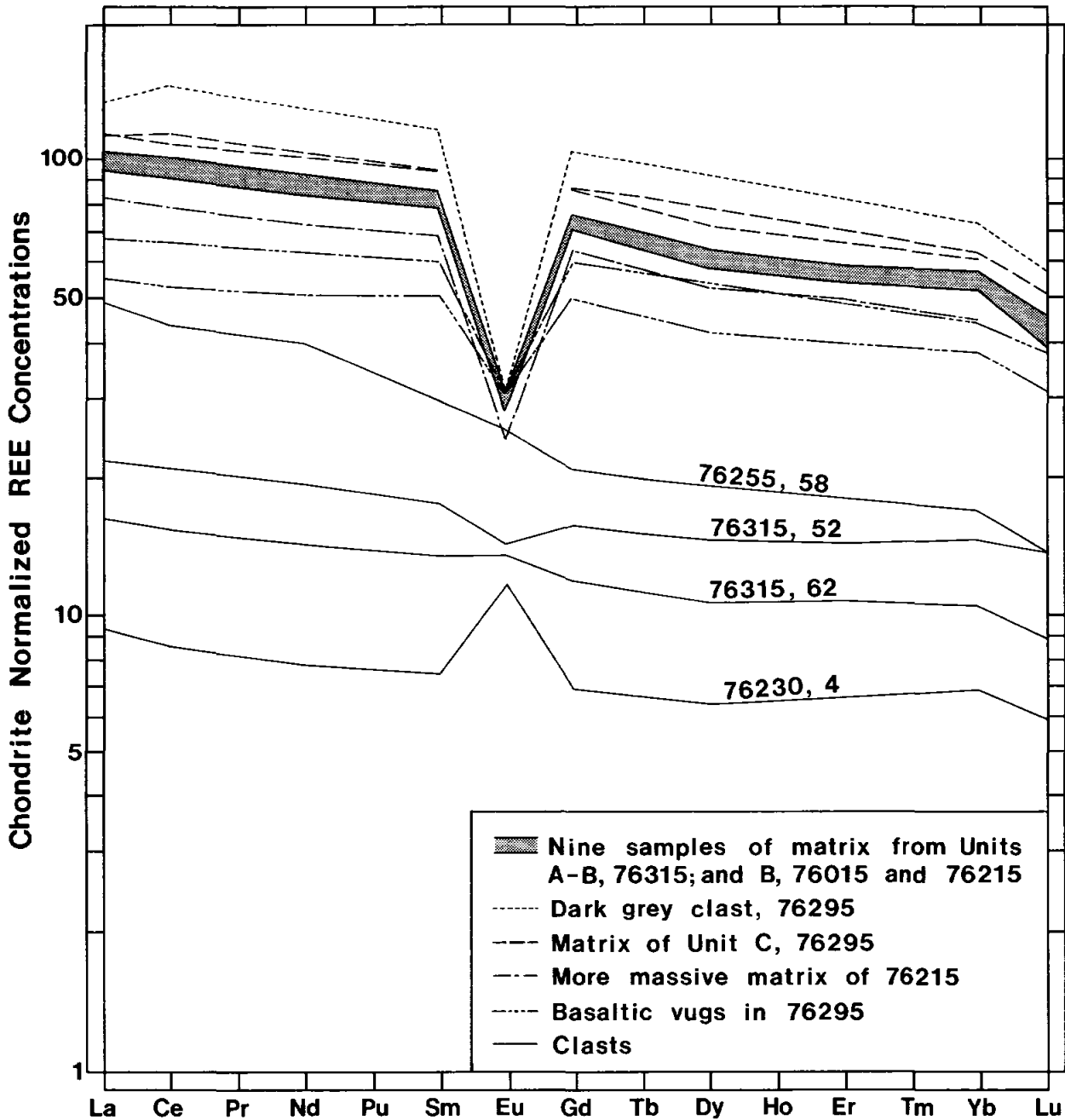


FIGURE 48: Rare Earth Element Patterns for various samples from the Station 6 Boulder, Apollo 17.

76295,46 and ,48 has much lower rare earth elements but much higher Ba, K and Rb than the matrices. The higher Ba, K and Rb are plausibly due to an "excess" or addition of K-feldspar or remobilized, low melting, ground mass. Three clasts: 76315,52; 76315,62; and 76230,4 are anorthositic and may represent early lunar crustal materials. Clast 76255,58 is another example of early lunar crustal material (Ref. 31A) but contains some contaminants. Its analysis is reported and the REE pattern plotted with the caution that there may be some aberrant values due to contaminants. One dark gray clast 76295,51 displays relatively high rare earth values and apparently is derived from a more KREEP-rich unit.

Meteoritic and Volatile Elements

Several samples from the Station 6 boulder were analyzed for trace elements, using radiochemical neutron activation analysis (Ref. 35-43). The results are given in Table 5.

Except for the troctolite clast, 76255,57 and the norite clast, 76255,56, samples are greatly enriched in the siderophile elements which are diagnostic of meteoritic material. Even the least enriched samples contain Ir, Re, and Au at 20-60 times the estimated indigenous levels.

A striking trend revealed by the ternary AuReIr plot, Fig. 49, is that matrix samples from Apollo 17 fall into Groups 2 or 3 while clasts, the basaltic vug, and crystalline or cataclastic rocks fall into other widely scattered groups. Most exceptions are in the gray foliated Boulder 1 from Station 2 (Wood consortium), whose matrix and clasts fall mainly into Group 3. This boulder came from near the crest of S. Massif, and may be derived from a different source than the Stations 6 and 7 rocks.

Of the three matrix samples from Station 6 that do not fall in Group 2 one is on the margin of Group 2 and the other 2 come from sample 76255 which is from the margin of a large norite clast and the matrix is extensively intermixed with the clast. Also all three of these matrix samples have very low siderophile element contents and hence would be the most susceptible to mixing, contamination, or errors.

Table 5. Siderophile and Volatile Trace Elements in Apollo 17 Rocks and Boulders (ppb, except Ni, Zn, Rb, F, Cl, Nb and Y ppm)

Ref.	Sample	Description	Ir	Re	Au	Ni	Sb	Ge	Se	Te	Ag	Br	Bi	Zn	Cd	Tl
36	76315,73	Un A bl mx	5.42	0.507	3.21	256	1.49	346	100	4.04	0.84	48	0.098	3.1	5.0	0.31
36	76315,74	Un A bl mx	5.97	0.575	3.48	260	1.54	354	107	5.1	0.88	44	0.28	3.4	6.4	0.34
38	76015,77	Un B mx	3.41	0.315	1.89	135	1.02	164	76		1.02	46.8	0.22	2.8	3.2	0.67
38	76215,48	Un B mx	0.829	0.070	0.526	54	0.44	31.5	60		0.87	50.5	0.34	2.5	1.08	0.63
38	76295,52	Un C dg c	5.42	0.456	3.93	203	2.11	423	68	1.9	1.20	37.5	0.56	2.6	1.28	0.33
38	76295,49	Bst vug	3.18	0.267	2.91	146	1.84	321	235	5.8	1.03	30.5	0.40	2.2	1.13	0.99
38	76295,37	Un C bl mx	7.88	0.566	4.36	250	3.93	316	103		4.55	78.7	0.97	27.1	6.56	1.41
38	76295,34	Un C t mx	6.10	0.486	3.43	379	1.68	374	132	4.6	5.09	27.9	0.80	2.5	1.00	0.64
38	76295,31	Un C lg c	5.98	0.480	2.65	90	1.03	198	75	2.4	0.87	23.5	0.46	2.3	1.88	0.44
36	76235,9	Un C wh c	22.5	1.69	6.66	62	1.45	328	38	2.6	0.66	9.6	0.15	1.2	0.63	0.097
41	76255,47	Un C mx 2	1.13	0.132	0.843	31	2.20	34.2	41	1.6	12.9	35.9	0.31	2.4	8.2	0.89
41	76255,52	Un C mx 1	1.21	0.112	0.380	≤15	0.20	9.6	19	2.5	1.29	15.8	0.37	2.3	6.4	1.0
41	76255,56	Un C norite C	0.042	0.028	0.178	387	0.11	6.6	49	1.1	0.70	9.2	0.20	2.0	2.0	0.96
41	76255,57	Un C wh c (troct)	0.019	0.0068	0.0093	423	2.40	2.2	0.6	5.9	0.34	7.8	≤2	0.5	67.5	5.4
41	76275,33	Un C ves c	7.76	0.725	5.10		2.00	383	125	9.8	1.22	72.7	≤0.5	4.0	8.8	1.4
41	76315,118	Un A lg c	18.6	1.85	6.40		0.85	57.7	71	3.4	0.72	39.2	0.44	2.0	12.1	1.6
43	76015,12	Un B mx										30				

bl = blue Bst = basaltic c = clast dg = dark gray ves = vesicular lg = light gray mx = matrix t = tan Un = unit wh = white

Table 5. (continued)

Ref.	Sample	Description	Rb	Cs	U	Os	Pd	In	F	Cl	Nb	Y
36	76315,73	Un A bl mx	5.91	245	1540							
36	76315,74	Un A bl mx	5.9	250	1490							
38	76015,77	Un B mx	5.77	156	1490							
38	76215,48	Un B mx	2.51	192	1120							
38	76295,52	Un C dg c	1.75	117	1940							
38	76295,49	Bst vug	12.5	383	757							
38	76295,37	Un C bl mx	9.20	154	1910							
38	76295,34	Un C t mx	4.22	302	1320							
38	76295,31	Un C lg c	3.31	196	1620							
36	76235.9	Un C wh c	0.448	29.5	190							
41	76255,47	Un C mx 2	5.36	184	3150	1.11	≤2.5	0.61				
41	76255,52	Un C mx 1	3.68	175	1170	1.91	≤2.5	9.76				
41	76255,56	Un C norite C	12.8	842	445	0.035	≤0.7	0.30				
41	76255,57	Un C wh c (troct)	0.19	6.3	19	≤0.03	≤4.3	0.77				
41	76275,33	Un C ves c	3.60	196	2350	8.60	19.8	12.4				
41	76315,118	Un A lg c	2.73	110	355	20.9	22.6	4.61				
43	76015,12	Un B mx							45.8	6.9	32	112

bl = blue Bst = basaltic c = clast dg = dark gray ves = vesicular lg = light gray mx = matrix
t = tan Un = unit wh = white

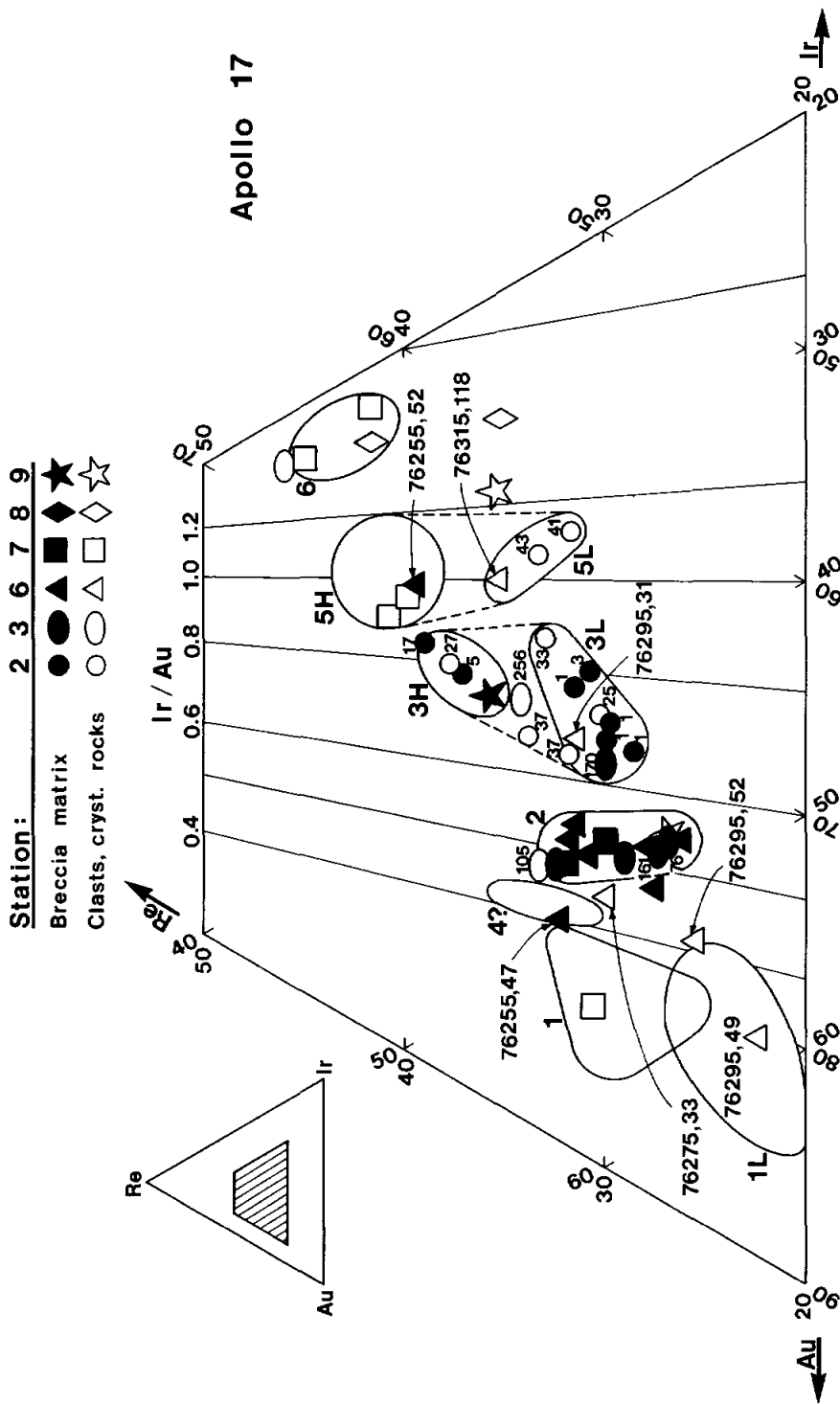


FIGURE 49: Meteoritic components, classified according to proportions of Au, Ir, and Re. Most Apollo 17 matrix samples fall into Groups 2 (Serenitatis projectile?) and 3. (The three exceptions all have low siderophile element contents and may hence be in error.) Clasts show a broader distribution. Numbers refer to samples from the Consortium Indomitabile (Morgan et al., 1975) or James Consortium (Morgan et al., 1976a).

The meteoritic component does not correlate with rock type. A given meteoritic component, such as 2, is found in rocks of widely different types.

The prevalence of Group 2 among the matrix samples has led to the suggestion that Group 2 represents the Serenitatis projectile (Refs. 38, 41).

The samples show differences in composition of non-meteoritic trace elements that do not correlate well with gross lithology. The two samples of green-grey, Unit B matrix differ appreciably in their content of Rb and U (the two elements most diagnostic of bulk chemistry and mineralogy).

Unit C blue matrix (76295,37) shows the highest abundance of the volatile elements Br, Bi, Zn, Cd, and Tl. Though this sample also has the highest content of 4 of the 6 meteoritic siderophiles, the enrichment in volatiles is disproportionately greater, and cannot come from the projectile alone. Much of it must be indigenous, and is probably related to the high KREEP, Rb, and U content of this sample. The tan matrix from Unit C (76295,34) and blue matrix from Unit A (76315,73 and 74) are substantially lower in Rb and U, as well as in most of the above volatiles.

The basaltic vug (76295,49) has the lowest U content, but surprisingly, the highest Rb and Cs content of 11 samples. The anomalous alkali content suggests enrichment by vapor deposition but of the remaining volatiles, only Se and Te show a substantial enrichment in this sample.

The clasts have high U-contents, but rather low Rb contents. These low Rb/U ratios and distinctive meteoritic components are the chief chemical differences between clasts and matrix registered by the suite of trace elements.

Carbon and Sulfur

Total carbon and sulfur analyses have been performed on thirteen samples from the Apollo 17 Station 6 boulder (Table 6). Total carbon abundances range from 36 to 105 $\mu\text{gC/g}$ for matrix material whereas the porous clast from 76015 contained 214 $\mu\text{gC/g}$. Total sulfur abundances ranged from 318 to 1019 $\mu\text{gS/g}$. The C and S abundances are similar to those observed previously for recrystallized breccias.

Table 6. Sulfur and Carbon in Station 6 Boulder

<u>Sample Number</u>	<u>μgS/g</u>	<u>Ref.</u>	<u>μgC/g</u>	<u>Ref.</u>	<u>Description</u>
76015,32	895 ± 40	33	51 ± 5	*	matrix; Unit B
76015,58	641 30	33	72 5	*	matrix, Unit B
76015,59	834 30	33	38 7	*	matrix, Unit B
76015,65	679 30	33	84 8	*	matrix, Unit B
76015,70	552 30	33	214 8	*	porous clast in Unit B
76215,26	1019 30	*	43 4	*	more porous matrix, Unit B
76215,29	695 20	*	73 8	*	less porous matrix, Unit B
76230,4	270 20	33			
76235,8	318 20	*	36 4	*	brecciated olivine norite clast in Unit C
76295,40	731 30	*	105 10	*	blue matrix, Unit C
76315,2	756 40	33	-	*	composite sample (PET), matrix, Unit A-B
76315,33	948 30	33	72 5	*	gray phase, noritic matrix, Unit A-B
76315,65	781 20	33	69 5	*	dark gray clast 3, Unit A-B

*E. Gibson (unpublished)

Three separate samples from the breccia 76315 produced sulfur concentrations of 755, 950 and 785 $\mu\text{gS/g}$ for (a) composite sample (split, 2), (b) dark gray phase (split, 33) and (c) blue-gray phase (split, 65). The carbon abundance for the dark gray phase was 72 $\mu\text{gC/g}$ and the blue-gray phase contained 69 $\mu\text{gC/g}$. The PET sample (split, 2) was not analyzed for carbon because the sample had been powdered in a boron carbide mortar and pestle and was obviously contaminated. The similarities in total carbon content between the gray phase and the blue-gray phase are in agreement with the trace element data of other analysts for different regions of 76315.

Four matrix samples and one porous clast from breccia 76015 were analyzed for total carbon and sulfur. Matrix samples contained carbon abundances of: 51, 72, 38 and 84 $\mu\text{gC/g}$. Sulfur abundances for the same samples were 895, 641, 834 and 680 $\mu\text{gS/g}$. Wide variations in C and S content within the matrix is of extreme importance in noting variations of composition within an individual rock. Total carbon and sulfur analysis of the porous clast indicated that the sample contained 214 $\mu\text{gC/g}$ and 552 $\mu\text{gS/g}$. The sample had been processed using both the band saw and wire saw. Caution was given for possible contamination with molybdenum sulfide within the sample. However, the total sulfur abundances found for the clast indicated it was either very low in sulfur (552 $\mu\text{gS/g}$) or no contamination from MoS had occurred. Total carbon analysis of the porous clast produced the highest carbon value found for a lunar breccia from Apollo 17 (214 $\mu\text{gC/g}$). At the present time carbon contamination cannot be ruled out.

Sample 76235 contained the lowest carbon and sulfur of any of the Station 6 samples. These low C and S values are a reflection of the sample's composition. Olivine norites are typically depleted in carbon and sulfur.

Variations in both total carbon and sulfur abundances within a single lunar rock are important observations. Interpretations of data from a single sample of fragmental rock of this nature should be taken with extreme caution.

Noble Gases

The abundances and isotopic compositions of the five noble gas elements have been measured in six different Station 6 boulder samples (Table 7). Three analyses, including our only data for 76255, were on preliminary surface chips.

The data for these three analyses are largely dominated by a solar wind component, either directly implanted or from contaminating fines. A neon isotope correlation plot (Fig.50) demonstrates that our sample of 76015,71 also contained considerable solar-wind gas; 76235,2 and 76315,63 may have contained a small amount of solar wind Ne. All other Ne data are consistent with a mixture of cosmic ray-produced Ne and atmospheric Ne (adsorbed and blanks). With the above exceptions, most samples analyzed contained low noble gas concentrations, and appear essentially devoid of solar wind gases.

Essentially all of the ^4He and ^{40}Ar present can be attributed to radiogenic decay. Other noble gas isotopes are dominated by a cosmic ray-produced component. Variable amounts of fission-produced Xe are present in concentrations comparable to the concentrations of cosmogenic Xe, which makes precise definition of the fission Xe or cosmogenic Xe spectra difficult. The amounts of fission Xe present are roughly consistent with measured U concentrations and a gas-retention age of 4 Aeons. Isotope correlation plots for Xe in the stepwise temperature extraction of 76315 were previously presented (Ref. 34). All additional boulder data (not tabulated) are essentially consistent with the trends shown for 76315. There is no evidence in these samples for fission Xe other than that produced by in situ decay of ^{238}U . All Kr isotopic data (not tabulated) is also consistent with adsorbed air plus a cosmogenic component (e.g., Fig. 51). The isotopic composition of the cosmogenic Ne and Xe also indicate irradiation under conditions of low shielding, i.e., essentially in the present position of the boulders.

Concentrations of cosmogenic ^{21}Ne and ^{38}Ar are nearly the same in the various samples, and those variations which exist are probably due to small differences in major element chemistry and shielding. Larger variations in cosmogenic ^{126}Xe are also probably due to target element variations; e.g., [Ba] measured in samples adjacent to 76315,34 and 76315,63 differed by nearly a factor of 5 (Ref. 45).

Table 7. Apollo 17, Station 6 Boulders: Noble Gas Abundances (cm³ STP/g)

Sample	type	wt. mg.	³ He 10 ⁻⁸	⁴ He 10 ⁻⁴	²² Ne 10 ⁻⁸	³⁶ Ar 10 ⁻⁸	⁴⁰ Ar 10 ⁻⁵	⁸⁴ Kr 10 ⁻¹⁰	¹³² Xe 10 ⁻¹⁰	²⁰ Ne ²² Ne	²² Ne ²¹ Ne	³⁶ Ar ³⁸ Ar	Spallation concentration (cm ³ /g)		
													²¹ Ne 10 ⁻⁸	³⁸ Ar 10 ⁻⁸	¹²⁶ Xe 10 ⁻¹²
76315,6	(b)	19.6	39.5	15.6	85.4	233	7.43	26.5	4.56	12.63 ± .03	19.74 ± .19	5.25 ±.04	1.6	(0.9)	(5)
76295,5	(b)	22.0	46.6	19.4	173	524	13.1	60.2	6.64	12.64 ± .03	25.07 ± .39	5.31 ±.03	1.3	(0.9)	(6)
76255,9	(b)	50.5	21.7	18.7	53.4	175	10.9	18.4	2.00	12.40 ± .03	17.03 ± .10	5.20 ±.02	1.45	(.10)	(2)
76315,34	matrix	129.6	8.25	8.02	2.5 ^a	<25	12.2	<8	2.27	3.51 ^a	1.68 ^a	4.28 ±.30	1.44	<1.3	7.4
76315,63	clast	99.6	4.31	0.975	3.9 ^a	<3.5	3.97	4.6	1.55	5.42 ^a	1.75	2.44 ±.03	0.95	0.87	0.8
76315,66	clast	83.7	7.01	7.89	4.3 ^a	< 3	12.8	4.0	2.60	3.06 ^a	1.46 ^a	4.17 ±.03	1.36	---	6.3
76015,71	clast	52.7	11.5	2.84	10.5	19	19.1	3.5	0.67	11.19 ± .06	6.60 ± .06	4.21 ±.03	1.30	(1.0)	---
76015,60	matrix	162.8	6.61	6.93	1.59	<2.5	11.8	2.2	0.31	1.34 ^a	1.21 ± .05	1.78 ±.10	1.31	0.97	3.0
76235,2	anortho- sitic clast	136.3	3.37	0.55	1.21	1.14	1.81	3.4	0.63	4.68 ±.10	1.64 ±.05	1.42 ±.03	0.72	0.68	0.1 ^c
76295,36	350°C	62.1	---	0.003	---	0.04 ^a	0.017	1.7 ^a	0.65 ^a						
	1640°C		7.66	10.4	<11	00.51 ^a	8.28	0.84 ^a	0.29 ^a	<8.7 ^a	<6.9 ^a	<1.0 ^a	1.35	0.71	1.9 ^c
76295,39	350°C	159.6	---	0.005	---	0.03	0.010	1.28	0.37						
	1640°C		7.16	8.03	<4.2	0.71	8.73	1.10	0.21	<6.6 ^a	<3.0 ^a	1.11 ±.05	1.32	0.58	2.2 ^c

Table 7. (continued)

Sample	type	wt. mg.	^3He 10^{-8}	^4He 10^{-4}	^{22}Ne 10^{-8}	^{36}Ar 10^{-8}	^{40}Ar 10^{-5}	^{84}Kr 10^{-10}	^{132}Xe 10^{-10}	$\frac{^{20}\text{Ne}}{^{22}\text{Ne}}$	$\frac{^{22}\text{Ne}}{^{21}\text{Ne}}$	$\frac{^{36}\text{Ar}}{^{38}\text{Ar}}$	Spallation concentrations (cm^3/g)		
													^{21}Ne 10^{-8}	^{38}Ar 10^{-8}	^{126}Xe 10^{-12}
76215,41	325°C	195.3	---	0.002	---	0.09	0.026	2.48	0.76	---	---	5.1	---	---	---
	800°C		8.23	5.56	0.057 ^a	0.25	2.49	0.73	0.41	$\leq 6.5^a$	$\leq 2.6^a$	1.08 +0.05	0.05	0.21	0.5
	1200°C		0.32	0.40	2.12 ^a	0.19 ^a	4.59	1.69	0.16	4.0 ^a	1.7 ^a	≤ 0.68	1.22	0.30	2.5
	1640°C		---	0.006	<0.2	<0.16	1.39	0.69	<0.045	$\leq 9^a$	$\leq 12^a$	1.05 +0.02	0.11 $\Sigma=1.38$	0.14 $\Sigma=0.65$	0.6 $\Sigma=3.6$
76315,34	500°C	919.4	3.91	3.92	0.019	0.58	0.87	0.67	0.43	5.7 +0.5	2.65 +0.27	4.93 +0.03	0.008	0.010	---
	700°C		3.22	3.10	0.062	0.53	2.15	0.13	0.050	2.34 +0.20	1.45 +0.04	3.98 +0.03	0.042	0.039	0.29
	900°C		0.35	0.24	0.82	0.66	4.10	0.16	0.039	0.91 +0.03	1.21 +0.01	3.01 +0.05	0.67	0.11	0.14
	1100°C		0.17	0.10	0.59	0.99	2.68	0.33	0.087	0.9 ^a	1.18 +0.03	2.64 +0.09	0.50	0.22	1.54
	1300°C		0.06	0.02	0.23 ^a	1.35	2.08	0.34	0.141	<4.7	1.3 ^a	2.25 +0.03	0.18	0.40	3.01
	1500°C		---	---	<0.26	1.03	0.17	0.10	0.35	5.5 ^a	---	2.28 +0.04	0.10 $\Sigma=1.50$	0.30 $\Sigma=1.08$	0.49 $\Sigma=5.5$

Most measured gas concentrations are estimated at +5-10% for He, Ne, ^{40}Ar , and Xe and +10-15% for ^{36}Ar and Kr. (a) This data had blank corrections >15%, which produces additional uncertainty in abundance. Concentrations marked as upper limits had blanks >50%, which were not applied. (b) These samples were preliminary surface chips. Spallation gas concentrations in () are approximate because of high trapped gas concentrations. (c) These spallation ^{126}Xe concentrations were calculated from ^{128}Xe concentrations and $^{128}\text{Xe}/^{126}\text{Xe} = 1.5$.

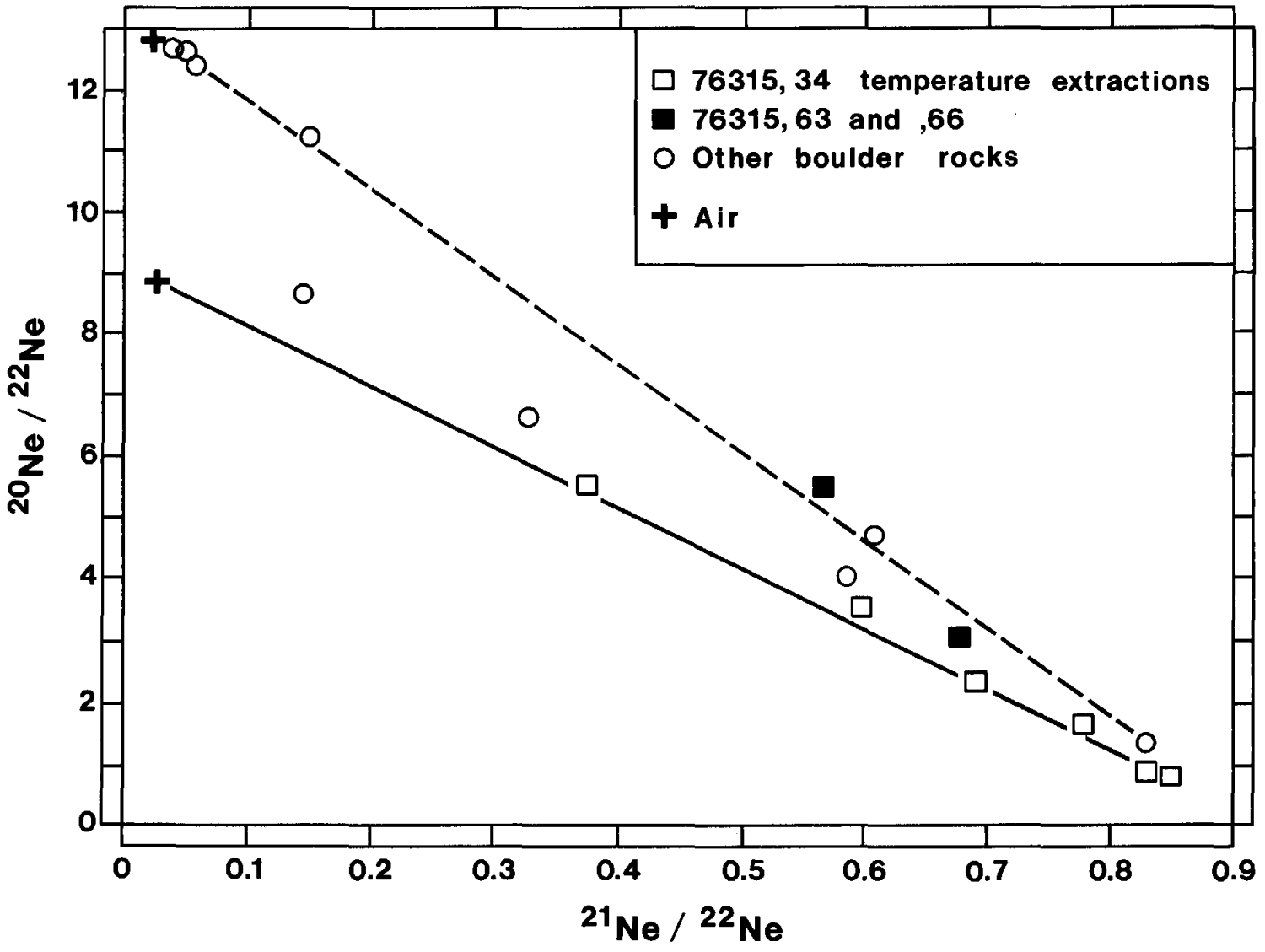


FIGURE 50: Neon isotope correlation plot comparing boulder samples from Station 6.

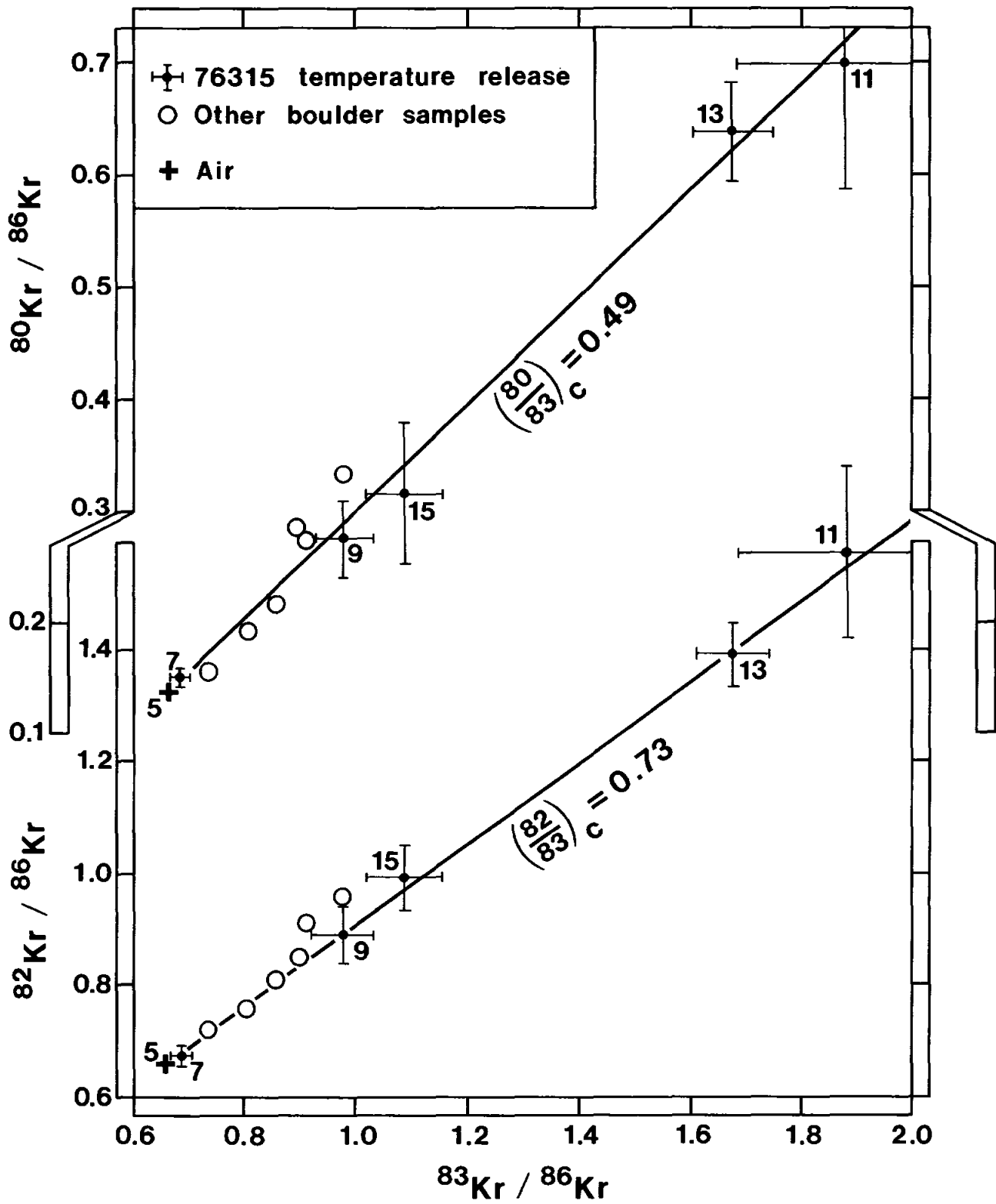


FIGURE 51: Krypton isotope correlation plot comparing boulder samples from Station 6.

Lower limits to the exposure ages of all these samples of ~10 m yr. can be calculated by using production rates derived for 2π irradiation geometry. In fact, self shielding of the large boulders makes the actual irradiation geometry for most samples more like 1.5π (USGS, Apollo 17 Interagency Report: Astrogeology 72). This factor would bring the noble gas ages into essential agreement with the more precise ^{81}Kr age for 76315 of 21 ± 2 m yr. (Ref. 49). However, rock 76015 had little self-shielding from the boulders, and its corrected noble gas exposure age would be consequently lower than for the other rocks (although its cosmogenic ^{21}Ne and ^{38}Ar concentrations are essentially identical to those for 76315). This is in agreement with the lower ^{81}Kr age reported for 76015 (Ref. 49).

Gamma Counting

The gamma ray counting data for Station 6 rocks (Table 8), obtained primarily during the Apollo 17 preliminary examination, indicates that all analyzed rocks have over 0.2% K_2O and confirms the estimates made from modal mineralogy that with the exception of 76230 all samples should have low-K KREEP chemistry. The K/U ratio of 5000 for 76255 is unique in accord with its unusual texture, which includes feldspar and exsolved pigeonite bound together with a low-K KREEP-like melt. Analyses of three soils from Station 6 are included to show the lower K, U, and Th values than exist in the rocks.

Geochronology

Eleven samples (Table 9) of the melt rock, or noritic breccia, which forms the matrix of the boulder produce a Rb-Sr isochron of about $4.03 \pm .21$ b.y. with an initial $^{87}\text{Sr}/^{86}\text{Sr}$ of $.69969 \pm 32$. Including the additional six samples of matrices from the other Apollo 17 noritic breccias listed in Ref. 45 further constrains the isochron to $4.02 \pm .09$ b.y. and an initial ratio of $.69973 \pm 15$ (Fig. 52). Four anorthositic rocks from Apollo 17 including two from the Station 6 boulder lie on a slightly older isochron at $4.09 \pm .33$ b.y. with initial ratio of $.69924 \pm 17$.

TABLE 8.- GAMMA-RAY COUNTING DATA FOR STATION 6 ROCKS

	Green-grey poikilitic rock	Green-grey poikilitic rock	Complex breccia with blue- grey area	Blue-grey impact basalt	Blue-grey impact basalt		Shadowed soil	Unshadowed soil nearby		Unshadowed soil
Sample	76015,0	76215,0	76255,0	76275,0	76295,0	76295,0	76240,2	76261,1	76261,1	76501,4
WEIGHT (g)	2819.0	642.8	393.2	55.93	260.7	260.7	104.98	100.7	100.7	97.89
LAB ^a	ES	RCL	BNW	BNW	ORNL	BNW	BNW	RCL	BNW	ORNL
Th (ppm)	8 ± 3	4.6 ± .2	2.33 ± .05	5.4 ± .4	5.30 ± .27	5.76 ± .17	2.30 ± .06	2.1 ± .3	1.92 ± .04	1.39 ± .14
U (ppm)	2 ± .3	1.27 ± .06	.58 ± .02	1.39 ± .10	1.50 ± .08	1.55 ± .05	.60 ± .02	.49 ± .02	.51 ± .02	.38 ± .04
K (%)	.30 ± .06	.215 ± .014	.291 ± .006	.222 ± .009	.227 ± .011	.230 ± .009	.110 ± .005	.102 ± .003	.097 ± .004	.090 ± .005
²⁶ Al (dpm/kg)	detected	56 ± 3	79 ± 4	111 ± 9	67 ± 5	71 ± 4	151 ± 6	182 ± 17	171 ± 5	90 ± 9
²² Na (dpm/kg)	detected	60 ± 4	71 ± 4	95 ± 6	54 ± 4	64 ± 3	42 ± 2	148 ± 8	142 ± 4	90 ± 9
⁵⁴ Mn (dpm/kg)	detected	22 ± 17	38 ± 9	103 ± 20	38 ± 15	70 ± 30	31 ± 8	93 ± 7	106 ± 8	60 ± 10
⁵⁶ Co (dpm/kg)	detected	45 ± 6	37 ± 4	64 ± 6	41 ± 7	35 ± 5	27 ± 3	240 ± 20	245 ± 8	120 ± 12
⁴⁶ Sc (dpm/kg)	detected	5 ± 3	3.9 ± 1.3	7 ± 2	5 ± 2	6.4 ± 2.6	8 ± 4	23 ± 2	27 ± 3	18 ± 4
⁴⁸ V (dpm/kg)		<24	5.7 ± 2.6				2.6 ± 1.4	18 ± 12	19 ± 10	15 ± 10
⁶⁰ Co (dpm/kg)		<.4		<1.1		<1.2	.8 ± .4	12 ± 5	<1.5	
⁷ Be (dpm/kg)	detected									
⁵¹ Cr (dpm/kg)	detected									
⁵⁷ Co (dpm/kg)										
⁵⁸ Co (dpm/kg)	detected									
Th/U	4 ± 1.6	3.6 ± .2	4.0 ± .2	3.9 ± .4	3.5 ± .3	3.7 ± .2	3.3 ± .2	4.3 ± .6	3.8 ± .2	3.7 ± .5
K/U	1500 ± 400	1690 ± 140	5000 ± 200	1600 ± 130	1510 ± 110	1500 ± 80	1800 ± 100	2100 ± 100	1900 ± 110	2400 ± 300

^aKey to laboratories

BNW - L. A. Rancitelli, R. W. Perkins,
W. D. Felix and N. A. Wogman
Battelle, Pacific Northwest Laboratories

RCL - J. E. Keith and R. S. Clark
NA - NASA-Johnson Space Center
W. R. Portenier and M. K. Robbins
Northrop Services, Incorporated

ES - Ernest Schonfeld
NASA-Johnson Space Center

ORNL - G. D. O'Kelley, J.
S. Eldridge and
K. J. Northcutt
Oak Ridge National
Laboratory

Table 9. Rb and Sr Data for Station 6 Boulder

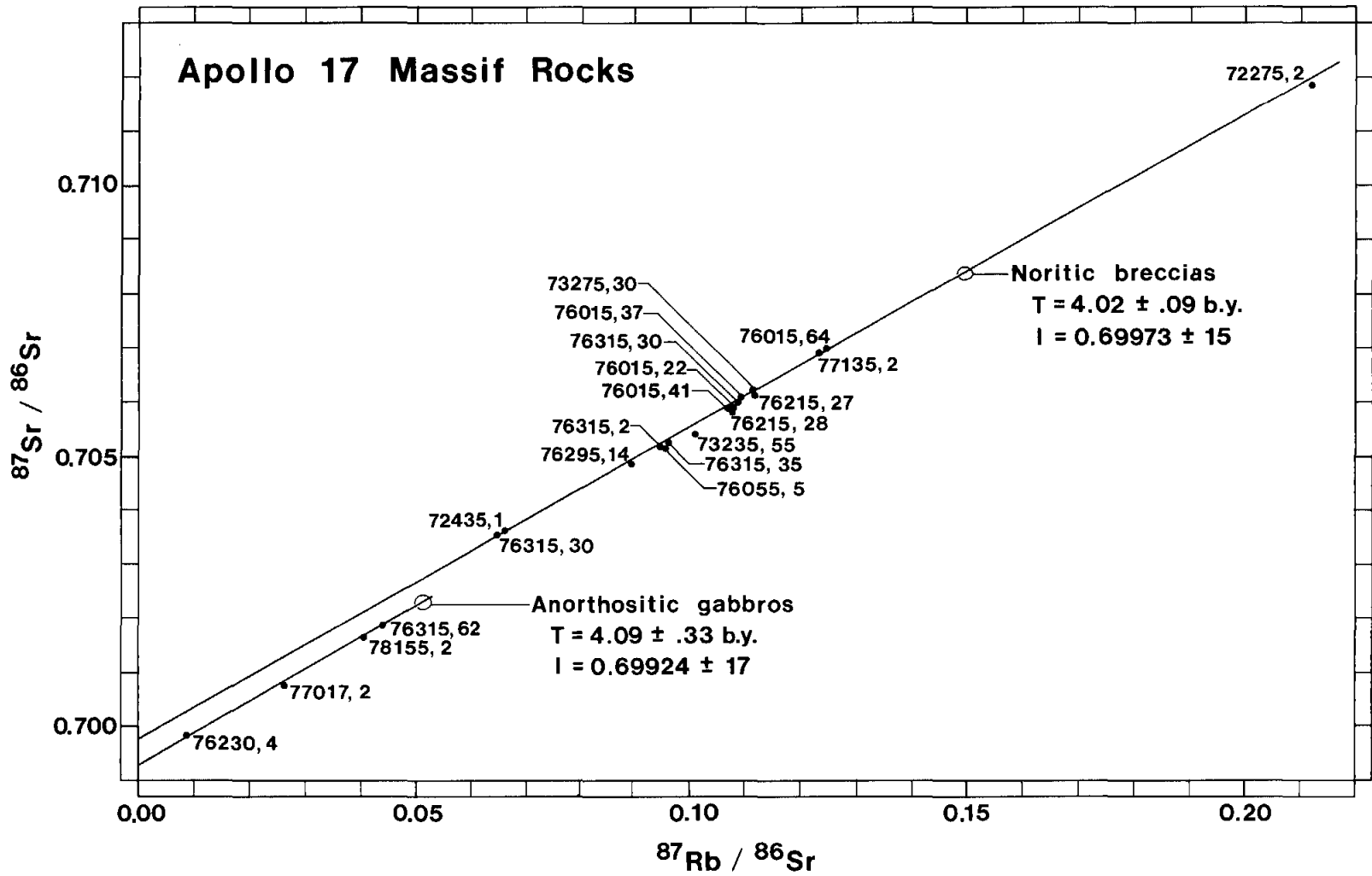
Sample	Pet. Type	wt. (mg)	Rb (ppm)	Sr (ppm)	$\frac{87\text{Rb}}{86\text{Sr}}$ ^(a)	$\frac{87\text{Sr}}{86\text{Sr}}$ ^(a)	TBABI ^(b) (AE)	Ref.
76015,22	Matrix	52	6.41	172	0.1079 ± 9	0.70589 ± 5	4.39 ± .07	45
,37	"	54	6.67	176	0.1088 ± 9	0.70605 ± 5	4.45 ± .07	45
,41	"	64	6.57	177	0.1076 ± 9	0.70589 ± 11	4.40 ± .11	45
,64	"	52	7.46	174	0.1242 ± 10	0.70693 ± 6	4.40 ± .07	45
76315,2	Matrix	52	5.88	180	0.0948 ± 8	0.70515 ± 6	4.45 ± .08	45
,30	Dark clast	67	3.85	172	0.0650 ± 6	0.70351 ± 10	4.72 ± .14	45
,30	Matrix	52	6.56	175	0.1086 ± 9	0.70595 ± 5	4.40 ± .08	45
,35	"	49	5.78	174	0.0960 ± 8	0.70521 ± 7	4.44 ± .09	45
,52	White rind	39	3.73	115	0.0937 ± 9	0.70491 ± 6	4.33 ± .08	45
,62	Light grey cl	52	2.34	153	0.0441 ± 5	0.70185 ± 5	4.35 ± .13	45
76215,27	Matrix, porous	66	6.89	178	0.1119 ± 10	0.70608 ± 6		(c)
,28	Matrix	54	6.10	164	0.1079 ± 10	0.70578 ± 6		(c)
76295,14	Matrix, blue	51	5.43	175	0.0899 ± 9	0.70489 ± 6		(c)
,46	Basaltic vug	47	20.5	191	0.311 ± 3	0.71717 ± 5	4.07 ± .04	(c)

(a) Uncertainties refer to last figures and are 2_{mean} for $^{87}\text{Sr}/^{86}\text{Sr}$

(b) For BABI = 0.69910

(c) Unpublished data from L. Nyquist

FIGURE 52: Rb-Sr isotopic data for the breccias and clasts from massif rocks at Apollo 17.



The Sr-Rb isotopic data for the basaltic vug sample, 76295,46, is worth mentioning. It has the highest $^{87}\text{Rb}/^{86}\text{Sr}$ ratio of any Apollo 17 "whole rock" material yet analyzed. Its ratio of 0.311 is a factor 3 higher than that of typical Apollo 17 noritic breccia matrices and comparable to, but slightly higher than, "typical" KREEP. The $^{87}\text{Sr}/^{86}\text{Sr}$ ratio is 0.71717 ± 0.00005 giving it a BABI model age of $4.07 \pm .04$ AE, an upper limit to its age. Assumption of initial $^{87}\text{Sr}/^{86}\text{Sr} = 0.69974 \pm 0.00015$ as determined from an Apollo 16 whole rock isochron for noritic breccias (Ref. 45) yields $T = 3.92 \pm 0.08$ AE. The Rb-Sr data for this sample are consistent with the previously determined whole rock isochron parameters but extend the range of $^{87}\text{Rb}/^{86}\text{Sr}$ by ~60%.

Three samples of 76315 were analyzed by the $^{40}\text{Ar}/^{39}\text{Ar}$ method; (1) ,36, a 47 mg fragment of typical matrix, (2),67, a 91 mg sample of clast 3 material and (3) a 42 mg fragment of poikiloblastic white clast 2 chipped from sub-sample 61 (Ref. 46). The results of these analyses are shown graphically in Figures 53, 54, and 55.

For matrix sample 76315,36, the high apparent ages in the initial gas release imply that this sample has lost very little radiogenic argon. These high ages continue in the form of a plateau at 3.98 ± 0.04 Gy before dropping to 3.8 Gy at high temperatures. It has become an accepted procedure to use the "intermediate plateau" as indicating the most meaningful argon retention age which in this case is 3.98 ± 0.04 Gy.

The low temperature ($^{38}\text{Ar}_c/^{37}\text{Ar}$) ratios are essentially constant, corresponding to release of argon derived solely from calcium. A cosmic ray exposure age of 16 ± 2 m.y. is determined on the basis of a nominal production rate of 1.4×10^{-8} cc

STP $^{38}\text{Ar}/\text{g}$ ca m.y. This calculation ignores variation in production rate with depth (spectral hardness) or the possibility of a less than 2π irradiation geometry for 76315.

$(^{38}\text{Ar}_\text{C}/\text{Ca})$ increases dramatically at high temperatures due to the release of $^{38}\text{Ar}_\text{C}$ produced by high energy spallation reactions on Fe in the pyroxene and olivine and also on Ti. This increase in $(^{38}\text{Ar}_\text{C}/\text{Ca})$ implies a very hard (primary) energy spectrum for the cosmic rays. This would imply that 76315 has been exposed to cosmic rays only in its present surface location, and that prior to Boulder 6 rolling down the hill 76315 was in a completely shielded situation.

The $(^{40}\text{Ar}^*/^{39}\text{Ar}^*)$ release pattern from 76315,67 (dark clast 3) is very similar to that from the matrix. A comparison of the $(^{39}\text{Ar}^*/^{37}\text{Ar})$ release pattern suggests that the two samples have almost identical chemistry apart from a higher (K/Ca) ratio in the "low temperature" sites of 76315,67. There is an extended age plateau corresponding to 3.97 ± 0.04 Gy, followed by the characteristic high temperature decrease.

Once again the drop in apparent age at high temperatures coincides with a remarkable increase in $(^{38}\text{Ar}_\text{C}/\text{Ca})$, indicating argon release from the Fe rich minerals. Based on the low temperature $(^{38}\text{Ar}_\text{C}/\text{Ca})$ ratios and using the same assumptions as before, a nominal cosmic ray exposure age of 18 ± 3 m.y. is obtained for clast 3 material.

Sample 76315,61 of light gray clast 2 displays significantly different patterns. After exhibiting a small degree of radiogenic argon loss, the apparent ages rise to a plateau at 3.98 ± 0.05 Gy while at higher temperatures there is a small but significant rise to 4.10 ± 0.05 Gy. The $(^{39}\text{Ar}^*/^{37}\text{Ar})$ ratios vary only slightly, after an initial decrease, suggesting a relatively uniform chemical composition, dominated by plagioclase, and in contrast to the matrix and dark clast.

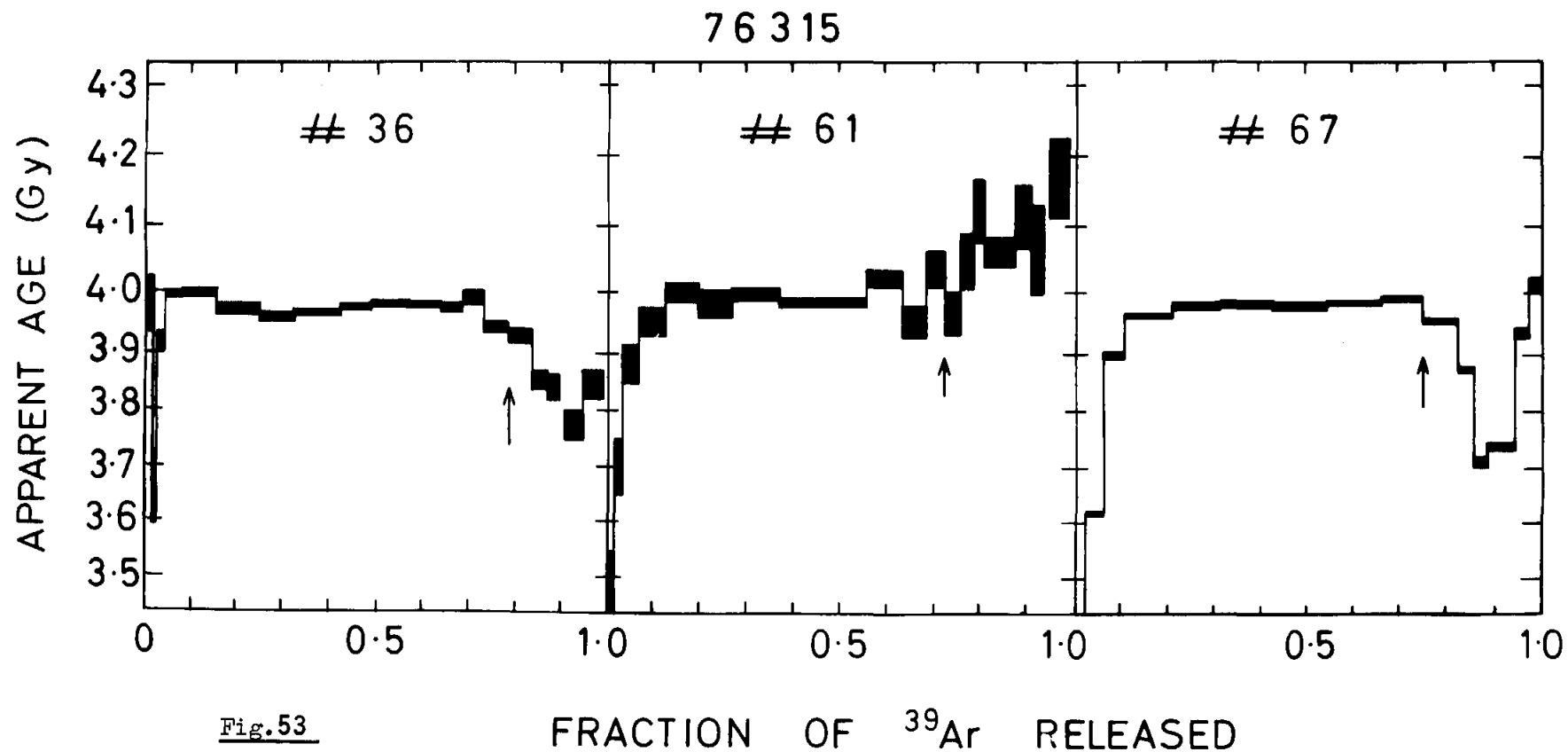


Fig.53

Apparent age as a function of $^{39}\text{Ar}^*$ release. All three samples yield identical plateau ages of (3.98 ± 0.04) Gy. The arrows indicate the temperatures above which excess $^{38}\text{Ar}_c$ is released. The matrix (76315, 36) and dark clast (76315, 67) show a decrease in apparent age above this temperature a characteristic of many lunar breccias. The light coloured clast (76315, 61) shows an increase which may indicate that it was originally formed at 4.10 GY or earlier.

76315

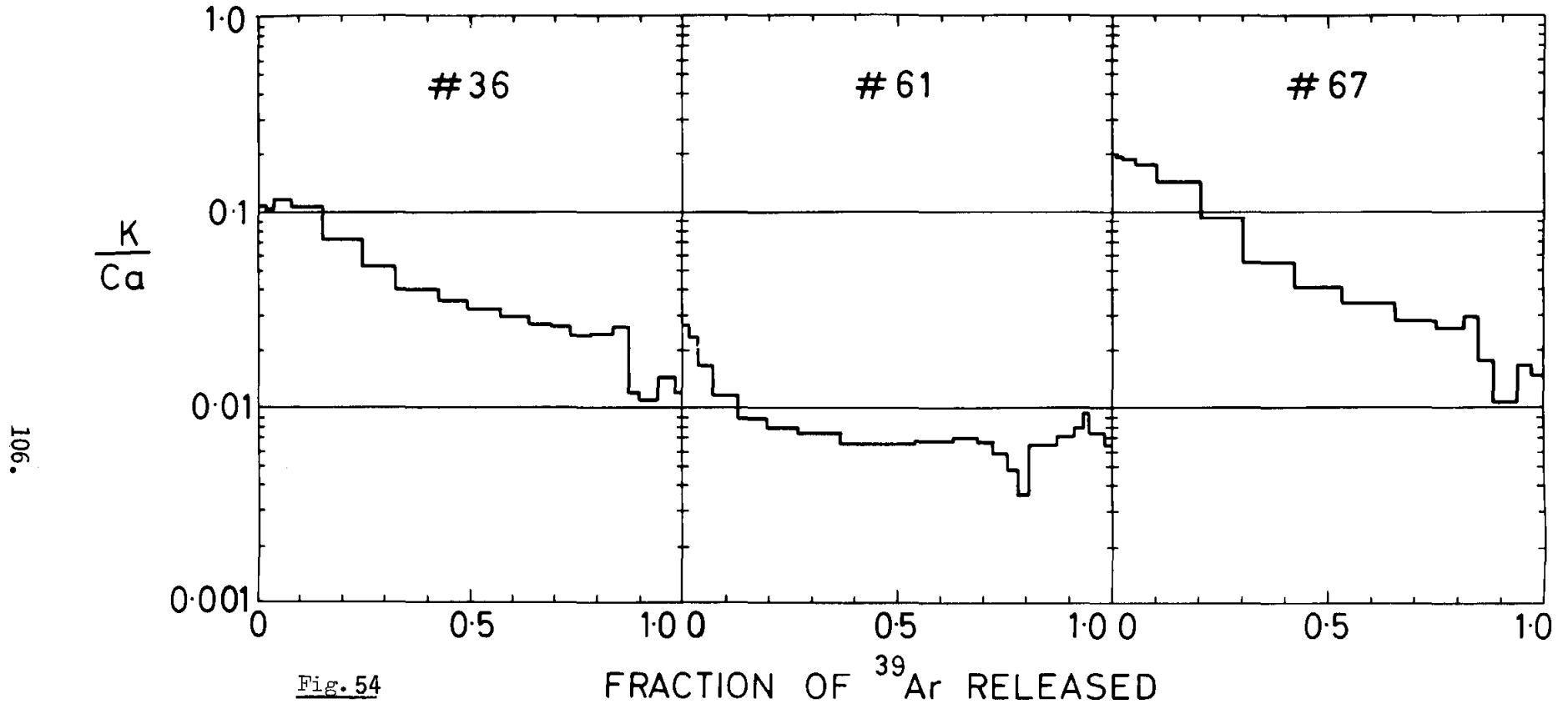


Fig. 54

FRACTION OF ^{39}Ar RELEASED

K/Ca, determined from $^{39}Ar^*/^{37}Ar$, as a function of $^{39}Ar^*$ release. The release patterns from matrix (76315, 36) and dark clast (76315, 67) show similar patterns, reflecting their chemical similarity. The slightly higher initial K/Ca from the dark clast indicates the presence of a higher proportion of unretentive K-rich sites. The pattern from the light coloured clast (76315, 61) is relatively constant, after an initial sharp decrease. This suggests a distinctly different and relatively uniform mineralogy presumably dominated by plagioclase.

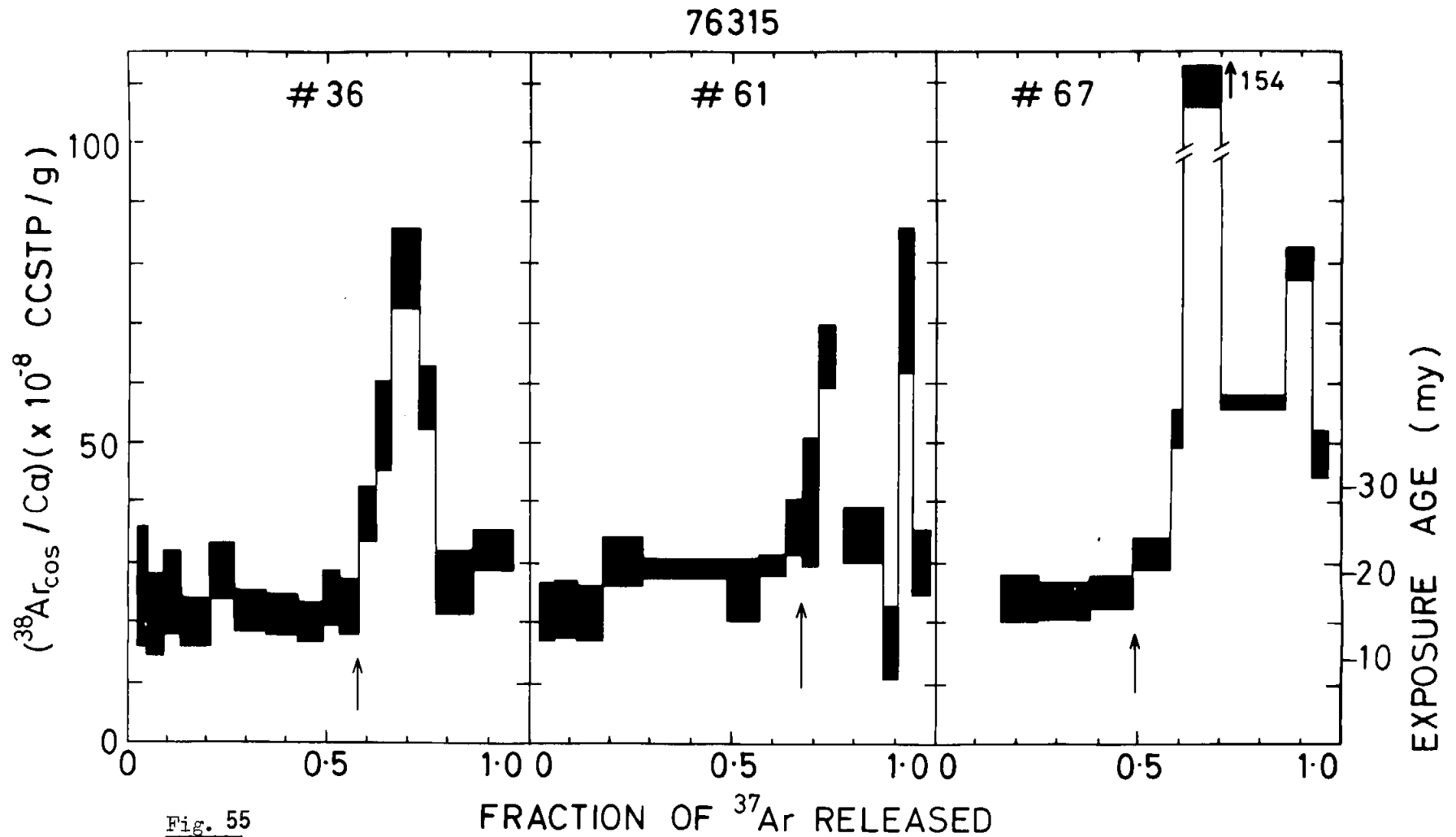


Fig. 55

$(^{38}\text{Ar}/\text{Ca})$, determined from $(^{38}\text{Ar}/^{37}\text{Ar})$, as a function of ^{37}Ar release. The arrows correspond to those shown in Fig. 1. Exposure ages from all three samples, based on the low temperature extractions, are essentially identical at (17 ± 3) My. All three samples release excess cosmogenic ^{38}Ar at high temperatures from heavy target elements (Fe, Ti). The effect is most pronounced in subsamples 36 and 67.

Uranium-Thorium-Lead

Table 10. U-Th-Pb in Station 6 Boulder

The following unpublished U, Th and Pb data were obtained by Leon Silver.

	U ppm	Th ppm	Pb ppm	Pb ²⁰⁶ / ₂₀₇	Pb ²⁰⁷ / ₂₀₄	Pb ²⁰⁸ / ₂₀₄
76015,53 matrix, Unit B	1.495	5.109	3.287	542.20	276.34	537.31
76295,28 matrix, Unit C	1.764	6.548	3.653	392.59	200.06	396.77
76315,71 matrix, Unit A-B	1.274	4.192	2.760	799.1	397.9	752.3
76315,72 dark clast in Unit A-B	0.758	2.793	2.894	56.79	36.93	72.37
76315,71 acid washed	1.084	3.845	2.227	1925.3	1084.1	1782.5
76315,72 acid washed	1.066	3.494	2.339	763.2	436.8	738.0

AGE:

76015,53: slightly discordant, above concordia line. Very similar to previous data on breccias.

76295,28: concordant at 4.28.

The (Fe/Ca) ratio in this sample is much lower than in the matrix or dark clast. In consequence the ($^{38}\text{Ar}_C/\text{Ca}$) ratios do not show a large high temperature enhancement. The low temperature ($^{38}\text{Ar}_C/\text{Ca}$) ratios imply a cosmic ray exposure age of 17 ± 3 m.y. identical to that of matrix and dark clast.

The rise in apparent age to 4.10 ± 0.05 Gy at high temperature may be indicative of an earlier period of existence for the clast material prior to incorporation in 76315. It is worth noting that the Rb-Sr data (Ref. 45) show that large scale Sr isotope homogenization between clast and matrix did not occur at 3.98 Gy and it is, therefore, conceivable that the clast was not fully outgassed of radiogenic ^{40}Ar at that time.

Matrix samples from four additional rocks (76215,30; 76015,38; 76275,39; 76295,1 and 76295,3) yielded $^{40}\text{Ar}/^{39}\text{Ar}$ ages similar to 76315. The overall average for the matrix is 3.97 Gy.

The additional samples also yielded cosmic ray exposure ages of about 15 to 20 m.y. this probably being the time when the boulder rolled down the slope of the North massif. The difference between this age and the slightly older Kr/Kr age (Ref. 49) represents an uncertainty in the appropriate production rate for $^{38}\text{Ar}_C$ from Ca and not a real conflict.

Surface Exposure Effects

76015 and 76215 are unique rocks in the Apollo collection in terms of their record of extra-lunar processes (e.g., solar fluxes, and meteoroid phenomena) which effect the lunar surface.

Microcraters, solar flare tracks and solar wind. 76015 has a large number of cavities or vugs, and each cavity views a different region of space as determined by the orientation of 76015 on the lunar surface established by the Field Geology Team. Samples from two cavities representing different viewing directions were studied.

Microcraters from 0.025 to 1.0 microns were observed on crystal surfaces from both cavities. The microcrater size frequency distribution for 76015,24 which intercepted micrometeorites traveling normal to the plane of the ecliptic was observed to be identical to the distribution for 76015,28 which intercepted particles with orbits confined to the plane of the ecliptic (Ref. 50). The mass distribution of micrometeoroids, therefore, was found to be isotropic over the diameter interval (≤ 0.025 to ≤ 1.0 microns) measured.

Surfaces from one of the large cavities of 76015 had relatively high densities of craters but very little adhering debris. One of these surfaces was examined by very high resolution scanning microscopy after preparation with improved coating techniques. Microcraters with diameters as small as 150^oÅ were observed. These craters were made by particles of 1/2 to 1/4 the crater diameter (e.g., tens of angstroms) and indicate the presence of interplanetary dust particles of 10^{-19} to 10^{-20} grams (Ref. 59A). Crater shapes indicate equidimensional particles.

Solar flare track distributions were measured on the same surfaces from which crater counts were taken. Because the samples were not eroded, solar flare track profiles requiring no correction for erosion were established over the depth range of 10-2000 microns. The gradients closely approach an E^{-A} shape with A values of 1.72 and 1.79 (Ref. 51). These track gradients are comparable to gradients measured on other uneroded samples (Ref. 50). Exposure ages were determined to be 4.6×10^5 years for 76015,28 and 76015,105 (the largest cavity of 76015) and 5.3×10^5 years for 76015,40 (and, 24) (Ref. 51). It was observed that the track density to crater density ratio was the same for each sample. Therefore the flux of micrometeorites producing craters of 0.025 to 1.0 microns was demonstrated to be isotropic in terms of time as well as in mass distribution.

Sample 76215 was broken from a large spall plate located near the base of Boulder 4. The location and orientation of the sample is extremely well documented. In fact, it is possible to match precisely the cavities in the rock visible in the lunar surface documentary photography with Lunar Receiving Laboratory documentary photographs. A series of samples were slabbed for 76215 representing three orientations. One set came from a face with a lunar strike of approximately N45W and a dip of about 85°N. A second set came from the top of the sample which was oriented approximately parallel to the local surface. Both were exposed for the first time when 76215 was dislodged from the parent boulder and had very low crater populations and virtually no patina. Both surfaces were examined and the larger craters counted with a binocular microscope. The third set of samples came from surfaces exposed on the parent boulder and had patinas of varying thicknesses.

The exposure of the 76215 samples was affected by the adjacent boulders which reduce fluxes by a factor of about 1.5. Microcrater and track populations were determined from relatively flat surfaces and no substantial corrections were required for shielding by sample microtopography as in the case of the cavities of 76015.

Micron and sub-micron diameter crater populations and craters with diameters larger than 250 microns were counted on 76215. The size frequency distributions observed were equivalent to those measured on other samples including 76015 (Ref. 51).

Solar flare tracks were measured on two chips, principally to check the track density versus depth profile observed by Blanford (Refs. 50 and 52). The results confirmed the previous observations lending credence to the track production model (Ref. 51).

The solar flare track gradient, the microcrater abundances, and solar wind species concentrations all were measured on a 2 x 1 mm feldspar crystal surface removed from 76215 to provide correlative data sets for these three lunar surface phenomena (Ref. 58) (S. Hafner also was allocated a piece of this crystal).

These data and the previous results show that the solar flare track exposure age of the fresh surfaces of 76215 exposed when the rock was removed from the Station 6 boulder is 16,000-20,000 years using the Blanford et al. (Ref. 50) track production model. Solar wind species abundances in 76215 measured by ion probe (Ref. 59) also indicate exposure ages of approximately 20,000 years in agreement with the track data.

The ratio of microcrater to track densities was observed to be the same for samples of 76215 and 76015 showing uniformity of flux of both micrometeorites and solar flare particles thereby demonstrating invariant solar and interplanetary fluxes over a 2×10^6 year period (Ref. 51). The size frequency distribution of microcraters agrees with later results from 12054 (Ref. 58). These data are compiled in Figure 56, and correspond to the mass distribution and flux of interplanetary dust over many orders of magnitude. The consistent results from 76015 and 76215 plus 12054 in terms of dust flux and solar flare track production invariability are shown in Figure 57. The Station 6 samples pin down both ends of the line and clearly were critical samples in determining the long range behavior of the interplanetary dust and solar flare fluxes.

Patination processes and solar wind erosion. Surfaces of 76015 which showed variations in the amounts of material adhering to them were examined. It was concluded that glassy particles, typically shaped like pancakes, were deposited on all exposed surfaces (Ref. 50). Temperatures of the particles deposited ranged from at least 1300°C to over 1700°C. The rate and pervasiveness of this process appears sufficient to have an effect on surface correlated properties on a scale ranging from a few hundred angstroms to microns. The patina produced by deposition of glass pancakes reduces the albedo of all exposed surfaces.

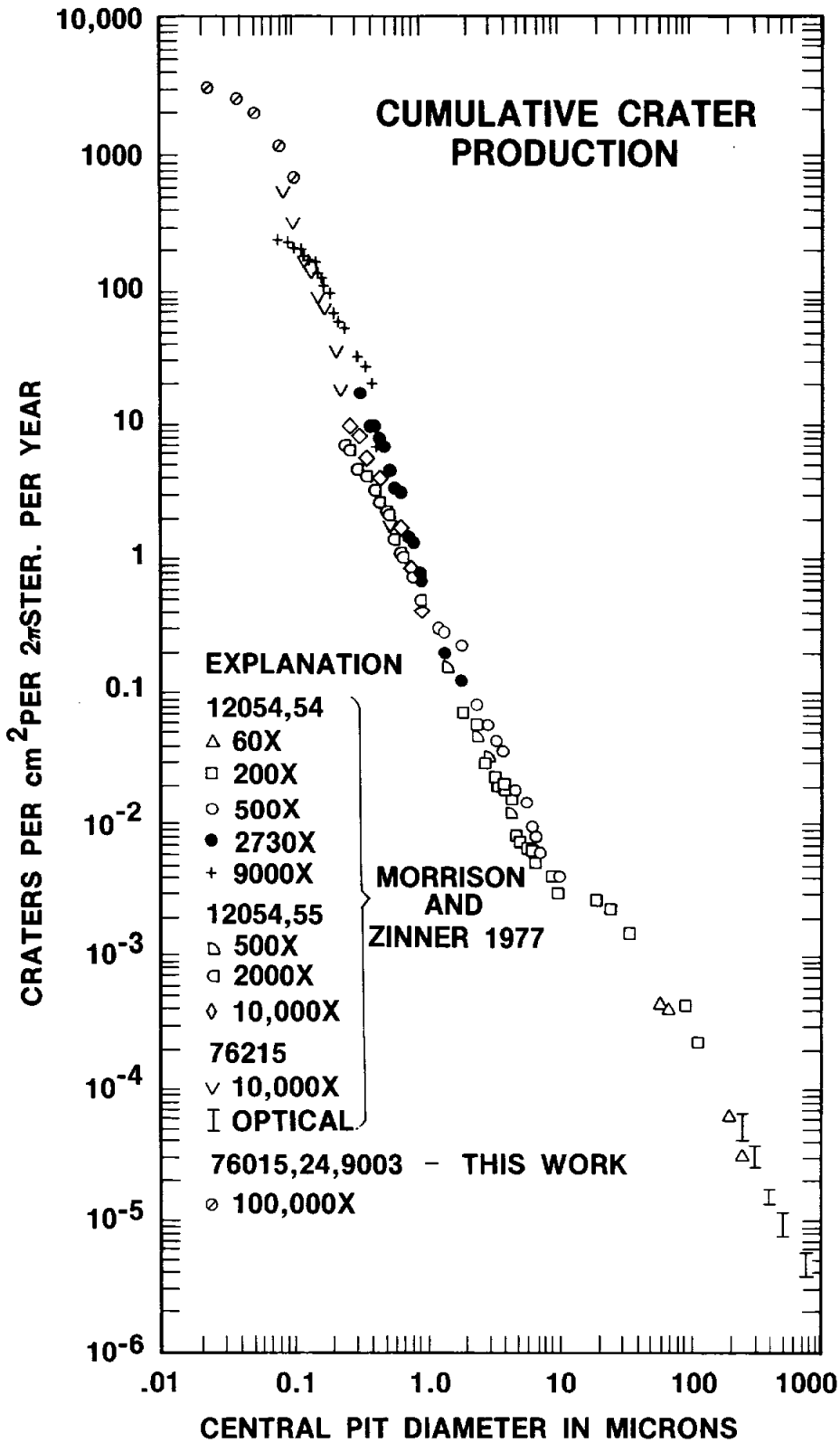


FIGURE 56: Cumulative crater distribution on 76215 and 76015 in comparison with 12054.

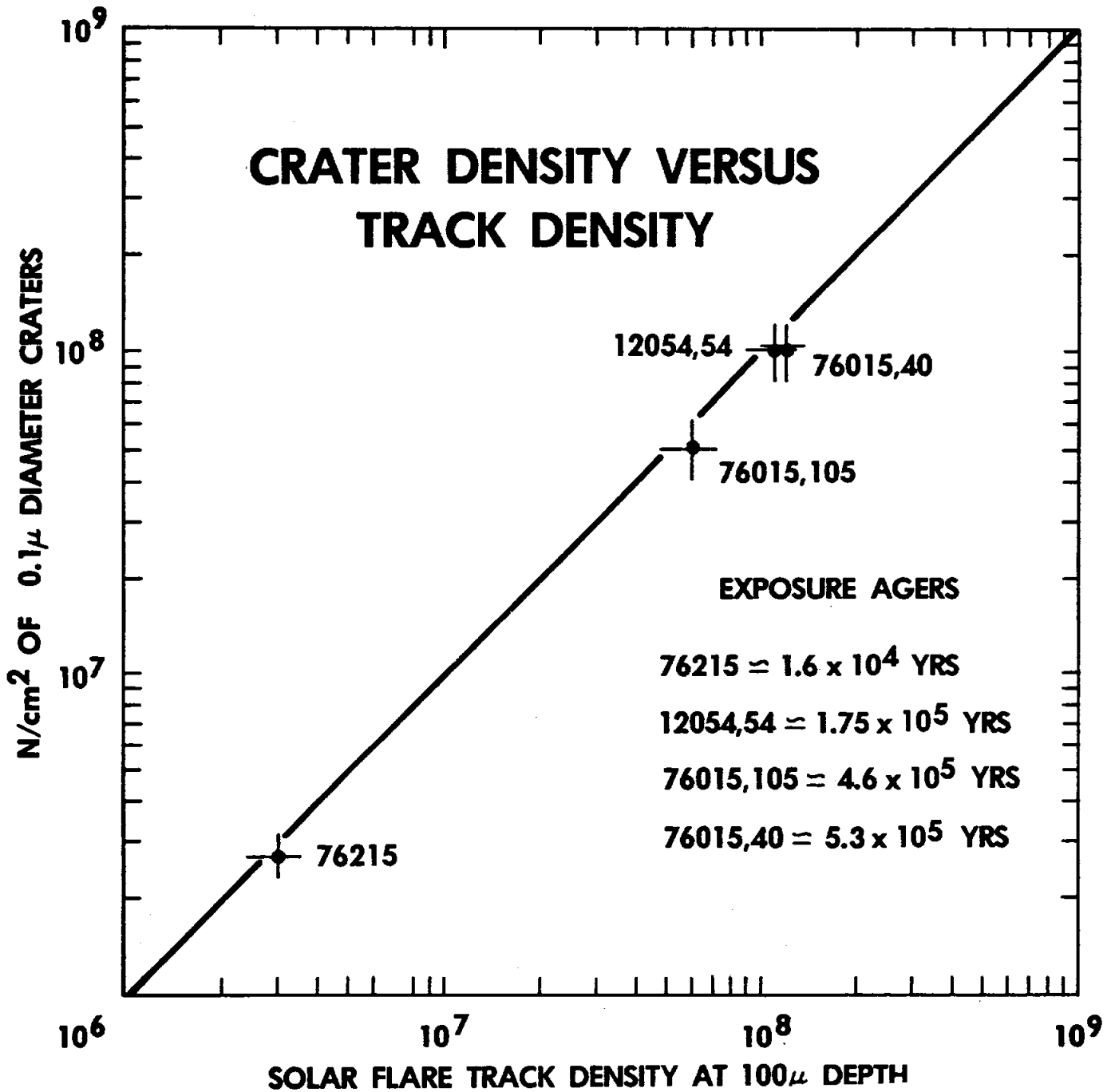


FIGURE 57: Correlation of crater density and solar flare track density on 76015, 76215 and 12054.

The preservation of small microcraters on the samples of 76015 exposed to the sun set an upper limit of 0.07\AA per year on solar wind erosion. Later work with small (≤ 0.1 to 1.0 microns) filaments (representing long cleavage flakes) on the surface of the feldspar crystal from 76215 shows no effect of solar wind erosion. This observation further limits solar wind erosion to less than or equal to 0.03\AA per year under recent lunar conditions (Ref. 58).

Magnetization

Twenty six samples from seven hand specimens, collected from the Station 6 boulder were studied magnetically (Ref. 63) The study of the natural remanent magnetization (NRM) of this boulder was undertaken primarily to test for uniformity of the direction of NRM within a handspecimen. This is a necessary although not sufficient condition for the rocks to carry a thermoremanence, i.e., a remanence acquired by cooling from above 770°C in the presence of a magnetic field. If the directions are uniform within each handspecimen then this information can be used to reassemble the boulder into one piece. After measuring samples from four handspecimens no simple picture emerged. However, as the measurements progressed a pattern did begin to emerge.

The direction of magnetization of samples from unit B which is almost devoid of large clasts cluster fairly well after alternating field demagnetization (Fig.58). Samples from unit C which is characterized by abundant large clasts up to 1 m in size do not contain a uniform direction of magnetization but the distribution is not random (Fig. 58). Based on these data it is proposed that the natural remanent magnetization in these breccias is the vector sum of two magnetizations, a pre-impact magnetization and a partial thermoremanence acquired during breccia formation. The relative contribution of the two components is controlled by the thermal history of the ejecta, which in turn is determined by its clast population. Depending

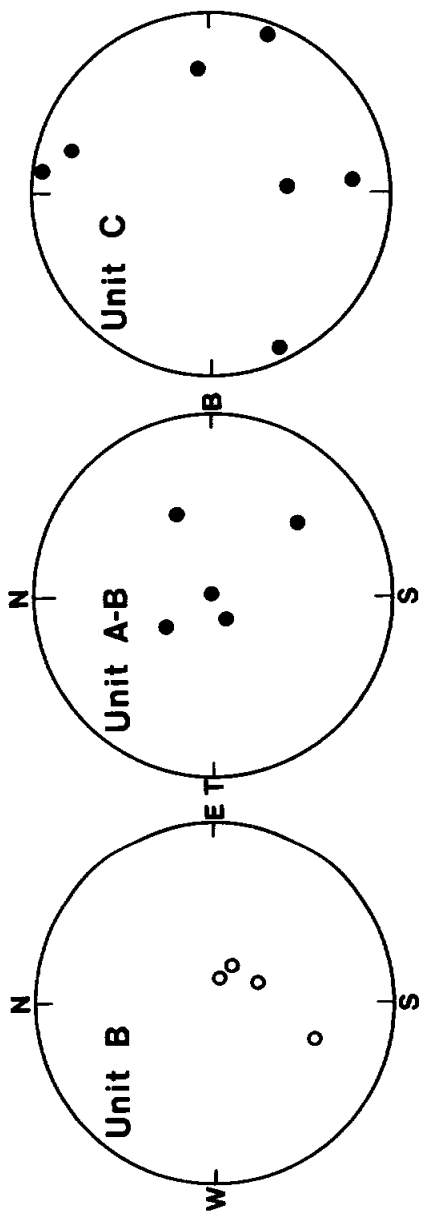


FIGURE 58: Distribution of the directions of stable magnetizations in individual samples of Unit B (76015), Unit A-B (76315) and Unit C (76295, 76275 and 76255).

on the clast population, the NRM can be a total thermoremanence, a partial thermoremanence plus a pre-impact magnetization, or a pre-impact magnetization. This model of thermal overprinting might be applicable to all lunar breccias of medium and higher metamorphic grade.

Interesting Problems that Remain

The clasts from the Station 6 boulder provide some interesting questions. For example the large cataclastic norite of 76255 has received only petrographic attention. Because of the unshocked nature of what appear to be primary coarse-grained, plutonic minerals it should be possible to study isotopic systematics on a lunar crustal rock whose mineral compositions indicate a relatively intermediate stage of differentiation.

The vuggy basalts that may be clasts in 76015 and 76295 display an unusually high Rb/Sr ratio and the highest $^{87}\text{Sr}/^{86}\text{Sr}$ ratio of lunar samples. Further chemical and isotopic study is necessary to delineate the origin of this unusual material. The occurrence of mare basalt clasts in 76255, a rock that formed about 3.98 b.y. ago, suggests that a search for such clasts in the boulder should be made for potential chemical and isotopic work.

In general the bulk of the work done by the consortium was concentrated on other than clasts. Further searches for and studies of clasts seems worthy of consideration.

References

General

1. Heiken, G. H., P. Butler, C. H. Simonds, W. C. Phinney, J. Warner, H. H. Schmitt, D. D. Bogard and W. G. Pearce (1973) Preliminary Data on Boulders at Station 6, Apollo 17 Landing Site. NASA TMX-58116.
2. Apollo 17, Station 6 Boulder Consortium, W. C. Phinney, Consortium leader (1974) Progress Report: Apollo 17, Station 6 Boulder Consortium. Lunar Science V, Supplement A, (The Lunar Science Institute, Houston), p. 7-13.
3. Phinney, W. C., J. L. Warner and C. H. Simonds (1974) Samples from a Lunar Highlands "Outcrop": Methodology of a Coordinated Study (abstract) Program Geol. Soc. Am. Annual Meeting, p. 1055-1057.

Petrology

4. Simonds, C. H., W. C. Phinney and J. L. Warner (1974) Petrography and Classification of Apollo 17 Non-Mare Rocks with Emphasis on Samples from the Station 6 Boulder. Proc. Fifth Lunar Sci. Conf., Geochim. Cosmochim. Acta, Suppl. 5, Vol. 1, Pergamon, p. 337-353.
5. Simonds, C. H., J. L. Warner and W. C. Phinney (1974) Source Material for Apollo 17 Impact-Melt Rocks (abstract) Program Geol. Soc. Am. Annual Meeting, p. 957-958.
6. Simonds, C. H., W. C. Phinney, J. L. Warner and G. H. Heiken (1975) Thermal Regimes in Crater Debris as Deduced from the Petrology of Apollo 17, Station 6 Boulder and Rake Samples, Lunar Science VI (Lunar Science Institute, Houston), p. 747-749.
7. Simonds, C. H. (1975) Thermal Regimes in Impact Melts and the Petrology of the Apollo 17, Station 6 Boulder, Proc. Lunar Sci. Conf. 6th, p. 641-672.

8. Warner, J. L., C. H. Simonds and W. C. Phinney (1975) Igneous Textured Gabbro from the Lunar Highlands (abstract), Trans. Amer. Geophys. Union (EOS), v. 56, p. 1071.
9. Warner, J. L., C. H. Simonds and W. C. Phinney (1976) Genetic Distinction between Anorthosites and Mg-Rich Plutonic Rocks: New Data from 76255, Lunar Sci. VII (Lunar Science Institute, Houston), p. 915-917.
10. Simonds, C. H., J. L. Warner and W. C. Phinney (1976) Clast-Melt Interactions in Lunar and Terrestrial Impact Melts, Lunar Sci. VII (Lunar Science Institute, Houston), p. 812-814.
11. Warner, J. L., C. H. Simonds and W. C. Phinney (1976) Apollo 17, Station 6 Boulder Sample 76255: Absolute Petrology of Breccia Matrix and Igneous Clasts, Proc. Lunar Sci. Conf. 7th, p. 2233-2250.
12. Phinney, W. C., J. L. Warner and C. H. Simonds (1977) Petrologic Evidence for Formation and Solidification of Impact Melts, Lunar Sci. VIII (Lunar Science Institute, Houston), p. 770-772.
13. Carter, J. L., U. S. Clanton, R. Fuhrman, R. B. Laughon, D. S. McKay and T. M. Usselman (1975) Morphology and Composition of Chalcopyrite, Chromite, Cu, Ni-Fe, Pentlandite, and Troilite in Vugs of 76015 and 76215. Proc. Lunar Sci. Conf. 6th, p. 719-728.
14. Clanton, U. S., J. L. Carter and D. S. McKay (1975) Vapor-Phase Crystallization of Sulfides? Lunar Sci. VI (Lunar Science Institute, Houston), p. 152-154.
15. Misra, K. C., B. M. Walker and L. A. Taylor (1976) Native Fe-Ni Metal Particles in Apollo 17 Station 6 Boulder. Lunar Sci. VII (Lunar Science Institute, Houston) p. 565-567.
16. Misra, K. C., B. M. Walker, and L. A. Taylor (1976) Textures and Compositions of Metal Particles in Apollo 17, Station 6 Boulder Samples. Proc. Lunar Sci. Conf. 7th, p. 2251-2266.

17. Warner, J. L., W. C. Phinney, C. E. Bickel and C. H. Simonds (1977) Felspathic Granulitic Impactites and Pre-Final Bombardment Lunar Evolution. Proc. Lunar Sci. Conf. 8th, p. 2051-2066.
18. Delano, J. W. (1977) Experimental Melting Relations of 63545, 76015, and 76055. Proc. Lunar Sci. Conf. 8th, p. 2097-2123.

Crystallography

19. Takeda, H., T. Ishii and M. Miyamoto (1976) Characterization of Crust Formation on a Parent Body of Achondrites and the Moon by Pyroxene Crystallography and Chemistry. Lunar Sci. VII (Lunar Science Institute, Houston), p. 846-848.
20. Takeda, H., T. Ishii, M. Miyamoto and A. M. Reid (1976) Characterization of Crust Formation on a Parent Body of Achondrites and the Moon by Pyroxene Crystallography and Chemistry. Proc. Lunar Sci. Conf. 7th, p. 3535-3548.
21. Takeda, H. and M. Miyamoto (1977) Inverted Pigeonites from Lunar Breccia 76255 and Pyroxene Crystallization Trends in Lunar and Achondritic Crusts. Lunar Sci. VIII (Lunar Science Institute, Houston), p. 922-924.
22. Takeda, H. and M. Miyamoto (1976) Inverted Pigeonites in Sample 76255 from North Massif, Taurus-Littrow (in Japanese). Abstr. Miner. Soc. Japan Fall Meeting, p. 122, Kagoshima.
23. Takeda, H. and M. Miyamoto (1976) Orientational Relationship of Augite-Orthopyroxene in Inverted Pigeonites and Their Inversion Mechanism. Abstr. Cryst. Soc. Japan Annual Meeting (in Japanese), p. 61, Cryst. Soc. Japan, Kanseigakuin Univ.
24. Takeda, H. and M. Miyamoto (1977) Inverted Pigeonites from Lunar Breccia 76255 and Pyroxene-Crystallization Trends in Lunar and Achondritic Crusts. Proc. Lunar Sci. Conf. 8th, 2617-2626.

Thermal Models

25. Simonds, C. H., J. L. Warner, W. C. Phinney and P. E. McGee (1976) Thermal Model for Impact Breccia Lithification: Manicouagan and the Moon, Proc. Lunar Sci. Conf. 7th, p. 2509-2528.
26. Onorato, P. K., D. R. Uhlmann and C. H. Simonds (1976) Heat Flow in Impact Melts: Apollo 17 Station 6 Boulder, Lunar Sci. VII (Lunar Science Institute, Houston), p. 656-658.
27. Onorato, P. I. K., D. R. Uhlman and C. H. Simonds (1976) Heat Flow in Impact Melts: Apollo 17 Station 6 Boulder and Some Applications to Other Breccias and Xenolith Laden Melts, Proc. Lunar Sci. Conf. 7th, p. 2449-2467.

Geochemistry

28. Rhodes, J. M., K. V. Rodgers, C. Shih, B. M. Bansal, L. E. Nyquist and H. Wiesmann (1974) The Relationship between Geology and Soil Chemistry at the Apollo 17 Landing Site. Lunar Sci. V (Lunar Science Institute, Houston), p. 630-632.
29. Rhodes, J. M., K. V. Rodgers, C. Shih, B. M. Bansal, L. E. Nyquist, H. Wiesmann and N. J. Hubbard (1974) The Relationship Between Geology and Soil Chemistry at the Apollo 17 Landing Site. Proc. Lunar Sci. Conf. 5th, p. 1097-1117.
30. Hubbard, N. J., J. M. Rhodes, L. E. Nyquist, C. Y. Shih, B. M. Bansal and H. Wiesmann (1974) Non-Mare and Highland Rock Types: Chemical Groups and their Internal Variations. Lunar Sci. V (Lunar Science Institute, Houston), p. 366-368.
31. Hubbard, N. J., J. M. Rhodes, H. Wiesmann, C. Y. Shih and B. M. Bansal (1974) The Chemical Definition and Interpretation of Rock Types Returned from the Non-Mare Regions of the Moon. Proc. Lunar Sci. Conf. 5th, p. 1227-1246.
- 31A. Warren, P. H. and J. T. Wasson (1978) Compositional-Petrographic Investigation of Pristine Nonmare Rocks. Proc. Lunar Planet. Sci. Conf. 9th, p. 185-217.

32. Gibson, E. K. and G. W. Moore (1974) Total Sulfur Abundances and Distributions in the Valley of Taurus-Littrow: Evidence of Mixing. Lunar Sci. V (Lunar Science Institute, Houston), p. 267-269.
33. Gibson, E. K. and G. W. Moore (1974) Sulfur Abundances and Distributions in the Valley of Taurus-Littrow. Proc. Lunar Sci. Conf. 5th, p. 1823-1837.
34. Bogard, D. D., L. E. Nyquist and W. C. Hirsch (1974) Noble Gases in Apollo 17 Boulders and Soils. Lunar Sci. V (Lunar Science Institute, Houston), p. 73-75.
35. Morgan, J. W., R. Ganapathy, H. Higuchi, U. Krähenbühl and E. Anders (1974) Lunar Basins: Tentative Characterization of Projectiles, from Meteoritic Elements in Apollo 17 Boulders, Lunar Sci. V (Lunar Science Institute, Houston), p. 527-529.
36. Morgan, J. W., R. Ganapathy, H. Higuchi, U. Krähenbühl and E. Anders (1974) Lunar Basins: Tentative Characterization of Projectiles, from Meteoritic Elements in Apollo 17 Boulders, Proc. Lunar Sci. Conf. 5th, p. 1703-1736.
37. Higuchi, H. and J. W. Morgan (1975) Ancient Meteoritic Component in Apollo 17 Boulders, Lunar Sci. VI (Lunar Science Institute, Houston), p. 364-366.
38. Higuchi, H. and J. W. Morgan (1975) Ancient Meteoritic Component in Apollo 17 Boulders, Proc. Lunar Sci. Conf. 6th, p. 1625-1651.
39. Higuchi, H., J. Gros and J. W. Morgan (1975) Errata. Cesium Content of Lunar Samples (10 papers). Proc. Lunar Sci. Conf. 6th, p. xii-xv.
40. Gros, J., H. Takahashi, J. Hertogen, J. W. Morgan and E. Anders (1976) Bombardment of Lunar Highlands: Constraints on Composition and Origin of Projectiles. Lunar Sci. VII (Lunar Science Institute, Houston), p. 339-341.
41. Gros, J., H. Takahashi, J. Hertogen, J. W. Morgan, and E. Anders (1976) Composition of the Projectiles that Bombarded the Lunar Highlands, Proc. Lunar Sci. Conf. 7th, 2403-2425.

42. Hertogen, Jan, M. Janssens, H. Takahashi, H. Palme and E. Anders (1977) Lunar Basins and Craters: Evidence for Systematic Compositional Changes of Bombarding Population. Proc. Lunar Sci. Conf. 8th, p. 17-45.
43. Palme, H., H. Baddenhausen, K. Blum, M. Cendales, G. Dreibus, H. Hofmeister, H. Kruse, C. Palme, B. Spettel, E. Vilesek, H. Wanke and G. Kurat (1978) New Data on Lunar Samples and Achondrites and a Comparison of the Least Fractionated Samples from the Earth, the Moon and the Eucrite Parent Body, Proc. Lunar Planet. Sci. Conf. 9th, p. 25-57.

Geochronology

44. Nyquist, L. E., B. M. Bansal, H. Wiesmann and B. M. Jahn (1974) Taurus-Littrow Chronology: Implications for Early Lunar Crustal Development. Lunar Sci. V (Lunar Science Institute, Houston), p. 565-567.
45. Nyquist, L. E., B. M. Bansal, H. Wiesmann and B. M. Jahn (1974) Taurus Littrow Chronology: Some Constraints on Early Lunar Crustal Development. Proc. Lunar Sci. Conf. 5th, p. 1515-1539.
46. Turner, G. and P. H. Cadogan (1975) The History of Lunar Bombardment Inferred from $^{40}\text{Ar} - ^{39}\text{Ar}$ Dating of Highland Rocks. Proc. Lunar Sci. Conf. 6th, p. 1509-1538.
47. Cadogan, P. H. and G. Turner (1976) The Chronology of the Apollo 17 Station 6 Boulder. Proc. Lunar Sci. Conf. 7th, p. 2267-2285.

Surface Exposure Effects

48. Crozaz, G., R. Drozd, C. Hohenberg, C. Morgan, C. Ralston, R. Walker and D. Yuhas (1974) Lunar Surface Dynamics: Some General Conclusions and New Results from Apollo 16 and 17. Lunar Sci. V (Lunar Science Institute, Houston), p. 157-159.

49. Crozaz, G., R. Drozd, C. Hohenberg, C. Morgan, C. Ralston, R. Walker and D. Yuhas (1974) Lunar Surface Dynamics: Some General Conclusions and New Results from Apollo 16 and 17. Proc. Lunar Sci. Conf. 5th, p. 2475-2499.
50. Blanford, G. E., R. M. Fruland, D. S. McKay and D. A. Morrison (1974) Lunar Surface Phenomena: Solar Flare Track Gradients, Microcraters, and Accretionary Particles. Proc. Lunar Sci. Conf. 5th, p. 2501-2526.
51. Morrison, D. and E. Zinner (1975) Studies of Solar Flares and Impact Craters in Partially Protected Crystals, Proc. Lunar Sci. Conf. 6th, p. 3373-3390.
52. Blanford, G., R. M. Fruland and D. A. Morrison (1975) Long-Term Differential Energy Spectrum for Solar Flare Iron Group Particles, Proc. Lunar Sci. Conf. 6th, p. 3557-3576.
53. Zinner, E., R. M. Walker, J. Chaumont and J. C. Dran (1976) Ion Probe Analysis of Artificially Implanted Ions in Terrestrial Samples and Surface Enhanced Ions in Lunar Sample 76215,77. Proc. Lunar Sci. Conf. 7th, p. 953-984.
54. Morrison, D. and E. Zinner (1976) The Size Frequency Distribution and Rate of Production of Microcraters. Lecture Notes in Physics, Interplanetary Dust and Zodiacal Light Proc. IAU Colloq. No. 31, Springer-Verlag, New York.
55. Morrison, D. and E. Zinner (1976) Submicron Crater Populations, Special Discussion on the Moon, Phil. Trans. R. Soc. London, 285, p. 379-384.
56. Zinner, E., R. M. Walker, J. Chaumont and J. C. Dran (1977) Surface Enhanced Elements and Microcraters in Lunar Rock 76215. Lunar Sci. VIII (Lunar Science Institute, Houston), p. 1044-1046.
57. Morrison, D. and E. Zinner (1977) Microcraters and Solar Cosmic Ray Tracks. Lunar Sci. VIII (Lunar Science Institute, Houston), p. 691-693.
58. Morrison, D. and E. Zinner (1977) 12054 and 76215: New Measurements of Interplanetary Dust and Solar Flare Fluxes. Proc. Lunar Sci. Conf. 8th, p. 841-863.

59. Zinner, E., R. M. Walker, J. Chaumont and J. C. Dran (1977) Ion Probe Surface Concentration Measurements of Mg and Fe and Microcraters in Crystals from Lunar Rock and Soil Samples. Proc. Lunar Sci. Conf. 8th, p. 3859-3883.
- 59A. Morrison, D. A. and U. S. Clanton (1979) Properties of Microcraters and Cosmic Dust of Less Than 1000Å Dimensions. Proc. Lunar Planet. Sci. Conf. 10th, p. 1649-1663.

Magnetism

60. Pearce, G. W., W. A. Gose and D. W. Strangway (1974) Magnetism of the Apollo 17 Samples. Lunar Sci. V (Lunar Science Institute, Houston), p. 590-592.
61. Pearce, G. W., D. W. Strangway and W. A. Gose (1974) Magnetic Properties of Apollo Samples and Implications for Regolith Formation. Proc. Lunar Sci. Conf. 5th, p. 2815-2826.
62. Gose, W. A., D. W. Strangway and G. W. Pearce (1976) Origin of Magnetization in Lunar Breccias: An Example of Thermal Overprinting. Lunar Sci. VII (Lunar Science Institute, Houston), p. 322-324.
63. Gose, W. A., D. W. Strangway and G. W. Pearce (1978) Origin of Magnetization in Lunar Breccias: An Example of Thermal Overprinting. EPSL, v. 38, p. 373-384.
64. Nagata, T., R. M. Fisher, F. C. Schwerer, M. D. Fuller and J. R. Dunn (1975) Basic Magnetic Properties of Apollo 17 Basaltic and Anorthositic Lunar Materials. Lunar Sci. VI (Lunar Science Institute, Houston), p. 584-586.
65. Nagata, T., R. M. Fisher, F. C. Schwerer, M. D. Fuller and J. R. Dunn (1975) Effects of Meteorite Impact on Magnetic Properties of Apollo Lunar Materials, Proc. Lunar Sci. Conf. 5th, p. 3111-3122.